CHALMERS

Ringhals Diagnostics and Monitoring, Annual Research Report 2015

V. DYKIN
C. MONTALVO
N. TRAN
H. NYLÉN
I. PÁZSIT

Nuclear Engineering Group
Division of Subatomic and Plasma Physics
CHALMERS UNIVERSITY OF TECHNOLOGY
Gothenburg, Sweden, 2015
CTH-NT-319/RR-20 December 2015

CTH-NT-319/RR-20 December 2015

Ringhals Diagnostics and Monitoring, Annual Research Report 2015

V. Dykin, C. Montalvo, N. Tran, H. Nylén and I. Pázsit

Division of Subatomic and Plasma Physics
Chalmers University of Technology
SE-412 96 Göteborg, Sweden
ISSN 0281-9775

Ringhals Diagnostics and Monitoring, Annual Research Report 2015

V. Dykin, C. Montalvo Martín, N. Tran, H. Nylén and I. Pázsit

Division of Subatomic and Plasma Physics,
Chalmers University of Technology
SE-412 96 Göteborg, Sweden

Abstract

This report gives an account of the work performed by the Division of Subatomic and Plasma Physics (former Division of Nuclear Engineering), Chalmers, in the frame of research collaboration with Ringhals, Vattenfall AB, contract No. 630217-031. The contract constitutes a 1-year co-operative research work concerning diagnostics and monitoring of the BWR and PWR units. The work in the contract has been performed between January 1st 2015, and December 31st, 2015. During this period, we have worked with five main items as follows:

1. Development of the mode separation model with an extension to describe 3-D core barrel vibrations;
2. Analysis of new ex-core measurements, taken in R-4 after power uprate;
3. Investigation of the correctness of the hypothesis that the reactivity component extracted from the ex-core detector signals can be due to fuel assembly vibrations with CORE SIM;
4. A basic study in neutron noise theory which could provide some indirect support for the determination of the void fraction from neutron noise measurements;
5. A preliminary study of the possibility of modelling 3-dimensional fuel assembly vibrations in a realistic PWR system with the CORE SIM simulator;

This work was performed at the Division of Subatomic and Plasma Physics, Chalmers University of Technology by Victor Dykin (project co-ordinator), Cristina Montalvo (visitor from the Technical University of Madrid), Hoai-Nam Tran (research collaborator from Duy Tan University), Imre Pázsit and Henrik Nylén, who was also the contact person at Ringhals.

Contents

1. INTRODUCTION

The long term goal of the contract is to utilize the research potential of the Division of Subatomic and Plasma Physics at Chalmers in treating reactor physics problems related to the operation of the power plant. This is achieved in a co-operative research project, in the course of which the understanding of relevant problems increases at the division as well as methods are elaborated and implemented for their solution. The results obtained in the earlier stages have been reported in [13]-[19].

The work in one-year contract period has been performed between January 1st 2015, and December 31st, 2015. During this period, we have worked with five items as follows:

1. Development of the mode separation model with an extension to describe 3-D core barrel vibrations;
2. Analysis of new ex-core measurements, taken in R-4 after power uprate;
3. Investigation of the correctness of the hypothesis that the reactivity component extracted from the ex-core detector signals can be due to fuel assembly vibrations with CORESIM;
4. A basic study in neutron noise theory which could provide some indirect support for the determination of the void fraction from neutron noise measurements;
5. A preliminary study of the possibility of modelling 3-dimensional fuel assembly vibrations in a realistic PWR system with the CORE SIM simulator;

A further general objective of the work is to gain experience with the important and characteristic features of power spectra and certain operational variables in the normal state, in order to be able to perform diagnostics of various phenomena.

A proposal for the continuation of the work for 2016 is also given at the end of this report.

2. DEVELOPMENT OF THE MODE SEPARATION MODEL WITH AN EXTENSION TO DESCRIBE 3-D CORE BARREL VIBRATIONS.

2.1. Introduction, background

Core barrel motion monitoring has been so far concentrated on two main types of core barrel vibration modes: the pendulum or beam mode vibrations and the shell mode vibrations [1]-[2]. The former Division of Nuclear Engineering (currently Division of Subatomic and Plasma Physics) in Chalmers, Gothenburg, and the Ringhals Nuclear Plant have investigated the core barrel vibrations in the Ringhals PWRs in the frame of a long-term research project over the last 20 years [3]-[4]. Based on the different symmetry properties of the vibration modes, a mode separation technique was developed to enhance the contributions from the different modes by taking different combinations of the time-resolved detector signals before performing the frequency analysis and subsequent determination of the vibration amplitudes by curve fitting to the enhanced vibration peaks [5]. In such a method only the upper or the lower detector signals have been involved, i.e. a pure 2D model has been used. Recently this methodology have been even extended to 3D in order to resolve two different components of the beam mode (the so-called "wobbly" or "tilting" mode and the "true" beam mode), lying close to each other in frequency [4]. Moreover, even the diagnostics of the beam mode vibrations, if e.g. the reactivity component is estimated from the sum of 8 detectors instead of 4, can benefit from such an extension to 3D.

Another argument in favour for such an study is the fact that the recent observations of wear at both the lower and upper core-barrel-support structures, i.e. the lower radial key and the reactor vessel alignment pins in the Ringhals PWRs also indicated that vibration modes of the core barrel other than pendulum (beam mode) and shell mode are likely to occur [6]. A beam mode type movement alone is not able to explain such a wear, and therefore, it is fair to assume that the vibration mode in question is a small amplitude periodic tilting movement of the core barrel around a horizontal, diagonal pivot at the half height of the core (crossing through the centre of mass of the core). *Fig. 1* below gives an illustration of the tilting mode and the symmetry relationships between the upper and lower, diagonally opposite ex-core detectors.

In addition, the method proposed above might also help to explain the extra peaks that were observed in the spectra of R2, which are possibly due to the difference of the thermal shield in R2 from those in R3 and R4.

In the following work, ex-core data taken in the Ringhals-4 PWR were analyzed in order to find evidence of such a tilting movement. First, cross spectra between various upper and lower ex-core detectors were calculated and analyzed to locate the frequency range of the new vibration mode. Then, the mode enhancement model, based on symmetry considerations, elaborated in [2] for the beam and shell modes by using either the four upper or four lower detectors only, was extended to include all eight detectors

simultaneously. The extension was made by assuming the presence of a tilting mode, and accounting for its symmetry properties. The measurements were evaluated by the new mode enhancement technique. The results show that it is possible to enhance such a mode and find it in the spectra by properly combining the signals in the time domain.

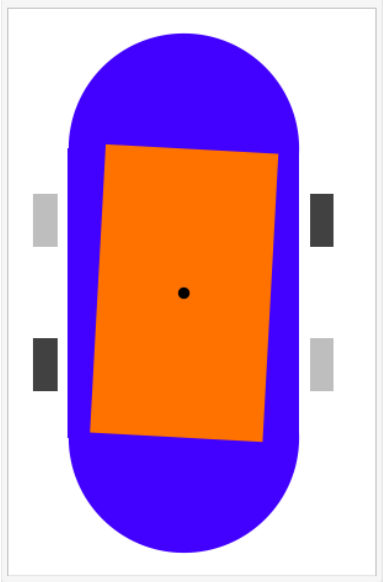

Fig. 1. Illustration of the tilting mode vibration of the core barrel and the symmetries of the detector signals.

2.2. Traces of the tilting mode in the ex-core data

One of the problems, we may encounter during the analysis of the new vibration type is that both the beam mode and the tilting mode exhibit a very similar behaviour what regards the type of vibration, and therefore it might be somewhat difficult to distinguish and separate those two modes especially if they both lie very close to each other in the frequency domain. The titled mode represents the case when the entire core barrel vibrates. Such a movement can be illustrated as if the core was fixed in the centre of its mass and at the same time exhibits pendulum vibrations such that one upper detector signal is in-phase with the radially opposite lower detector signal i.e. N41U is in-phase with N42L, N42U is in-phase with N41L and so forth. The same illustration can also be applied to the beam mode with the only difference that the core barrel is fixed in the top. Thus, according to the symmetry properties of the assumed type of movement (see *Fig. 1*) it is possible to presume the phase relationships between different pairs of ex-core detectors and compare them to the ones found for the beam mode. This information is thus summarized in Table 1.

Table 1 Phase relationship of pair of detectors in the beam and tilting mode.

Pair of detectors	Phase relationship in tilting mode	Phase relationship in Beam Mode
N41U-N42L	In-phase	Out-of-phase
N42U-N41L	In-phase	Out-of-phase
N43U-N44L	In-phase	Out-of-phase
N44U-N43L	In-phase	Out-of-phase

Table 1 basically reveals that opposite detectors at different axial levels would show in-phase relationship in a tilting type of movement whereas for a pendulum type (beam mode), there would be an out-of-phase relationship.

First, the amplitude and the phase of the CPSDs between the opposite detector signals are plotted and compared with the corresponding CPSDs calculated between one upper and one lower detectors placed on the same diagonal (see *Fig. 3*-*Fig. 2*).

As one can see from *Fig. 3*, the amplitude and the phase behaviour look pretty much similar for the beam mode detector pairs N41U-N42U and N41L-N42L and the tilting detector pairs N41U-N42L and N42U-N41L. In the beam mode region (6-8 Hz) the phases of the CPSDs clearly show out of phase behaviour whereas the coherence is also very high.

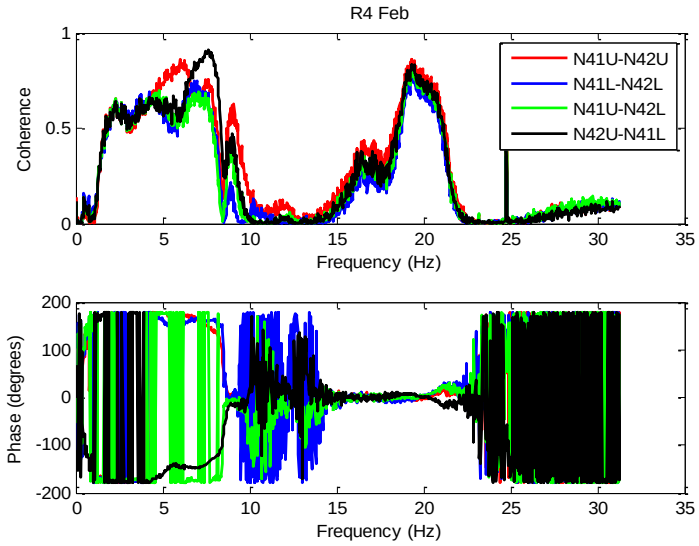

Fig. 3 The amplitude and the phase of the CPSD calculated from the measurements taken in February 2014 at Ringhals 4 for N41U-N42U, N41L-N42L, N41U-N42L, N42U-N41L detector pairs.

Fig. 2 shows the CPSDs calculated for other diagonal detector pair N43-N44. *Fig. 2* also demonstrates clear out of phase relationship between all detector pairs in the region of beam mode. In addition, several sinks in the amplitude such as at 6 Hz in N43U-N44L case and another one at 9 Hz for all detector pairs can be pointed out.

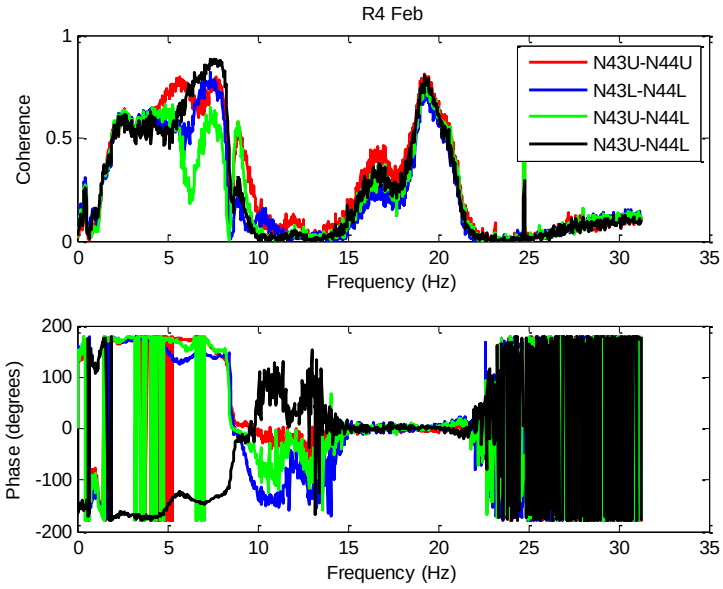

Fig. 2 The amplitude and the phase of the CPSD calculated from the measurements taken in February 2014 at Ringhals 4 for N43U-N44U, N43L-N44L, N43U-N44L, N43U-N44L detector pairs.

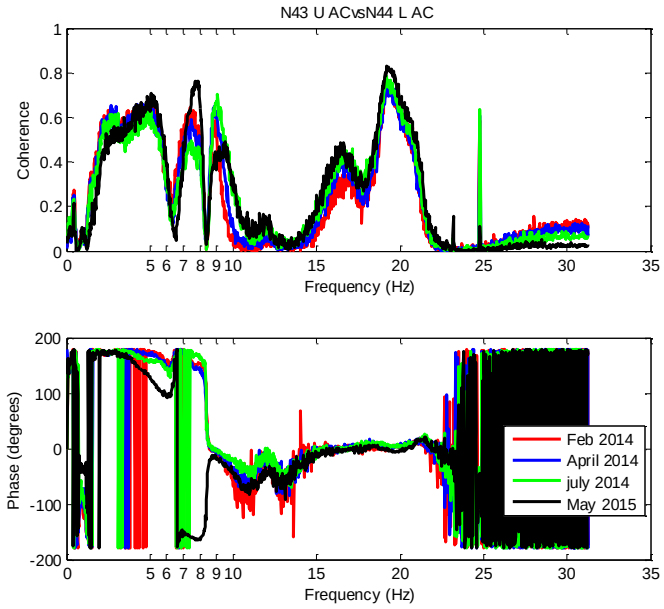

Fig. 4 The amplitude and the phase of the CPSD calculated between N43U and N44L detector signals for different sets of measurements (2014-2015).

Although there are frequencies at which the tilting detector pairs show pure in phase behaviour, it is not clear whether those peaks correspond to the wobbly movement or not since the frequency region where in phase relationship is observed actually belong to the shell mode region (around 20 Hz). At the same time, the observed peak around 9 Hz might also be related to the fuel induced vibrations. The similar peak has also been noticed in the reactivity mode (obtained via the developed enhancement method) in the earlier analysis.

Next, the amplitude and the phase of the CPSDs calculated for the detector pair N43U-N44L are shown in *Fig. 4* for different set of measurements. The data from 2014 belongs to one cycle and the data from 2015 to the next cycle. Taking into account previous studies based on Ringhals data, the strong peak around 7-8 Hz that shows out-of-phase relationship might be associated with the beam mode component. In such a case the peak around 8 Hz with zero phase, might actually be attributed to the tilting mode motion.

In order to prove or disprove the above mentioned hypothesis, the amplitude and the phase of the CPSD between two opposite detector signals placed at the same axial level were calculated and plotted (see *Fig. 5*). In such a case the tilting mode is expected to show a pure out of phase behaviour. Nevertheless, the thorough analysis of *Fig. 5* indicates that the peak around 8 Hz again shows close to zero phase behaviour and therefore cannot be attributed to the tilting mode. Moreover, the previous studies [7] based on the analysis of Ringhals measurements show that the peak around 8 Hz is actually caused by fuel assembly vibrations due to the turbulent flow.

Taking into account these results obtained above where the tilting mode was not clearly identified, another approach has also been tested. Namely, a special model representing different vibration modes of the core barrel was set up in order to extract and enhance the tilting mode (similar to the case of beam mode vibrations [5]-[6]).

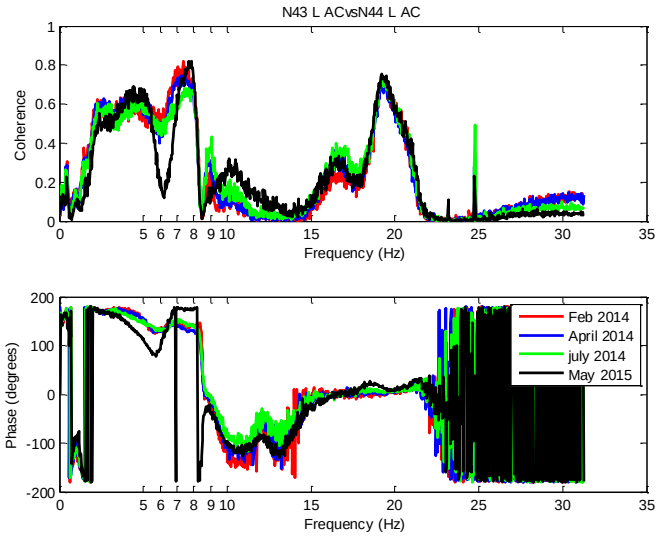

Fig. 5 The amplitude and the phase of the CPSD calculated between N43L and N44L detectors for different sets of measurements (2014-2015).

2.3. Proposed model and mode enhancement technique.

Following the same approach as in [2], the ex-core detector signals are assumed to contain several different components such as uncorrelated (background) noise, point kinetic or reactivity component, beam mode and shell mode. By also including a tilting mode component, the signal from each of eight ex-core detectors (N41U, N42U, N43U, N44U, N41L, N42L, N43L and N44L) can be given as:

$$\delta\phi_{N41U} = \delta r_{N41U}(t) + P(t) + D(t) - \mu x(t) + \lambda x(t), \quad (1)$$

$$\delta\phi_{N42U} = \delta r_{N42U}(t) + P(t) + D(t) + \mu x(t) - \lambda x(t), \quad (2)$$

$$\delta\phi_{N43U} = \delta r_{N43U}(t) + P(t) - D(t) + \mu y(t) - \lambda y(t), \quad (3)$$

$$\delta\phi_{N44U} = \delta r_{N44U}(t) + P(t) - D(t) - \mu y(t) + \lambda y(t), \quad (4)$$

$$\delta\phi_{N41L} = \delta r_{N41L}(t) + P(t) + D(t) - \mu(1+\alpha)x(t) - \lambda x(t), \quad (5)$$

$$\delta\phi_{N42L} = \delta r_{N42L}(t) + P(t) + D(t) + \mu(1+\alpha)x(t) + \lambda x(t), \quad (6)$$

$$\delta\phi_{N43L} = \delta r_{N43L}(t) + P(t) - D(t) + \mu(1+\alpha)\,y(t) + \lambda\,y(t), \tag{7}$$

$$\delta\phi_{N44L} = \delta r_{N44L}(t) + P(t) - D(t) - \mu(1+\alpha)\,y(t) - \lambda\,y(t), \tag{8}$$

Here, $\delta\phi_i(t)$ stands for the fluctuations (AC component) of the signal of the specified detector, and $\delta r_i(t)$, $P(t)$, $D(t)$, $\mu x(t)$ and $\lambda y(t)$ are the uncorrelated noise, the reactivity component, the shell mode, the beam mode and the tilting mode components, respectively. Notice that, unlike in the original work [2], we assume that the lower detectors have a larger amplitude of the beam mode component, by introducing the factor $1+\alpha$. This is

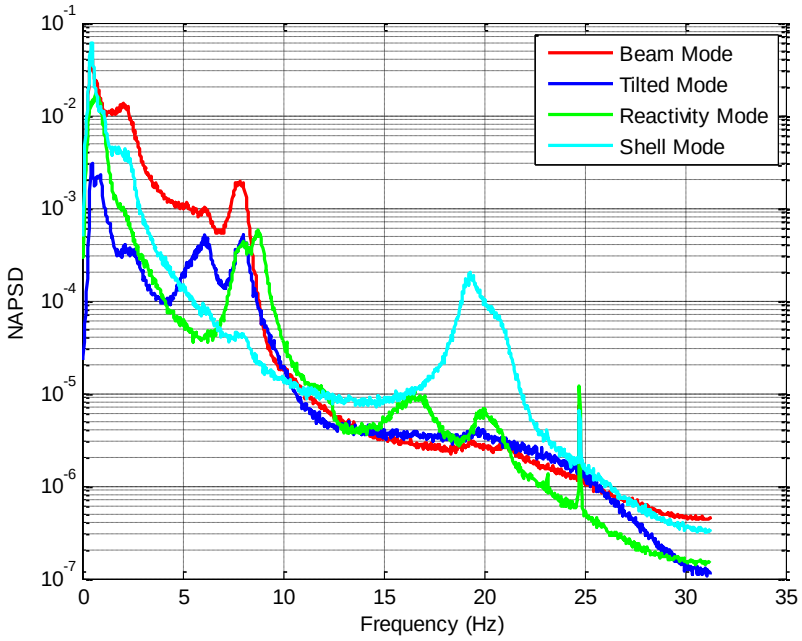

Fig. 6 APSDs of beam, tilting, reactivity and shell modes extracted from the data taken at Ringhals 4 in 2014 .

justified by the fact that, in contrast the approach presented in [2], here we need to consider the signals from all 8 detectors (both the upper and lower ones) simultaneously. The tilting mode $\lambda x(t)$ and $\lambda y(t)$ in x and y direction respectively which are simulated as a beam mode component in terms of its symmetry. Similar to the case of beam mode vibrations, here it is also assumed that the core barrel movement takes place along two core diagonals whereas the in-phase behaviour is specified for two opposite detectors instead: one is the upper detector and another one is the lower.

By combining the signals from various detectors in the time domain, it is possible to enhance the tilting mode component and one thus obtains:

- for the x-component:

$$\frac{\delta\phi_{N41U}(t) + \delta\phi_{N42L}(t)}{2} - \frac{\delta\phi_{N42U}(t) + \delta\phi_{N41L}(t)}{2} = \mu\alpha\,x(t) + 2\lambda\,x(t). \tag{9}$$

- for the y-component:

$$\frac{\delta\phi_{N43U}(t)+\delta\phi_{N44L}(t)}{2}-\frac{\delta\phi_{N44U}(t)+\delta\phi_{N43L}(t)}{2}=-\mu\alpha\, y(t)-2\lambda\, y(t). \qquad (10)$$

As it can be seen from Eqs (9)-(10), a beam mode component ${}^{\mu}\alpha_{x(t)}$ (${}^{\mu}\alpha_{y(t)}$) represented by the first term on the right hand side, is still present in the expressions above whereas the second term represents the enhanced tilting mode. From the above, it becomes clear that if the difference in the amplitude of the beam mode for the upper and lower detector signals would be negligible, the procedure presented by equations (9)-(10) would enhance the tilting mode in the x-and y-directions, respectively.

The Eqs (9) and (10) can be transformed into the frequency domain, such that Eq. (9) will represent $TM_x(\omega)$ and Eq. (10) -$TM_y(\omega)$ and then after averaging two spectra one obtains:

$$TM(\omega)=\frac{TM_x(\omega)+TM_y(\omega)}{2}. \qquad (11)$$

which thus represents the Auto Power Spectral Density (APSD) of the tilting mode. For the illustration purpose, in *Fig. 6* the APSDs for all different components/modes are plotted for the measurement data taken in 2014 at Ringhals 4. As it can be seen from *Fig. 6*, the tilting mode is represented by a peak in the APSD (blue curve) around 6 Hz which cannot be clearly distinguished in the APSDs of any other enhanced modes. The applied enhancement method seems to be very efficient in removing the reactivity and shell modes but it is not able to completely eliminate the beam mode component due to the fact that the beam mode amplitude in the lower detector signals is larger as compared to the one measured by the upper detector.

Further, in *Fig. 7*, the time evolution of the amplitude of the titled mode within one cycle (from February to July) extracted from the measurements performed in 2014 at Ringhals 4 is plotted. From this figure one can notice that even though the beam mode is still present after the enhancement, a new peak is found at around 6 Hz which was not clearly visible before in the spectra of the separated mode components (reactivity, beam and shell modes). Taking into account that both movements (the beam mode and the tilting mode) are very similar to each other in their qualitative behaviour, the presence of two closely seated peaks in the APSD is justified by the fact that the applied enhancement technique is not able to completely remove the beam mode component as it has already been mentioned earlier in the discussion. Moreover, since the beam mode component is usually the strongest one in the detector signal in the frequency region of 8 Hz, it thus covers any other components which are present in the signal. Therefore, in the CPSD calculated between two diagonally placed upper and lower detectors (see *Fig. 4*), there were neither any peak nor any in-phase behaviour at 6 Hz observed. In addition, from *Fig. 4*, it can be clearly seen that the amplitude of the beam mode component is larger than that of the tilting mode

component, which thus confirms our earlier hypothesis about the dominance of the BM component in the APSD as compared to the tilting mode.

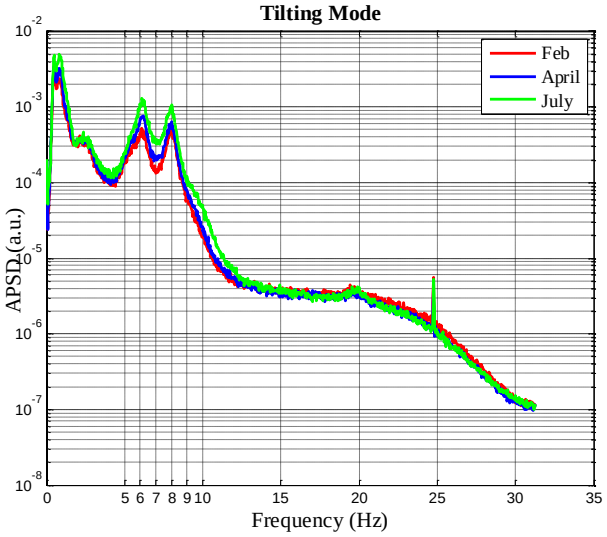

Fig. 7 Time evolution (within one cycle) of the APSD of the enhanced tilting mode for calculated from the measurements taken I 2014 at Ringhals-4 Unit.

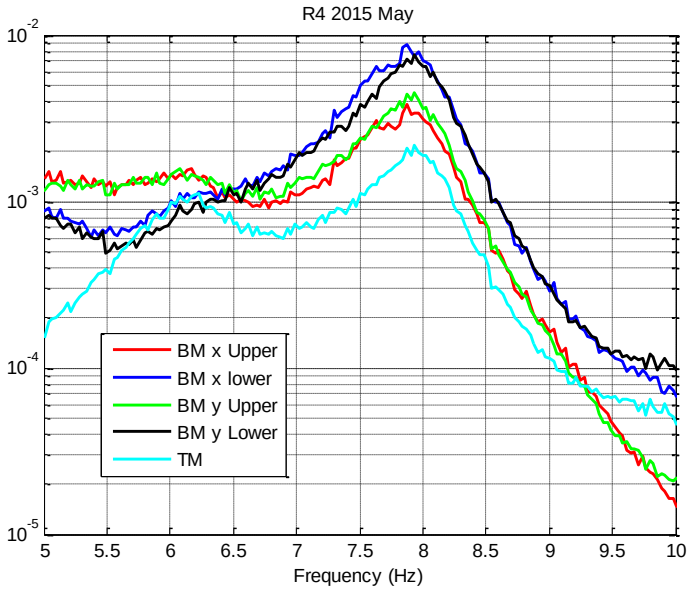

Fig. 8 APSDs of Beam and Tilting modes extracted from the measurement data taken at Ringhals 4 in May 2015, respectively .

Another interesting feature which can also be noticed from *Fig. 7* is the fact that the amplitude of the tilting mode gradually changes (increases) within a cycle,

To demonstrate yet another interesting observation related to tilting mode, In *Fig. 8* the APSDs of the beam and tilting mode components are plotted again but in a somewhat different manner. Namely, on the one hand there is the amplitude of the beam mode in the x direction plotted for the upper and the lower detector signals. On the other hand, the amplitude of the beam mode in y-direction for both upper and lower detector signals are also plotted as well as the APSD of the tilting mode. As one can see from the figure, the amplitude of the beam mode corresponding to the upper detectors has larger amplitude for the peak at 6 Hz whereas the amplitude of the beam mode for the peak at 8 Hz shows larger amplitude for the lower detectors. That is, if the 6 Hz peak is related to the tilting mode type, the vibrations should not necessarily have to show larger amplitude in the lower detector signals as the beam mode does. In fact, it demonstrates the opposite effect.

2.4. Validation of the tilting mode: in and out of phase process separation

As it was mentioned earlier in **Subsection 2.3**, for cross detectors at different axial levels, the beam mode vibrations appear as an out of phase process whereas the tilting movement type vibrations are in phase Nevertheless, the cross spectra are not able to demonstrate the existence of the tilting mode probably because the beam mode is dominant in the frequency range where both modes lie. Therefore it would be interesting to validate the existence of the tilting mode by using another methodology which could separate in-phase and out of phase processes. In [8]-[9] there is a model that represents the ex-core detector signals by the sum of in phase and out of phase contributions. Let $X(t)$ denote the in phase signal and $Y(t)$ the out of phase one, two detectors signals $S_1(t)$ and $S_2(t)$ could be represented by:

$$S_1(t) = X(t) + Y(t) + s_1(t), \tag{12}$$

$$S_2(t) = X(t) - Y(t) + s_2(t). \tag{13}$$

where $s_1(t)$ and $s_2(t)$ are independent (uncorrelated) random noise sources. By performing the cross-correlation analysis for both detector signals (i.e. calculating the CPSD between the two signals) and after some algebra, the following expressions below for the spectra of the in phase and out of phase processes separately ($APSD_X(\omega)$ and $APSD_Y(\omega)$, respectively) can be deduced:

$$APSD_X(\omega) = \left\{ \frac{1 \pm COH_{12}(\omega)}{2COH_{12}(\omega)} \right| CPSD_{12}(\omega) \Big| \tag{14}$$

$$APSD_Y(\omega) = \left\{ \frac{1 \mp COH_{12}(\omega)}{2COH_{12}(\omega)} \right| CPSD_{12}(\omega) \Big|. \tag{15}$$

where $APSD_X(\omega)$ stands for the Auto Power Spectral Density of the in phase processes and $APSD_Y(\omega)$ - for the APSD of the out of phase processes, $CPSD_{12}(\omega)$ is the Cross Power Spectral Density calculated between two detector signals $S_1(t)$ and $S_2(t)$ and $COH_{12}(\omega)$ denotes the coherence function. Eqs (14)-(15) give a clue how by calculating $APSD_X(\omega)$ and $APSD_Y(\omega)$ for different detector pairs, one can separate the beam mode contribution from the tilting mode component. In present work, it is advisable to use the opposite detectors at different axial levels in order to calculate the spectra of equations (14) -(15), since those ones contains both contributions: out of phase components corresponding to the beam mode vibrations and the in phase components representing the tilting mode motion. For further details, see [8]-[9].

- *Detector pairs corresponding to the tilting mode*

Fig. 9 shows an example of the in-phase/out-of-phase separation technique for the pair N43U-N44L. Here it can be seen that the out of phase processes are much stronger than the in phase ones so that the amplitude of the in phase is always much smaller than that of the out of phase ones. Further, the tilting mode at 6 Hz clearly appears as an in-phase process, whereas the beam mode results in an out-of-phase behaviour. It is also possible to point out the fact that very close to the beam mode at 8 Hz there is an in-phase peak observed in red coloured curve. The first peak obviously corresponds to a pendulum core barrel motion (out-of-phase process) whereas the second one is induced by the vibration of the fuel assemblies (in-phase process). Regarding the shell mode, for two diagonally opposite detectors at different axial levels it should also appear as an in-phase process. This latter can be easily confirmed from *Fig. 9* where a broad peak around 20 Hz is detected for the in-phase curve. It should be pointed out here that the applied separation procedure is valid

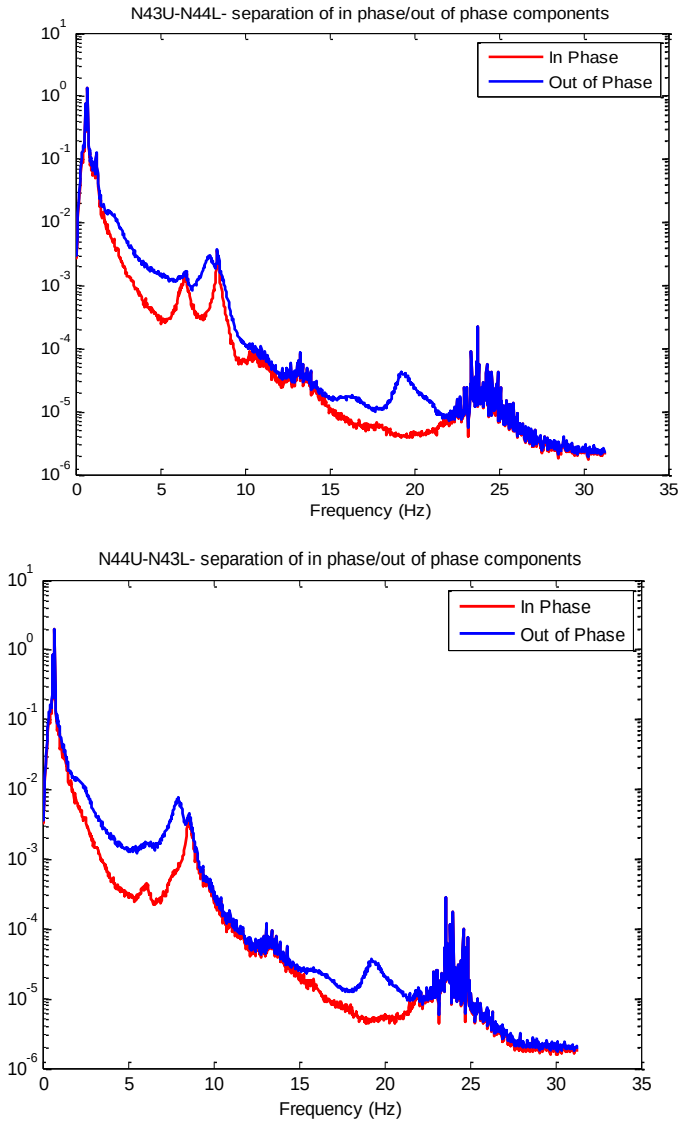

Fig. 9 APSDs of the in-phase and out-of-phase components for the pairs N43U-N44L (upper figure) and N44U-N43L (lower figure) .

only for a specific frequency region (in the present case for 5-10 Hz) since during the calculations a specific sign relation between the detector signals in the CPSD was assumed. Therefore the obtained spectrum can be analyzed only within 5-10 Hz frequency range.

In *Fig. 10* the results of the application of the same separation procedure for another detector pair (corresponding to another diagonal) are presented.

One can notice that *Fig. 9* does not demonstrate the same result for the separation technique as *Fig. 10*. In the latter case, 6 Hz peak is clearly separated from the beam mode peak whereas in *Fig. 9* such a distinction between two peaks is not clearly visible. Moreover, the obtained beam mode can even be characterized as combination of in phase and out of phase processes at the same time.

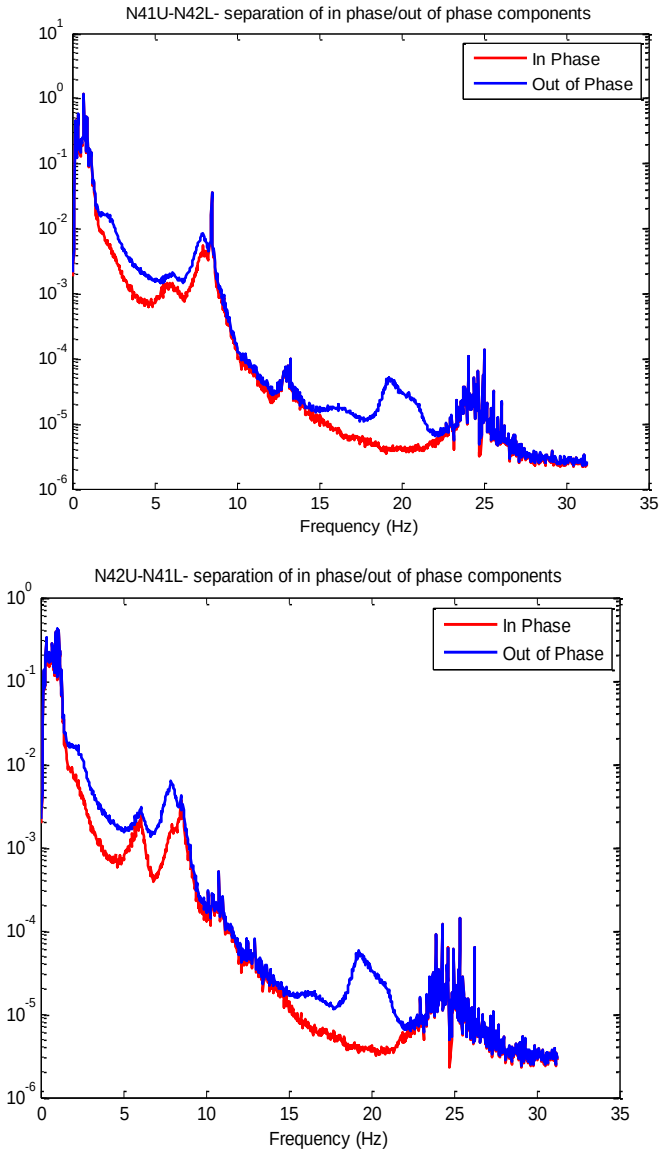

Fig. 10 APSDs of the in-phase and out-of-phase components for the pairs N41U-N42L (upper figure) and N42U-N41L (lower figure) .

- *Opposite upper detectors*

The results of the separation procedure performed for two opposite upper detector placed in the same axial level are shown below.

As one can see from *Fig. 11* in the case of opposite upper detectors sitting at the axial level, the beam and the tilting mode peaks are both present in the out-of-phase spectrum even though the peak at 6 Hz corresponding to the tilting mode has very low amplitude.

- *Opposite lower detectors*

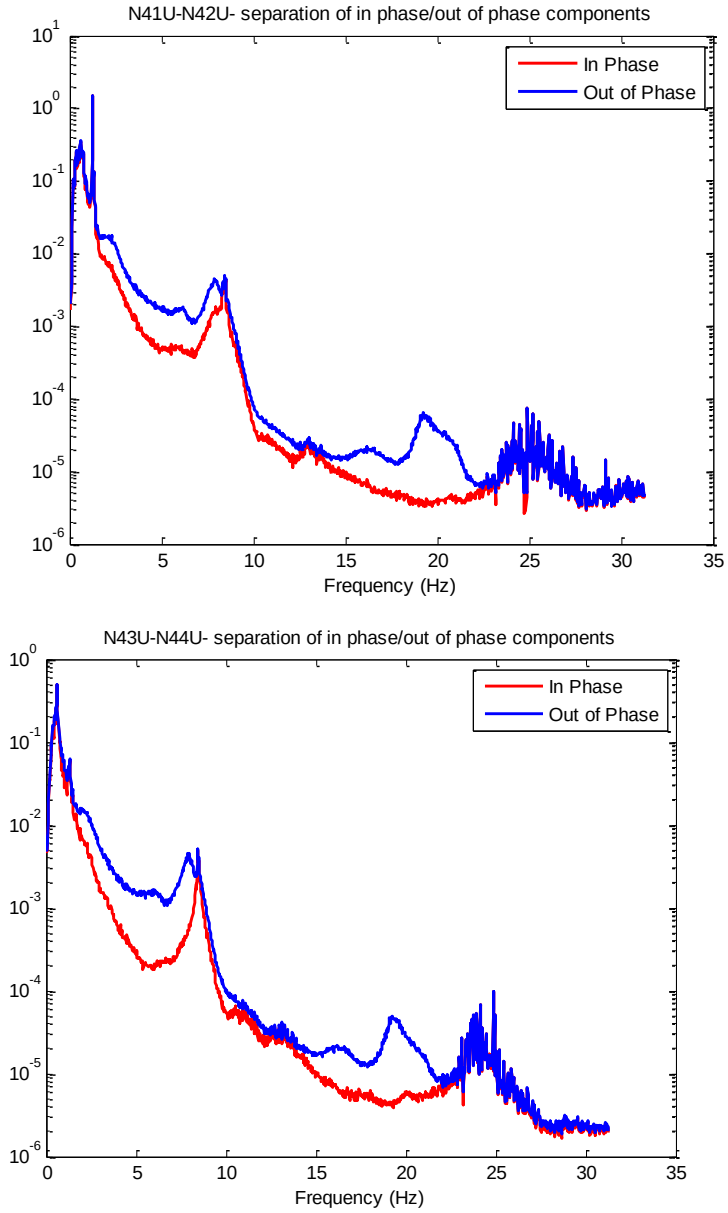

Fig. 11 APSDs of the in-phase and out-of-phase components for the pairs N41U-N42U (upper figure) and N43U-N44U (lower figure) .

The results of the separation procedure performed for two opposite lower detectors placed in the same axial level are then shown in *Fig. 12*.

In this case, the interpretation of the results becomes very complicated and non-conclusive since the peak at 6 Hz seems to be present in both in phase and out phase spectra.

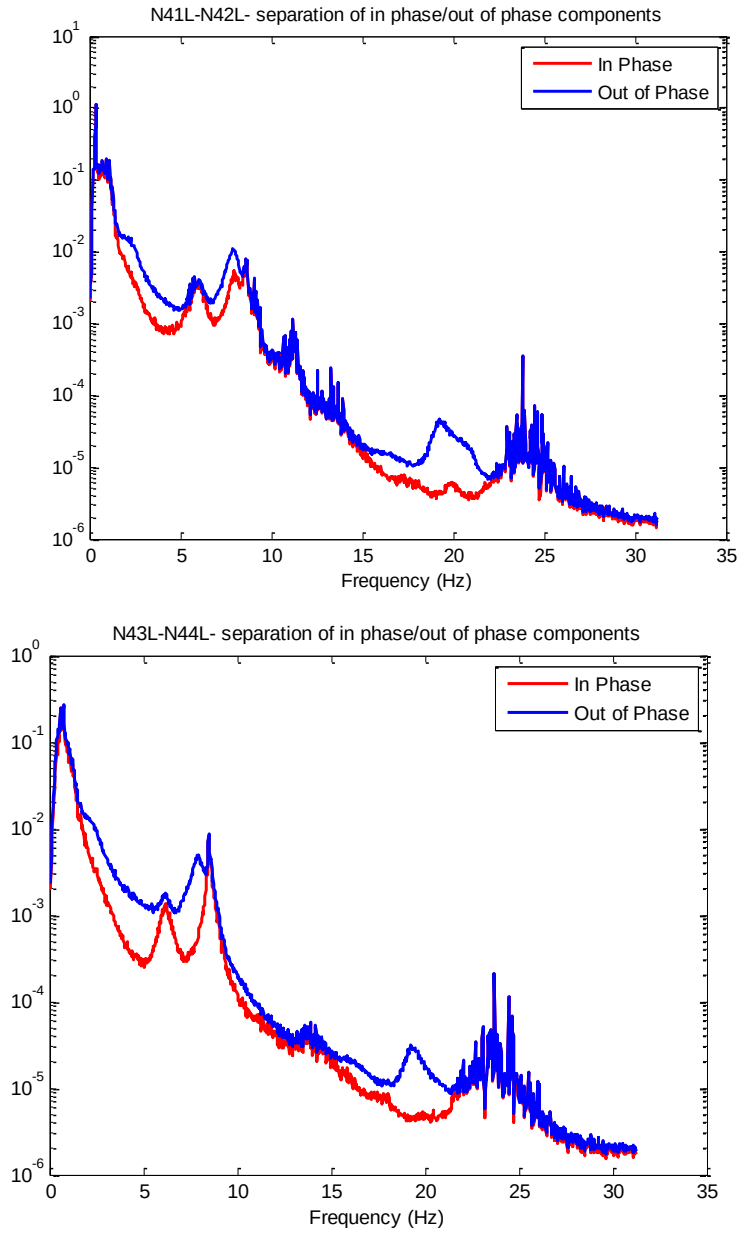

Fig. 12 APSDs of the in-phase and out-of-phase components for the pairs N41L-N42L (upper figure) and N43L-N44L (lower figure) .

2.5. Qualitative analysis of the behaviour of the tilting and beam modes via a double harmonic oscillator model.

As it has already been pointed out earlier in **Subsection 2.2**, there were several sinks (as such as one at 6 Hz and another one at 9 Hz) observed in the amplitude of the CPSDs calculated for the diagonal detector pair N43-N44 (see *Fig. 2*). Such behaviour is not natural for this frequency region and can be caused by several different reasons. The main purpose of the present study is to investigate the nature of those dips. For this purpose, a specific model based on the two harmonic oscillators representing the beam and the titled mode respectively is set up and analysed below.

Let us assume that the tilting and the beam mode movements can be simulated vibrations represented by two damped harmonic oscillators driven by a white noise. Each oscillator is assumed to have its own eigenfrequency, i.e. one at 6 Hz which corresponds the tilting mode and another one at 8 Hz for the beam mode. Then, the fluctuations in the flux (noise) caused by these two vibration components can then be modelled as follows:

$$\ddot{\delta\phi}_{TM}(t) + 2D_1\omega_{01}\dot{\delta\phi}_{TM}(t) + \omega_{01}^2\delta\phi_{TM}(t) = F(t), \tag{16}$$

$$\ddot{\delta\phi}_{BM}(t) + 2D_2\omega_{02}\dot{\delta\phi}_{BM}(t) + \omega_{02}^2\delta\phi_{BM}(t) = F(t). \tag{17}$$

where $F(t)$ stands for a white noise driving force, $\delta\phi_{TM}$ is the neutron noise due to the tilting mode and $\delta\phi_{BM}$ is the neutron noise due to the beam mode vibrations. After performing Fourier transform, taking into account $\omega = 2\pi f$, $\omega_{01} = 2\pi f_1$, $\omega_{02} = 2\pi f_2$ and after some algebra, from Eqs (16)-(17) one obtains:

$$\delta\phi_{TM}(f) = \frac{F(f)}{f_1^2 - f^2 + i2D_1 f_1 f} = F(f)H_1(f), \tag{18}$$

$$\delta\phi_{BM}(f) = \frac{F(f)}{f_2^2 - f^2 + i2D_2 f_2 f} = F(f)H_2(f). \tag{19}$$

where $H_1(f)$ and $H_2(f)$ stand for the transfer functions of each of two harmonic oscillators.

Next, performing Fourier transform on Eqs (1)-(6) representing the signals detected by N41 and N42 detectors and replacing the beam and tilting components via Eqs (18) and (19), one gets:

$$\delta\phi_{N41U}(f) = \delta r_{N41U}(f) + P(f) + D(f) - \mu H_2(f) + \lambda H_1(f), \tag{20}$$

$$\delta\phi_{N42U}(f) = \delta r_{N42U}(f) + P(f) + D(f) + \mu H_2(f) - \lambda H_1(f), \tag{21}$$

$$\delta\phi_{N41L}(f) = \delta r_{N41L}(f) + P(f) + D(f) - \mu(\alpha+1)H_2(f) - \lambda H_1(f), \tag{22}$$

$$\delta\phi_{N42L}(f) = \delta r_{N42L}(f) + P(f) + D(f) + \mu(1+\alpha)H_2(f) + \lambda H_1(f). \tag{23}$$

Then, assuming that all above components are uncorrelated and that the contribution of the shell mode component in the beam mode frequency range is negligible, the CPSD between the detector pairs representing the beam and the tilting modes as well as the CPSD for N41U-N41L and N42U-N42L detector pairs can be expressed as:

$$\text{BM pairs}\begin{cases} CPSD_{N41U-N42U} = \left|P(f)\right|^2 - \mu^2\left|H_2(f)\right|^2 - \lambda^2\left|H_1(f)\right|^2 \\ CPSD_{N41L-N42L} = \left|P(f)\right|^2 - \mu^2(1+\alpha)^2\left|H_2(f)\right|^2 - \lambda^2\left|H_1(f)\right|^2 \end{cases}, \tag{24}$$

$$\text{TM pairs}\begin{cases} CPSD_{N41U-N42L} = \left|P(f)\right|^2 - \mu^2(1+\alpha)\left|H_2(f)\right|^2 + \lambda^2\left|H_1(f)\right|^2 \\ CPSD_{N42U-N41L} = \left|P(f)\right|^2 - \mu^2(1+\alpha)\left|H_2(f)\right|^2 + \lambda^2\left|H_1(f)\right|^2 \end{cases}, \tag{25}$$

$$\text{N41U-N41L/N42U-N42L}\begin{cases} CPSD_{N41U-N41L} = \left|P(f)\right|^2 + \mu^2(1+\alpha)\left|H_2(f)\right|^2 - \lambda^2\left|H_1(f)\right|^2 \\ CPSD_{N42U-N42L} = \left|P(f)\right|^2 + \mu^2(1+\alpha)\left|H_2(f)\right|^2 - \lambda^2\left|H_1(f)\right|^2 \end{cases}. \tag{26}$$

Since coherence function is defined as the ratio between the absolute value of the CPSD weighted with the square root of the convolution between the APSDs of the individual signals, the coherence could become zero in some of the cases above. One possible explanation for this latter fact can be formulated as follows. Since within the beam mode frequency range the contribution of the latter one into the CPSD is usually the largest one, all the terms related to $\left|H_2(f)\right|$ will also contribute with the largest weight. Moreover, taking into account the fact that the tilting mode contribution and the reactivity have opposite sign with a respect to the sign of the beam mode component, the coherence function calculated for the case of tilting mode detector pairs might become zero. In addition, this mechanism can also result in much lower coherence for the rest of the CPSD. This latter fact can partly be confirmed by the fact that several sinks have also been observed in the coherence function calculated for the detector pairs other than the tilting mode detector pairs. Nevertheless, the sinks are still more visible in the coherence calculated for the detector pair representing the tilting mode.

Further, we assume that between 6-8 Hz, the main contributors into the neutron flux fluctuations (noise) are only the vibrations related to the beam and the tilting modes. As a result, the neutron noise can be represented as a combination of two induced vibrations i.e. two damped harmonic oscillators, each having its own eigenfrequency and transfer function. Then, applying a white noise as an input for each of these transfer functions, two outputs are obtained. Such a simulation can easily be performed in MATLAB by specifying two transfer functions in the frequency domain driven by a white noise. The output from each of two systems is obtained in the time domain, such that:

$$F(t) \rightarrow H_1(f) \rightarrow x_{TM}(t), \tag{27}$$

$$F(t) \rightarrow H_2(f) \rightarrow x_{BM}(t). \tag{28}$$

where $F(t)$ represents the input white noise, $x_{TM}(t)$ stands for the vibration signal induced by the tilting mode motion and $x_{BM}(t)$ is the vibration signal caused by the pendular core barrel motion. According to Eqs (1)-(6), the signal from each detector could be modelled as follows:

$$\delta\phi_{N41U}(t) = -\mu_1 x_{BM}(t) + \lambda x_{TM}(t), \tag{29}$$

$$\delta\phi_{N41L}(t) = \mu_1\mu_2 x_{BM}(t) + \lambda x_{TM}(t). \tag{30}$$

Sine both $x_{TM}(t)$ and $x_{BM}(t)$ signals are defined internally via a MATLAB simulation, detector signals $\delta\phi_{N41U}(t)$ and $\delta\phi_{N42L}(t)$ are obtained by carefully choosing the parameters μ_2, μ_1 and λ. In *Fig. 13*, the results of the simulation for the amplitude (coherence function) and the phase of the CPSD calculated between N41U and N42L detector signals are shown. There, one clear sink is visible in the coherence curve together a corresponding shift in the phase curve.

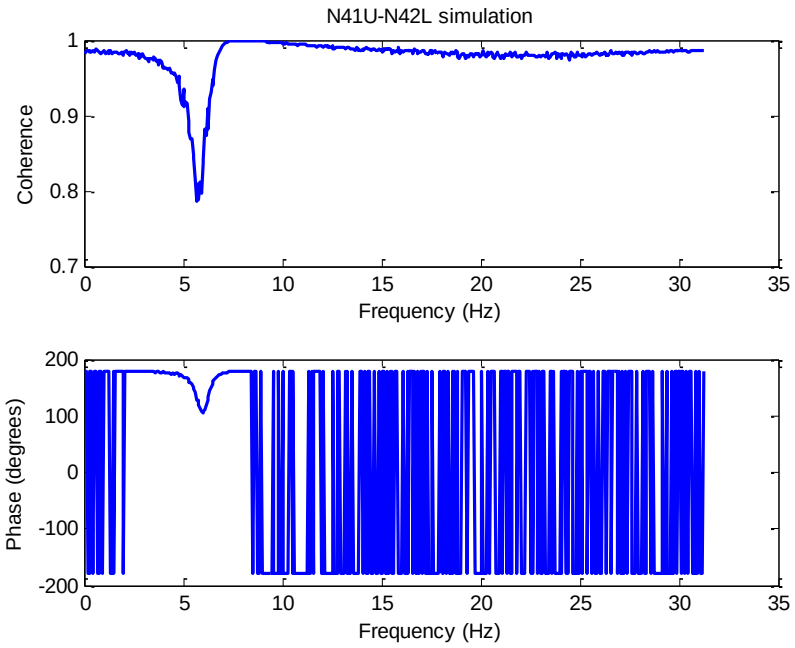

Fig. 13 Coherence and phase between N43L and N44L detectors.

As we can see from the simulation above, even though there is an in phase process present at 6 Hz, the overall phase shows essentially out of phase behaviour for all frequencies of interest, except for the localized phase shift and dip in the coherence at 6 Hz which were also observed earlier in real measurement data (see Fig. 4-Fig. 5).

By summing up the results presented above, one can conclude that apparently there are two processes which drive the detector signals in the beam mode frequency region.

These are the tilting mode motion and the pendulum CB motion. When both detector signals show an in-phase behaviour for the tilting mode motion, such as, for instance, for N44U-N43L detector pair, they will at the same time show an out of phase behaviour for the beam mode motion (see equations (1)-(6)). However, since these two processes are taking place very close to each other in frequency, it is very difficult to observe any trace of in phase behaviour for the 6 Hz peak, even though a slight shift in the phase can be detected.

2.6. Conclusions

The results presented in this work show the existence of a core barrel vibration mode different from the beam and the shell modes. The observations of wear in the core-barrel support structures, which prompted the investigation as well as the analysis performed in this work support the idea of a small amplitude periodic tilting movement of the core barrel around a horizontal, diagonal pivot at the half height of the core.

The analysis was made based on a model where the detector signals are composed of different sources, one of them being the vibration resulting from the tilting movement. By properly combining the signals of the ex-core detectors in the time domain, such mode is enhanced and it is possible to appreciate it as a 6 Hz peak in the spectra of the combined signals.

In order to validate this procedure, another methodology based on a technique for separating in-phase and out-of-phase processes is used. This method is able to separate the tilting mode from the beam mode and also works to identify other known modes of vibration such as the shell mode or the fuel assemblies' vibrations.

3. ANALYSIS OF NEW EX-CORE MEASUREMENTS, TAKEN IN R-4 AFTER POWER UPRATE.

3.1. Introduction and background

Within the last decade, a series of studies dedicated to core barrel vibrations have been performed in order to analyze and find a suitable explanation for the recent observations of wear at both the lower and upper core-barrel-support structures, i.e. the lower radial key and the reactor vessel alignment pins in the Ringhals PWRs. In the last few years the main focus in this area was put on the investigation of a double peak observed in the Auto Power Spectrum in the frequency region of the beam mode component. Several attempts were undertaken in order to understand and clarify the origin of this peak by using different techniques and methods such as spectrum analysis, curve fitting and trend analysis. In particular, the confirmation or disproval of the hypothesis about the nature of this peak (where it was suggested that the lower frequency peak is due to the beam mode vibrations and the upper peak is due to fuel assembly vibrations) was one the main target of those analysis. Up to the last stage none of significant progress has been done which could provide conclusive results. In 2014 a new separation technique to separate and enhance different components in the ex-core detector spectrum was developed and tested with a fruitful outcome on the measurements taken at Ringhals-4. Finally, it became possible to distinguish between the beam mode component due to core barrel vibrations and reactivity component associated to the single fuel assembly vibrations. In additions it was also possible to confirm the constant amplitude within one fuel cycle in the former case and varying amplitude (again within one cycle) in the latter case which were in very good agreement with the original hypothesis. For more details one refers to [5].

In the present stage, one of the main tasks with the spectral analysis of the ex-core detector measurements was to investigate the possibility of existence of yet another vibration component, the so called “tilting mode” component. For this purpose a new separation technique based on the symmetry of different vibration components involving all eight available ex-core detector signals was developed in order to enhance the tilting mode component and to separate it from other components. The results of such an analysis performed on the measurements data taken in 2014 in Ringhals-4 have been presented in the previous section and showed very promising results. The main conclusion was that such a component does exist. In addition a thorough trend analysis of the tilting mode within one cycle has been also performed which showed the gradual change in the amplitude of the APSD with burn-up of such vibrations. More details can be found in the previous section

Both investigations mentioned above have been undertaken on the measurement data taken at Ringhals-4. In 2015 the total effect of Ringhals-4 was increased by 18.6 %. Therefore, it is natural to perform the similar analysis on a new set of measurements in order to investigate the effect of power increase on the measured neutron noise, in particular core barrel and fuel assembly vibrations and associated vibrations components

(beam, shell, reactivity and titled modes). Thus, the analysis will be done along two lines. First the qualitative analysis and comparison between APSDs of the measurement taken in 2014 before the power uprate and in 2015 after the power uprate will be performed. Further, titled mode extraction technique developed in the previous section will be tested on 2015 measurements in order to indentify any differences related to the power uprate.

3.2. Details of the measurements in R4

Three sets of measurements were selected for the analysis. These were performed in R4 in 2014, on 10 April, 24 July and 19 May 2015. The measurements made correspond to cycle 33 and 34 of Ringhals 4.The sampling frequency in the present measurements was 62.5 Hz for all three sets of measurements. The measurement points are shown in Table 2. More detailed data regarding settings and general parameters can be found in the measurement protocol [10]-[12]. Some sample spectra, showing the APSD for each of the 8 individual ex-core detectors, calculated from the corresponding measurement will be presented in the next section

Table 2 Some data of the three measurements in Ringhals 4 during 2014-2015

Channel	Measurement point
0	Time
1	N41U DC
2	N42U DC
3	N43U DC
4	N44U DC
5	N41L DC
6	N42L DC
7	N43L DC
8	N44L DC
9	N41U AC
10	N42U AC
11	N43U AC
12	N44U AC
13	N41L AC
14	N42L AC

15	N43L AC
16	N44L AC

3.3. The analysis of the measurements taken in Ringhals-4 between 2014-2015 before and after power uprate

In this study, the APSDs calculated from Ringhals-4 measurements in the period 2014-2015 were plotted and visually analyzed. The spectra for four neutron detectors N41 Upper, N42 Upper, N43 Upper and N44 Upper are given in *Fig. 14*. In *Fig. 15* , the APSDs calculated for corresponding lower detectors are also plotted. The analyses will be focused only on the frequency regions related to the beam and shell modes, i.e. at the peaks around 6-8 and 20 Hz.

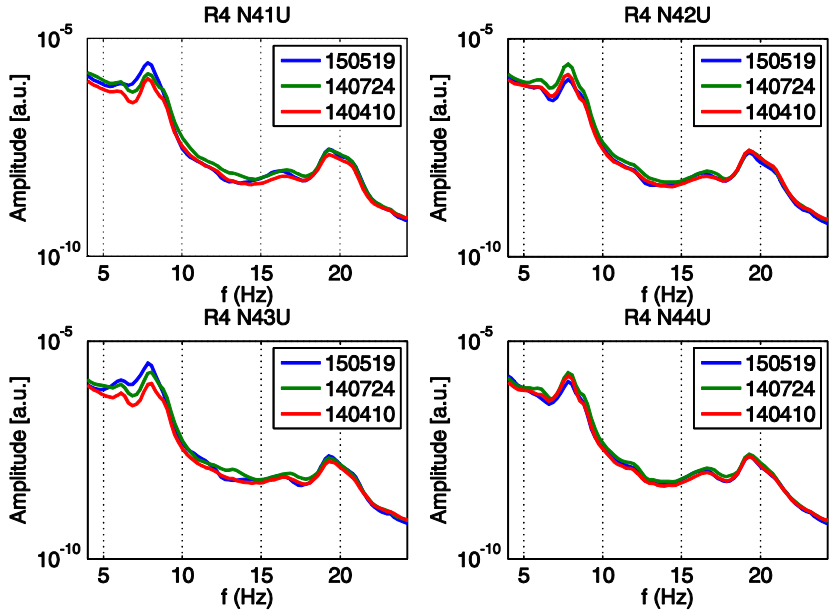

Fig. 14 Evolution of the APSDs of the upper ex-core detector measurements made in April, July 2014 and May 2015 in Ringhals-4.

The thorough analysis of the present plots does not show any remarkable differences in the spectra behaviour between different detectors within the 2014-2015 period. The spectra are almost identical and do not vary much from each other. The similar tendency in the spectral behaviour can also be seen within time evolution from 2014 to 2015. There are however, some observations that can be pointed out. The first one is relate to the slightly increase in the amplitude of the APSDs around 6-8 Hz corresponding to the beam mode in 2015 as compared to 2014 observed for the majority of ex-core detectors except for N42U and N44U/L. Such an increase in the amplitude is natural after the power uprate taking into account that the noise level is usually proportional to the total power of the reactor. The second one is related to the different time evolution behaviour of the amplitudes around 6-8 Hz between the upper and lower detector spectra within 2014-2015. Thus, in the case of

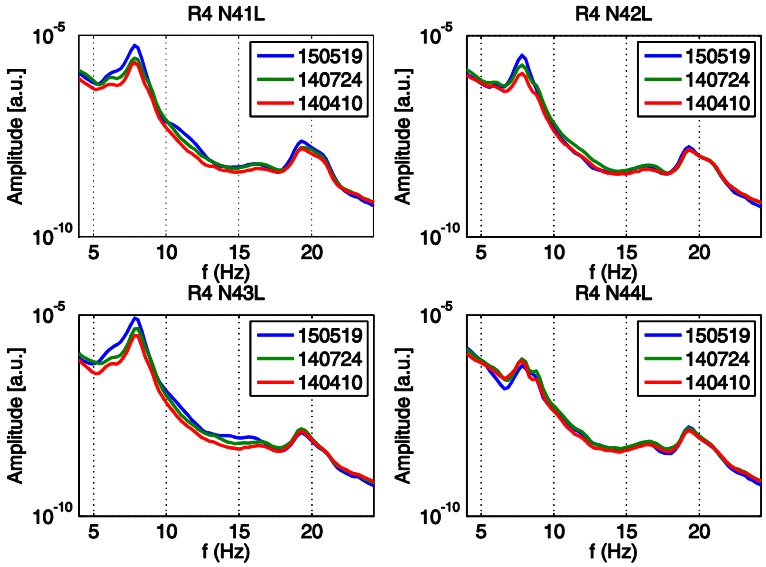

Fig. 15. Evolution of the APSDs of the lower ex-core detector measurements made in April, July 2014 and May 2015 in Ringhals-4.

N41U detector the APSD of the measured neutron noise shows a monotonous increase in the amplitude from April 2014 to May 2015. The same observation can be done for other detectors such as N43U/L, N42L and N41L. However, this is not the case for the rest of the detectors where non-monotonic behaviour with time can be conformed. This latter difference can be attributed to the different location of the detectors as well as anisotropy in the different vibration components including beam, shell and tilting modes. What regards the shell mode peak at 20 Hz, none of the solid conclusions about amplitude increase can be done since the spectra almost coincide with each other and do not show any common tendency in their behaviour.

3.4. The analysis of the titled and beam modes for 2015 measurements taken in Ringhals-4

In this section the results of the analysis of the titled mode for the measurements performed in on the 19th of May 2015 at Ringhals-4 are presented and discussed. Here, one should point out that since only one set of measurements was available for the analysis, there are no trend analysis of the amplitude during one fuel cycle was made. The analysis was made by separating the tilting mode, beam mode, reactivity and shell mode components, from the eight ex-core detectors, according to the description given in the previous section, and qualitatively analyzing the corresponding peak amplitudes. Some illustrations of the mode separation for the upper and lower detectors are shown below in *Fig. 17- Fig. 16*, respectively.

From the analysis of the APSDs presented in *Fig. 17- Fig. 16* the following interesting features can be pointed out what regards the behaviour of different modes of vibration:

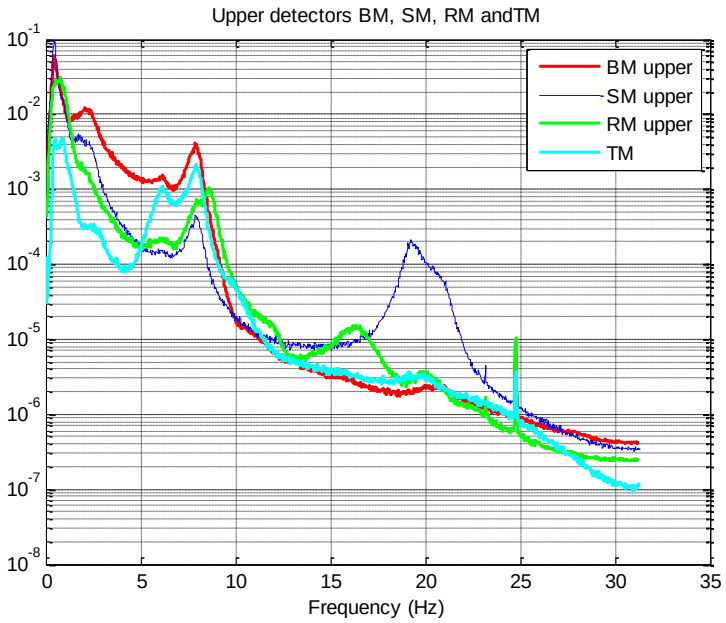

Fig. 17 APSDs of beam, shell, reactivity (upper detectors) and tilting modes extracted from the measurements taken at Ringhals 4 in May 2015, respectively .

- It can be clearly noticed that the amplitude of the tilting mode contains two

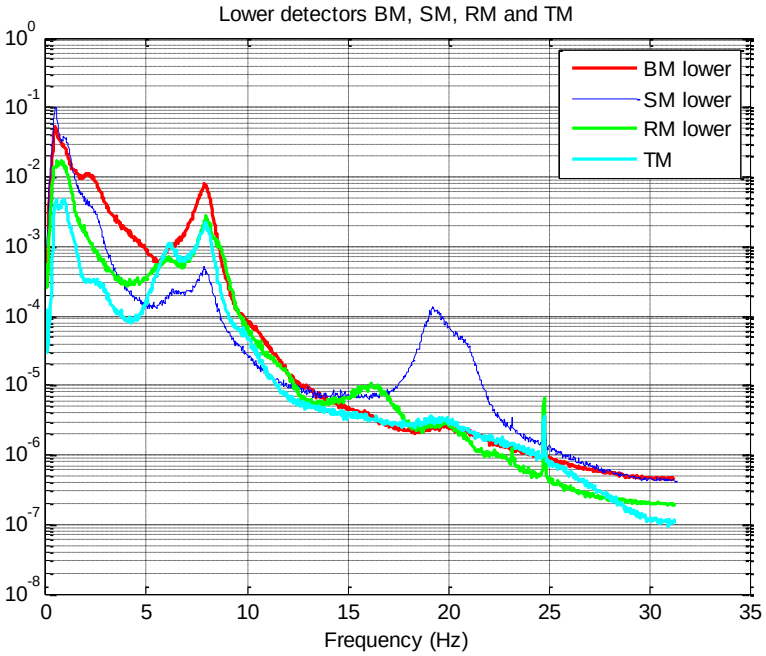

Fig. 16 APSDs of beam, shell, reactivity (lower detectors) and tilting modes extracted from the measurements taken at Ringhals 4 in May 2015, respectively .

distinct peaks; one - at 6 Hz and another one - at 8 Hz corresponding to the beam mode region.

- The amplitude of the beam mode is larger than that of the 6 Hz peak as it can be confirmed from *Fig. 18* where the titled mode was plotted separately for better visibility.

Further in *Fig. 19-Fig. 21* the comparison between the CPSDs calculated for the

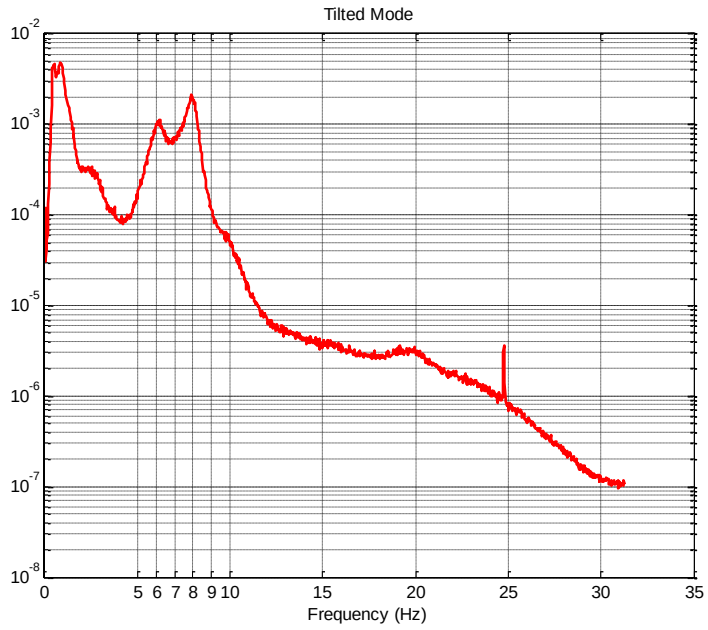

Fig. 18 APSDs of tilting modes extracted from the measurement taken at Ringhals 4 in May 2015.

tilting mode detector signal pairs and those for the beam mode detector signal pairs are shown. The detectors laying on the same diagonal but located at different spatial positions (axially and radially) are referred to as the tilting mode detector pairs. These are N41U-N42L, N42U-N42L, N43U-N44L and N44U-N43L. The beam mode detector pairs are defined as the ones placed at the same axial level but radially opposite to each other. These are N41U-N42U, N43U-N44U, N41L-N42L, and N43L-N44L.

As one can see from *Fig. 19-Fig. 20*, in the frequency range of the first peak of the APSD of the tilting mode component, the coherence has a sink observed in all tilting detector signal pairs (but only in one beam mode detector signal pair). This sink is due to a small shift in the phase. This sink can also be seen in the amplitude of the CPSD calculated between two detectors sitting at the same radial position but at different axial levels. (see *Fig. 21*).

In the corresponding literature, one can also find similar examples where such sinks were also observed in other measurements. For example, in [8] by Kosaly there is one example of such a behaviour of the CPSD calculated between cross-diagonal detector

signals that shows both in phase and out of phase behaviour. According to [8] the coherence can become low if the spectra of the in-phase and out-of-phase processes are approximately equal. In fact, this is not the true zero coherence from the physical point of view but rather from a mathematical one.

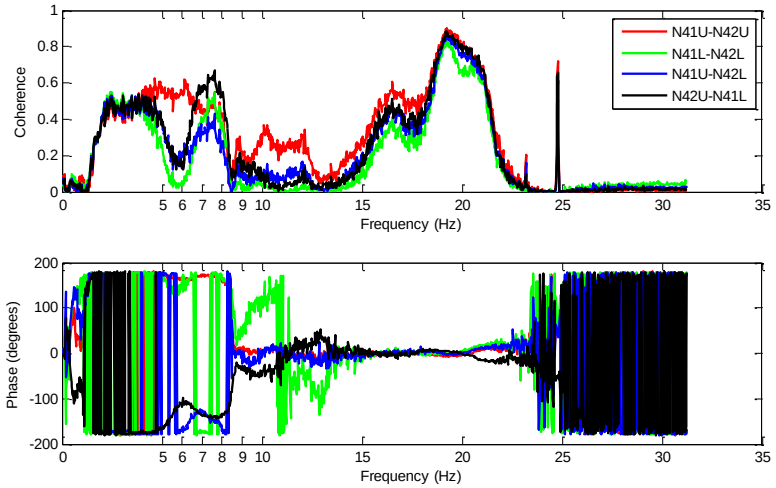

Fig. 19 The amplitude and the phase of the CPSD calculated for N41U-N42L, N42U-N42L, N43U-N44L and N44U-N43L detector pairs.

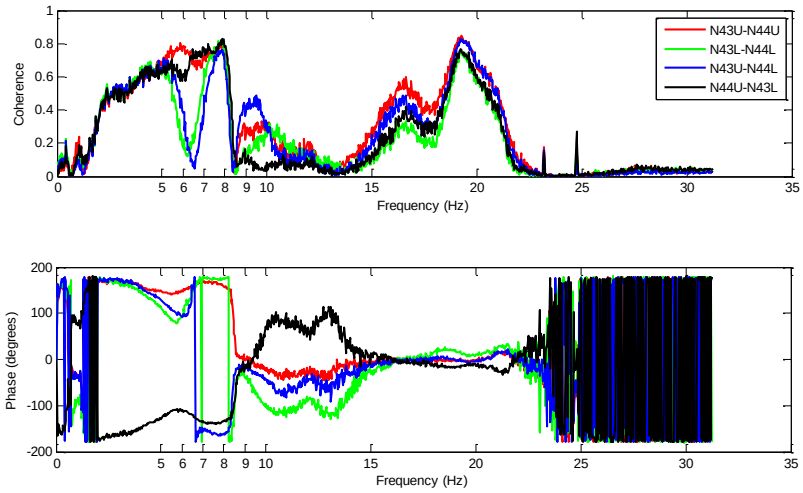

Fig. 20 The amplitude and the phase of the CPSD calculated for N41U-N42U, N43U-N44U, N41L-N42L, and N43L-N44L detector pairs.

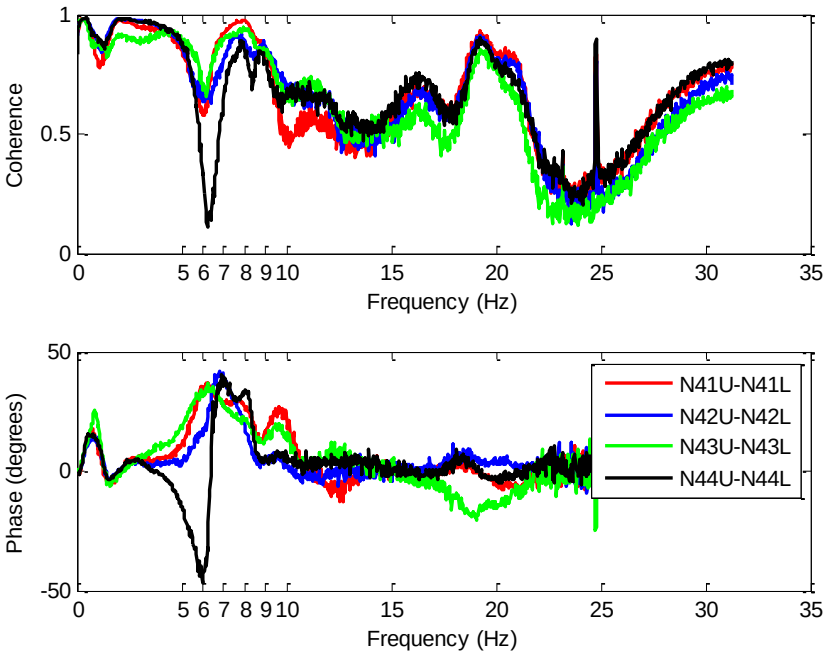

Fig. 21 The amplitude and the phase of the CPSD calculated for axially opposite N41U-N41L, N42U-N42L, N43U-N43L, and N44U-N44L detector pairs.

3.5. Conclusions

As it has been mentioned in the introduction the analysis of the 2015 measurements at Ringhals-4 after the power uprate by 18.6 %presented in this section has been performed along two lines.

First, the visual inspection of the APSDs of each individual ex-core detector signal has been performed and compared with the corresponding results from 2014 in order to identify any changes in the spectra caused by the power uprate. This analysis shows that the spectra from 2014 and 2015 are almost identical with a slight increase of the amplitude observed for some of the detectors. In addition, no new peaks have been detected.

The second point was dedicated to the extraction and the analysis of the titled mode. The analysis of the 2015 measurements has not brought any new results as compared to similar analysis made for 2014 measurements. Similarly to the case of 2014 data, two distinct peaks (at 6 and 8 Hz, respectively) were observed in the tilting mode spectra where the lower one was associated with beam mode and the upper one with titled mode. The amplitude of the former was larger then that of the latter one. Once again, sinks in the CPSDs calculated the detector pairs corresponding to different mode components (so-called beam mode detector pair and titled mode detector pairs) have been detected and probably caused by the interference between in-phase and out of phase components.

4. INVESTIGATION OF THE CORRECTNESS OF THE HYPOTHESIS THAT THE REACTIVITY COMPONENT EXTRACTED FROM THE EX-CORE DETECTOR SIGNALS CAN BE DUE TO FUEL ASSEMBLY VIBRATIONS WITH CORE SIM.

4.1. Introduction

Several attempts in the past [13] -[18] have been undertaken in order to explain the presence and the amplitude increase of a double peak around the frequency of the Beam Mode (BM) of the Core Barrel Motion (CBM) (7-8 Hz) which was for the first time observed in 1991 in the Auto Power Spectral Density (APSD) of the ex-core detector measurements taken at Ringhals 4. By analyzing both in-core and ex-core measurements and by studying the development of the amplitudes of the two peaks around 7-8 Hz separately within one reactor cycle, a hypothesis about the origin of two peaks was formulated.

The hypothesis suggests that the double peak corresponds to two vibration modes with different physical origins: the one, around 7 Hz is related to the core barrel motion itself, whereas another one, around 8 Hz, corresponds to flow induced vibrations of single fuel assemblies. The increase of the corresponding peak of the measured APSD can be due either to the amplitude increase of the fuel assembly vibrations, or to the change of the conversion factor between mechanical vibrations of fuel assemblies and the induced neutron noise, as measured by ex-core detectors. This latter possibility was studied recently [20]-[21] but the results obtained were not fully conclusive.

Several other attempts have been made in order to confirm the hypothesis by repeated measurements using advanced curve-fitting procedure to analyze the properties of the spectra but no success had been achieved [13]-[17]. In 2013 [18], another approach for studying these peaks was suggested where a new method for separating two peaks by manipulating different detector signals and using their symmetry was developed and implemented with positive outcome. In this approach, it is assumed that the beam mode component of the core barrel vibrations does not have any reactivity component. On the other hand the effect of the fuel assembly vibrations induces only the reactivity noise whereas the space-dependent component of the noise is assumed to be negligible. This latter assumption about the space-dependent component of the neutron noise can also be justified by the fact the flux measurements are performed by ex-core neutron detectors which are usually located outside of the reactor core and thus far away from the noise source itself (assuming that the noise source i.e. the vibrating fuel assembly is located at the centre part of the core but not at the periphery). In such a case, it is natural to assume that the amplitude of the space dependent noise due to fuel assembly vibrations which actually reaches the ex-core detector will be small enough due to the spatial relaxation of the flux and thus can be neglected. Such an assumption is an intuitive one and should be

confirmed or disproved by some numerical simulations which are an ultimate goal of this study.

In the previous work [20]-[21], a study was performed on calculating the ex-core noise by fuel assembly vibrations by the use of the dynamic core simulator CORE SIM [22], in order to see if the scaling factor between mechanical vibrations and the normalised detector current increases during the cycle. The same CORE SIM model to investigate the correctness of the hypothesis that the neutron noise induced by fuel assembly vibrations and measured by the ex-core detectors is associated primarily with the reactivity noise is also adopted in the present study.

For this purpose, the neutron noise in four selected ex-core detectors at the same axial level are calculated, and there reactivity effect is thereafter extracted by means of the same signal analysis method as the one used in the actual experiments [18]-[19]. On the other hand, the exact reactivity effect of the vibrations can also be calculated directly by CORE SIM. In possession of the symmetry properties one then test whether this component can also be obtained approximately by a signal addition and subtraction method from the measured signals. In addition, one could also calculate the space dependent component of the induced neutron noise by subtracting the reactivity component from the total noise, and its symmetries could be investigated. As a result, such a study could give a useful justification of the assumptions made for the newly-developed separation method used to confirm the hypothesis on the physical origin of the peaks in the measured spectra.

4.2. Calculation of the neutron noise due to fuel assembly vibrations

The methodology used to simulate the flux fluctuations induced by fuel assembly vibrations was adopted from [20]-[21]. There two-dimensional vibrations of selected fuel assembles were modelled with the help of neutronic numerical tool CORESIM.

The calculation are based on the data of Ringhas-3 PWR, cycle 15.To evaluate the detector signals, the ex-core detectors are placed in the reflector region and the corresponding response is recorded. The reactivity component is also calculated from the total noise by performing a convolution integral in space with the pre calculated adjoint solution. The results are then compared against each other.

4.2.1. The two-group neutron noise equations solved by CORE SIM.

CORE SIM represents two-energy group diffusion MATLAB-based core simulator providing both the static and dynamic solutions for commercial Light Water Reactors with rectangular mesh [22]. The dynamic solution is obtained in space-frequency domain and is based on the application of first order perturbation theory, i.e. splitting all the quantities into their mean values and fluctuating parts, subtracting the static equations, performing a Fourier transform and neglecting second order terms. As an input, the static cross-sections together with kinetic and geometrical core data, as well as the distribution of noise source should be provided. Below we give a brief reminder of the dynamic equations solved by CORE SIM. The first order noise equations in generic form can be written as

$$\left[\nabla \overline{\overline{D}}(\mathbf{r}) \nabla + \overline{\overline{\Sigma}}_{dyn}(\mathbf{r},\omega) \right] \times \begin{bmatrix} \delta\phi_1(\mathbf{r},\omega) \\ \delta\phi_2(\mathbf{r},\omega) \end{bmatrix} = \begin{bmatrix} S_1(\mathbf{r},\omega) \\ S_2(\mathbf{r},\omega) \end{bmatrix} \tag{31}$$

where

$$\overline{\overline{D}}(\mathbf{r}) = \begin{bmatrix} D_1(\mathbf{r}) & 0 \\ 0 & D_2(\mathbf{r}) \end{bmatrix}, \tag{32}$$

$$\overline{\overline{\Sigma}}_{dyn}(\mathbf{r},\omega) = \begin{bmatrix} -\Sigma_1(\mathbf{r},\omega) & \nu\Sigma_{f2}(\mathbf{r},\omega) \\ \Sigma_{rem}(\mathbf{r}) & -\Sigma_{a2}(\mathbf{r},\omega) \end{bmatrix}, \tag{33}$$

$$\Sigma_1(\mathbf{r},\omega) = \Sigma_{a1}(\mathbf{r},\omega) + \Sigma_{rem}(\mathbf{r}) - \nu\Sigma_{f1}(\mathbf{r},\omega), \tag{34}$$

$$\nu\Sigma_{f1,2}(\mathbf{r},\omega) = \frac{\nu\Sigma_{f1,2}(\mathbf{r})}{k_{eff}} \left(1 - \frac{i\omega\beta_{eff}}{i\omega + \lambda} \right), \tag{35}$$

$$\Sigma_{a1,2}(\mathbf{r},\omega) = \Sigma_{a1,2}(\mathbf{r}) + \frac{i\omega}{\upsilon_{1,2}}. \tag{36}$$

The r.h.s vector in Eq. (31) represents the noise source in the fast and thermal groups. The noise source can be modelled through the fluctuations of macroscopic cross-sections as a result of mechanical or thermal processes in the core, and is written as follows:

$$\begin{bmatrix} S_1(\mathbf{r},\omega) \\ S_2(\mathbf{r},\omega) \end{bmatrix} = \underline{\phi}_{rem}(\mathbf{r}) \delta\Sigma_{rem}(\mathbf{r}) + \overline{\overline{\phi}}_a(\mathbf{r}) \begin{bmatrix} \delta\Sigma_{a1}(\mathbf{r},\omega) \\ \delta\Sigma_{a2}(\mathbf{r},\omega) \end{bmatrix} + \overline{\overline{\phi}}_f(\mathbf{r}) \begin{bmatrix} \delta\nu\Sigma_{f1}(\mathbf{r},\omega) \\ \delta\nu\Sigma_{f2}(\mathbf{r},\omega) \end{bmatrix} \tag{37}$$

where the δX_i , i = $\{rem,\ a_1,\ a_2\}$ etc. stand for the fluctuations of the macroscopic cross sections, corresponding to the actual perturbation (in this case to the fuel assembly movement), and further:

$$\underline{\phi}_{rem}(\mathbf{r}) = \begin{bmatrix} \phi_1(\mathbf{r}) \\ -\phi_1(\mathbf{r}) \end{bmatrix}, \tag{38}$$

$$\overline{\overline{\phi}}_a(\mathbf{r}) = \begin{bmatrix} \phi_1(\mathbf{r}) & 0 \\ 0 & \phi_2(\mathbf{r}) \end{bmatrix}, \tag{39}$$

and

$$\overline{\overline{\phi}}_f(\mathbf{r}) = \begin{bmatrix} \phi_1(\mathbf{r}) & -\phi_2(\mathbf{r}) \\ 0 & 0 \end{bmatrix}. \tag{40}$$

The rest notations in the above equations have their usual meaning. After the discretisation with a finite difference method, equation (31) reads in the following matrix form:

$$\overline{\overline{M}}_{dyn} \times \delta\bar{\phi} = \bar{S}, \tag{41}$$

where $\delta\bar{\phi}$ is a vector containing the noise in both the fast and thermal energy groups and $\delta\bar{S}$ designates the noise source vector.

In the above, the noise source represents the perturbation of the cross-sections caused by various technological processes in the core, such as core barrel vibrations, fuel assembly vibrations and so on.

The vibrating fuel assembly, whose characteristic size is much smaller than the core size can be modelled as follows Assuming that the vibrations occur with the same amplitude at each axial level, the axial dependence of the noise can be factorized and thus disregarded. As a result, the problem can be considered as two-dimensional. When the fuel assembly vibrates, it moves on a two-dimensional stochastic trajectory around the equilibrium position such that its momentary position is given by $\mathbf{r}_p + \bar{\varepsilon}(t)$, where $\left|\bar{\varepsilon}(t)\right| \ll R$ and R is the core radius. Utilizing the smallness of the fuel assembly as compared to the core size, it can be modelled as a delta function. Thus, the perturbation of the cross sections caused by the fuel assembly vibrations can be given as

$$\delta X S(\mathbf{r}, t) = \gamma \quad \delta(\mathbf{r} - \mathbf{r}_p - \bar{\varepsilon}(t)) - \delta(\mathbf{r} - \mathbf{r}_p) \tag{42}$$

where γ is the so-called Galanin constant, describing the strength of a localized absorber, or the fuel assembly, and $\mathbf{r}_p$ is its equilibrium position around which it vibrates according to the time dependent displacement vector function $\bar{\varepsilon}(t) = \quad \varepsilon_x(t), \varepsilon_y(t)$.

Further, using the first order of Taylor expansion of the displacement function, after a temporal Fourier transform, Eq. (42) $\delta X S(\mathbf{r}, t)$ in the frequency domain reads as:

$$\delta X S(\mathbf{r}, \omega) = \gamma\bar{\varepsilon}(\omega)\nabla_{\mathbf{r}_p} \delta(\mathbf{r} - \mathbf{r}_p) \tag{43}$$

4.2.2. Calculation of the noise due to fuel assembly vibrations

Eq. (41) can be solved by using a well-known Green's function technique which allows calculating the space- and frequency dependent noise induced by any noise source once the Green's function is known, i.e. the Green function is solved only once for all cases for a given system. This technique has been used widely in analytical solutions for homogeneous systems, and numerically in heterogeneous systems in the noise simulator [22]-[23]. The equation for the Green's function is similar to Eq. (41) except for the fact that the source on the right hand side is replaced with a Dirac delta function source. Thus for the Green's function one obtains:

$$\overline{\overline{M}}_{dyn} \times \overline{\overline{G}}^{\delta XS}(\mathbf{r}, \mathbf{r}_p, \omega) = \bar{\delta}_{XS}(\mathbf{r} - \mathbf{r}_p), \tag{44}$$

where in the case of two groups, the Green's matrix reads as $\overline{\overline{G}}^{\delta XS}(\mathbf{r},\mathbf{r}_p,\omega)$:

$$\overline{\overline{G}}^{\delta XS}(\mathbf{r},\mathbf{r}_p,\omega)=\begin{bmatrix} G_{1\leftarrow 1}(\mathbf{r},\mathbf{r}_p,\omega) & G_{1\leftarrow 2}(\mathbf{r},\mathbf{r}_p,\omega) \\ G_{2\leftarrow 1}(\mathbf{r},\mathbf{r}_p,\omega) & G_{2\leftarrow 2}(\mathbf{r},\mathbf{r}_p,\omega) \end{bmatrix}. \tag{45}$$

In the above $G_{g\leftarrow g'}(\mathbf{r},\mathbf{r}_p,\omega)$ stands for the noise source at point $\mathbf{r}$ in energy group g induce by a point-wise perturbation at position $\mathbf{r}_p$ in energy group g'. The neutron noise can then be calculated through the Green's function as follows:

$$\delta\overline{\phi}(\mathbf{r},\omega)=\int_{V_c}\overline{\overline{G}}^{\delta XS}(\mathbf{r},\mathbf{r}_p,\omega)\bullet S(\mathbf{r}_p,\omega)d\mathbf{r}_p. \tag{46}$$

where V_c stands for reactor core volume. Thus, for each noise source, the space-dependence of neutron noise can be determined through only solving equation (44). The Green's function has a potential use to simulate neutron noise induced by any kind of noise source or vibration without directly solving a specific equation with the noise source as the inhomogeneous part of the equations (such as, for example Eq. (41)) .

Finally, the neutron noise induced by the vibrating noise source reads as:

$$\delta\overline{\phi}(\mathbf{r},\omega)\equiv\begin{bmatrix}\delta\phi_1(\mathbf{r})\\ \delta\phi_2(\mathbf{r})\end{bmatrix}\overline{\gamma}(\omega)\nabla_{r_p}\left[\overline{\overline{G}}^{\delta XS}(\mathbf{r},\mathbf{r}_p,\omega)\bullet\overline{\phi}(\mathbf{r}_p)\right], \tag{47}$$

From the above, it can be seen that using Eq. (47) for noise calculation requires the calculation of the derivatives of the Green's function with respect to the second variable, i.e. with respect to the source coordinates $\mathbf{r}_p = x_p, y_p$ defining the equilibrium position of the vibrating source. Therefore, the application of Green's function in 2-D and 3-D models with a large number of meshes to calculate the neutron noise might become a complicated task.

4.2.3. Simulation of the noise source for the case of fuel assembly vibrations

After thorough analysis of the solution (47), it turns out that the direct application of Eq. (47) to calculate the noise induced by vibrating fuel assemblies might be complicated or even impossible in some cases. The main obstacle in utilizing Eq. (47) is related to the definition of a noise source, i.e. the fluctuations of the cross sections, which can only be changed one node at a time. In other words, any vibration could only be defined with a spatial resolution not smaller than the node size. Another possible problem refers to the calculation of the direct Green's function itself given by Eq.(44), where the inhomogeneous part can not be defined as a Dirac delta function, but rather as a step-function over one node.

There are two possibilities to overcome these problems. The one is to use the adjoint Greens function instead of the direct one. In the case of the adjoint equations the inhomogeneous part of the equation is defined by the detector cross sections both in energy and space (there is no any noise source which has to be defined) and the variables of the solution turn into the source coordinates instead. Hence the calculation of the noise induced by a vibrating localised component requires only getting an estimate of the dynamic adjoint, the static flux, and their spatial derivatives at the position of the vibrating component.

Yet another possibility is to solve the direct noise equations, but with a mesh which is finer than the node size, and to calculate the derivative of the Green's function by moving the inhomogeneous part of the equation with one mesh. Such a method which is utilized in the present study can easily be applied for one dimensional system, whereas for higher dimensions using a finer mesh it might lead to excessive memory problems and running times. In order to simulate the vibration with a realistically small displacement (in the sub-millimetre range) while avoiding a large number of meshes (and thus memory and calculation time problems), the spatial discretisation was re-organised for the vibrating assembly by adding a very fine mesh around its border while keeping the same mesh size for all other assemblies. The size of the additional meshes could be defined as small as the amplitude of the displacement. Such an approach can easily be applied in 2D simulation, where a very small displacement from vibrations can be simulated while the total number of meshes does not increase appreciably, and therefore no significant numerical difficulty arises from the increase of different mesh sizes.

Further, there is also a third alternative which does not even require any calculation of the derivative of the flux and the Green's function. This third method has already been described and utilized earlier in the report for modelling three dimensional fuel assembly vibrations in Section. Here, we just give a brief reminder about the main principles of the method. In this method while modelling the vibrating component (i.e. a vibrating fuel assembly), it is assumed that the assembly has a finite width which is much larger than the vibration amplitude itself. Such an assumption leads to the possibility to represent the assembly vibrations as two point-wise absorbers of variable strength, separated by the width of the absorber and with strength oscillating in opposite phase. The noise induced by a variable strength absorber can then easily be modelled with a delta function point source.

In the present study, the two-dimensional fuel vibration is modelled as the displacement of fuel rod and water through a source defined via the difference of the cross sections between fuel rod and water. The magnitude of the difference of the cross sections is calculated and then located around the vibrating assembly. What regards the fuel assembly displacement, it is set to 0.1 mm which is considered close to the realistic displacement amplitude. In the present work, the pendulum vibration of the fuel assemblies was assumed so that the numerical simulation could be simplified in a 2D model.

Yet another interesting point which is worth to mention here prior to the simulation of fuel assembly vibrations, is related to the fact that the vibration of the fuel assembly by

nature is a random process. Therefore, in the actual measurements we obtained the signals induced by a random process of vibration, i.e. there is no preferable direction of the vibration. However, in the simulation one cannot really model such a random process. Instead, one has to first specify the vibrating direction in order to determine the noise source and then construct Eq. (47). In the present simulations, in order to overcome this problem we simply consider a simpler case of mono-directional vibrations i.e. assume that the vibrating direction is either in x-direction or y-direction. Actually it could be interesting to investigate both two directions since the two vibrations are usually not symmetrical for all assembly locations. Each vibration will induce different noise properties of the ex-core detectors. The case will postpone to the later studies.

Finally, one should also mention here that depending on the size of the fuel assembly vibrations, one can classify two types of fuel assembly vibrations. The first one is when displacement of the vibrating assembly is within its own location (roughly 1 mm, no impacting), i.e. the vibration of fuel material does not overlap with the neighbouring assemblies. In this case the vibrations of individual fuel assemblies do not require collective motion of the neighbouring assemblies. The second possibility is when the displacement of the vibrating assembly overlaps the location of the neighbouring assemblies (roughly 4 mm, with impacting). In reality, this model assumes the collective vibrations of neighbouring fuel assemblies. From a practical point of view the first case appears to be more realistic rather than the second one. Moreover the first model gives the results which are more consistent with the experimental observations. Therefore in the present study only the first case is considered.

4.2.4. Reactivity component

In order to investigate the contribution of the reactivity component into the total induced noise, the point-kinetic term should also be known. The reactivity component of the frequency dependent neutron noise can be written in the following standard form:

$$\delta\phi_{1,2}^{pk}(\mathbf{r},\omega) = \frac{\delta P(\omega)}{P_0}\phi_{1,2}(\mathbf{r}) \tag{48}$$

where the fluctuation of the amplitude factor $\delta P(\omega)$ is calculated using the orthogonality property between the neutron noise $\delta\bar{\phi}(\mathbf{r},\omega) = \begin{bmatrix} \delta\phi_1(\mathbf{r},\omega) \\ \delta\phi_2(\mathbf{r},\omega) \end{bmatrix}$ and the static adjoint solution $\bar{\phi}^{\dagger}(\mathbf{r}) = \begin{bmatrix} \phi_1^{\dagger}(\mathbf{r}) \\ \phi_2^{\dagger}(\mathbf{r}) \end{bmatrix}$ and thus for the case of two energy group reads as:

$$\frac{\delta P(\omega)}{P_0} = \frac{\int_{V_c}\left[\frac{1}{\upsilon_1}\phi_1^{\dagger}(\mathbf{r})\delta\phi_1(\mathbf{r},\omega) + \frac{1}{\upsilon_2}\phi_2^{\dagger}(\mathbf{r})\delta\phi_2(\mathbf{r},\omega)\right]d\mathbf{r}}{\int_{V_c}\left[\frac{1}{\upsilon_1}\phi_1^{\dagger}(\mathbf{r})\phi_1(\mathbf{r}) + \frac{1}{\upsilon_2}\phi_2^{\dagger}(\mathbf{r})\phi_2(\mathbf{r})\right]d\mathbf{r}} \tag{49}$$

where υ_i , $i = 1,2$ stands for neutron velocity in the fast and thermal energy group, respectively.

4.2.5. Calculation procedure

Numerical calculations for investigating the possibility to reproduce the reactivity component of the neutron noise induced by the vibrations of fuel assemblies from four ex-core detector signals, have been performed based on the Ringhals-3 PWR core at cycle 15, using the 2D neutron noise simulator CORE SIM. The core configuration with four ex-core detectors, assumed to be located at the outer periphery of the reflector, is illustrated in *Fig. 22*.

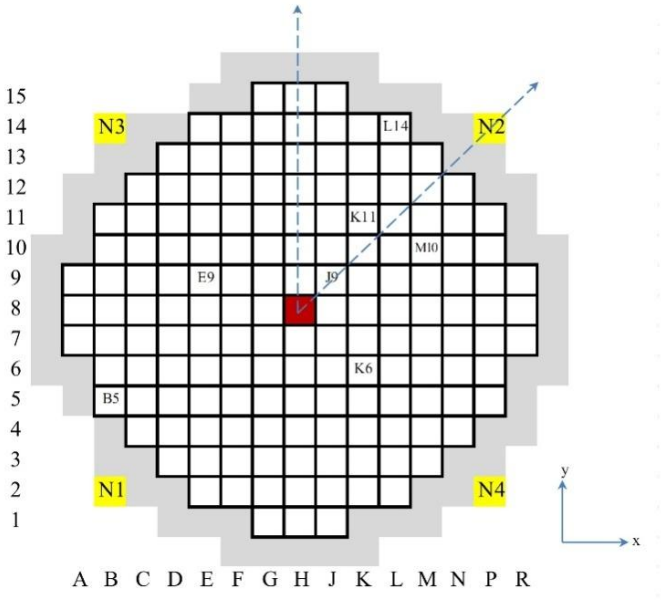

Fig. 22 Configuration of the Ringhals-3 PWR.

The calculations have been performed for the core at the middle of cycle (MOC), with dynamic parameters as given in **Table 3**. As a final result of the simulations with CORE SIM, the fast and thermal neutron space-frequency dependent flux distributions in the core have been obtained.

Table 3 Kinetic parameters for Ringhals-3 core, cycle 15.

k_{eff}	β_{eff} (pcm)	λ (1/s)	v_1 (cm/s)	v_2 (cm/s)
1:001699	551.1	0.087121	1.81783×10^7	4.13994×10^5

As it was mentioned earlier, in the present study only the pendular vibrations of fuel assemblies are of interest and thus were simulated in a 2D two-group model. In such a case the group constants and kinetic parameters for a 2D model should be provided. The input parameters for CORE SIM i.e. the cross sections and the kinetic parameters were generated by SIMULATE-3. Since SIMULATE-3 provides two-group cross sections in 3D representation, to obtain these data in 2D, the 3D cross section data have to be collapsed into a 2D data set. The data collapsing was carried out using the static fluxes from CORE SIM as weighting functions and preserving the axial neutron leakage. Then, the dynamic calculations were performed for the space and frequency-dependent noise induced by vibrating fuel assemblies, and the ex-core noise was investigated. The corresponding model for the noise source caused by vibrating fuel assemblies have already been described and discussed earlier in the previous subsections.

In the numerical simulation of the vibrations, the direct (forward) Green's function was used by having the perturbation (fluctuations of the cross sections) as the inhomogeneous part of the equation.

The main purpose is to investigate the possibility to reproduce the behaviour of the reactivity component from the total neutron noise induced by fuel assembly vibration by using four ex-core detector signals and compare the result with the exact reactivity component. For this purpose, the total noise induced by the vibrations of a fuel assembly have been calculated by solving Eq. (41) via Eqs (44) and (47) in CORE SIM for four selected radial positions of the ex-core detector. The locations of the ex-core detectors correspond to those encountered in a real Ringhals-3 reactor core and shown in *Fig. 22* (N1, N2, N3, N4 corresponding to N41 N42 N43 and N44 in the Ringhals-3 core). The simulations were performed for three different location of the vibrating fuel assembly: i.e. for the central fuel assembly, the fuel assembly at the periphery and the fuel assembly located in between (at the middle). Thereafter for each case studied, the reactivity component of the induced noise has been evaluated by summing up the normalized (to the static flux) signals from all 4 ex-core detectors. At the same time, the point-kinetic component has been calculated in exact manner from Eq. (49). Both results have been compared in terms of relative noise , i.e. $\left|\frac{\delta\phi_2}{\phi_2}\right|$ as well as the qualitative analysis of their time evolutions within a fuel cycle (i.e. BOC, MOC and EOC) have been performed. In addition the contribution of the space dependent component have been also evaluated by subtracting the reactivity component from the total noise and thereafter analyzed. What regards the preferable direction of the vibration, the direction along x-axis has been selected (see *Fig. 22*).

4.3. Preliminary results and discussion

Here we will present some results of the ex-core neutron noise induced by fuel assembly vibrations modelled in CORE SIM simulator. Due to the geometrical symmetry of the core, we focus only on the vibration of the fuel assemblies located in one octant of

the core located close to detector N2. The core layout of the Ringhals-3 PWR core which was used in the simulations together with ex-core detector locations have already been demonstrated earlier and can be recovered from *Fig. 22* . The results of the performed calculations are summarized in **Table 4-18** and will be discussed in more details below.

Table 4, 6 and 8 show the amplitude and the phase of simulated total neutron noise (both in the fast and thermal energy groups) for each of four ex-core detectors (N1, N2, N3 and N4) induced by the directional vibration of fuel assemblies along x axes. For the convenience of further analysis, some additional data such as the frequency of vibrations, location of the vibrating fuel assembly and the direction of vibrations are also pointed out in those tables. The calculations were performed at the frequency of 8 Hz corresponding to the vibration frequency of fuel assemblies observed earlier in the measurements [14]. A number of fuel assemblies have been selected, which can be classified into three groups depending on their locations: in the core centre (fuel assembly J9), in the middle of the core radius (fuel assembly K11) or at the periphery of the core (fuel assembly L14).

Further, in **Table 5, 7, 9**, the amplitude and the phase of the reactivity and space-dependent components of the corresponding neutron noise (both fast and thermal) due to fuel assembly vibrations are given. The relative weights between two components (the reactivity and the space-dependent) are also summarized in these tables.

Finally, in Error! Reference source not found. , the results for the point-kinetic component of the neutron noise are shown. For comparison purpose, the point kinetic component has been calculated in two ways. In the first case, the point kinetic component has been evaluated from four ex-core detector signals by averaging them aver the reactor core. At the same time, the reactivity component has been calculated in an exact manner via adjoint solution (see Eq. (49)).

From the results above, one can notice that the contribution of the reactivity component to the total noise is significant in the vibrations of most of fuel assemblies. For the fuel assemblies located at the periphery region which are closer to the detector N2 and would dominate the detector response, the reactivity component contribution in the detector response is generally greater than 30% of the total noise. This confirms the assumption that the reactivity noise is significant in the vibration of the fuel assembly, but it would not generally dominate the ex-core detector noise. More comprehensive quantitative results and discussion will be performed in the continuation.

Here, one should notice that the calculations have been performed for both fast and thermal noise. The reason for this is that in the present simulation with CORE SIM there is no possibility to model ex-core detector signals in exact manner. Ex-core detector signals in an actual PWR core are usually located roughly a half meter away from the core periphery. This part of the core is not and can not be modelled in the CORE SIM based on the diffusion theory. Instead some other techniques such as Monte Carlo simulations should be used. However, as a first approximation one can assume that the largest contrition in the detector response comes only from the fast noise at the boundaries which leaves a reactor core and then being thermalized. In such a case the contribution of the

thermal noise will very small due to the faster relaxation length as compared to that of fast neutrons. Therefore, in the recent analysis the main focus is mostly made on the noise induced in the fast group.

All the results presented so far were given for the beginning of a fuel cycle. Further in **Table 10-18,** the results for the point kinetic component calculated both from ex-core detector signals and in an exact manner from the total noise are given for the BOC, MOC and EOC. These results are given both for the fast and thermal noise as well as for the normalized and non-normalized (to the static flux) quantities. To simplify the analysis of the above mentioned results, in *Fig. 23-Fig. 25* the time evolution within a fuel cycle of the point kinetic components (the exact one and the one obtained from detector signals) is plotted for three different locations of the fuel assembly. As one can see from these results, the more or less correct prediction of the point kinetic behaviour for ex-core detectors is obtained only for the fuel assembly at the periphery of the core. In the other two cases, the predicted behaviour of the point kinetic component within a fuel cycle is not monotonic and does not follow the true behaviour.

Table 4 Total ex-core normalized neutron noise induced by a vibrating fuel assembly (FA J9, BOC)

Det	Region	Vibrating fuel assembly	Direction of vibration	Freq [Hz]	Total fast noise $\delta\phi_{1}^{N_i,tot}$ [a.u.]		Total thermal noise $\delta\phi_{2}^{N_i,tot}$ [a.u.]	
					Amplitude	Phase	Amplitude	Phase
N1	Core centre	J9	x	8	$2.93\cdot10^{-5}$	-0.18	$2.56\cdot10^{-5}$	-0.16
N2	Core centre	J9	x	8	$1.78\cdot10^{-5}$	-3.03	$1.88\cdot10^{-5}$	-3.08
N3	Core centre	J9	x	8	$6.36\cdot10^{-6}$	-2.84	$7.15\cdot10^{-6}$	-2.99
N4	Core centre	J9	x	8	$4.85\cdot10^{-5}$	-0.14	$4.37\cdot10^{-5}$	-0.12

Table 5 Space-dependent component calculated from ex-core normalized neutron noise induced by a vibrating fuel assembly (FA J9, BOC)

Det	Fast space-dependent noise $\delta\phi_{1,exact}^{N_i,sd}$ [a.u.]	Thermal space-dependent noise $\delta\phi_{2,exact}^{N_i,sd}$ [a.u.]	Rel. fast noise $\frac{\delta\phi_{1,exact}^{N_i,sd}}{\delta\phi_{1,exact}^{N_i,pk}}$ [a.u.]	Rel. therm. noise $\frac{\delta\phi_{2,exact}^{N_i,sd}}{\delta\phi_{2,exact}^{N_i,pk}}$ [a.u.]

	Amplitude	Phase	Amplitude	Phase	Amplitude	Amplitude
N1	$6.68 \cdot 10^{-6}$	-0.16	$5.89 \cdot 10^{-6}$	-0.17	0.30	0.29
N2	$4.00 \cdot 10^{-5}$	3.09	$3.83 \cdot 10^{-5}$	3.09	1.77	1.94
N3	$2.84 \cdot 10^{-5}$	3.06	$2.66 \cdot 10^{-5}$	3.06	1.25	1.35
N4	$2.59 \cdot 10^{-5}$	-0.09	$2.40 \cdot 10^{-5}$	-0.09	1.14	1.22

Table 6 Total ex-core normalized neutron noise induced by a vibrating fuel assembly (FA K11, BOC)

Det	Region	Vibrating fuel assembly	Direction of vibration	Freq [Hz]	Total fast noise [a.u.]		Total thermal noise [a.u.]	
					Amplitude	Phase	Amplitude	Phase
N1	Middle of core	K11	x	8	$1.01 \cdot 10^{-5}$	-0.23	$8.56 \cdot 10^{-6}$	-0.20
N2	Middle of core	K11	x	8	$6.33 \cdot 10^{-5}$	-3.13	$6.32 \cdot 10^{-5}$	-3.14
N3	Middle of core	K11	x	8	$1.52 \cdot 10^{-6}$	-2.45	$1.77 \cdot 10^{-6}$	-2.81
N4	Middle of core	K11	x	8	$2.94 \cdot 10^{-5}$	-0.13	$2.67 \cdot 10^{-5}$	-0.12

Table 7 Space-dependent component calculated from ex-core normalized neutron noise induced by a vibrating fuel assembly (FA K11, BOC)

Det	Fast space-dependent noise $\delta\phi^{N_i,sd}_{1,exact}$ [a.u.]		Thermal space-dependent noise $\delta\phi^{N_i,sd}_{2,exact}$ [a.u.]		Rel. fast noise $\frac{\delta\phi^{N_i,sd}_{1,exact}}{\delta\phi^{N_i,pk}_{1,exact}}$ [a.u.]	Rel. therm. noise $\frac{\delta\phi^{N_i,sd}_{2,exact}}{\delta\phi^{N_i,pk}_{2,exact}}$ [a.u.]
	Amplitude	Phase	Amplitude	Phase	Amplitude	Amplitude
N1	$1.53 \cdot 10^{-6}$	-3.07	$1.61 \cdot 10^{-6}$	-3.07	0.13	0.16
N2	$7.47 \cdot 10^{-5}$	-3.17	$7.32 \cdot 10^{-5}$	-3.17	6.44	7.23

N3	$1.26 \cdot 10^{-5}$	-3.23	$1.17 \cdot 10^{-5}$	-3.23	1.09	1.16
N4	$1.78 \cdot 10^{-5}$	-0.09	$1.66 \cdot 10^{-5}$	-0.09	1.54	1.64

Table 8 Total ex-core normalized neutron noise induced by a vibrating fuel assembly (FA L14, BOC)

Det	Region	Vibrating fuel assembly	Direction of vibration	Freq [Hz]	Total fast noise [a.u.]		Total thermal noise [a.u.]	
					Amplitude	Phase	Amplitude	Phase
N1	Periph. of core	L14	x	8	$2.58 \cdot 10^{-5}$	-0.31	$6.20 \cdot 10^{-6}$	-0.29
N2	Periph. of core	L14	x	8	$3.73 \cdot 10^{-5}$	-2.81	$3.33 \cdot 10^{-5}$	-0.11
N3	Periph. of core	L14	x	8	$2.60 \cdot 10^{-6}$	-0.31	$7.64 \cdot 10^{-6}$	-0.26
N4	Periph. of core	L14	x	8	$5.94 \cdot 10^{-5}$	-0.19	$1.53 \cdot 10^{-5}$	-0.18

Table 9 Space-dependent component calculated from ex-core normalized neutron noise induced by a vibrating fuel assembly (FA L14, BOC)

Det	Fast space-dependent noise $\delta\phi^{N_i,sd}_{1,exact}$ [a.u.]		Thermal space-dependent noise $\delta\phi^{N_i,sd}_{2,exact}$ [a.u.]		Rel. fast noise $\frac{\delta\phi^{N_i,sd}_{1,exact}}{\delta\phi^{N_i,pk}_{1,exact}}$ [a.u.]	Rel. therm. noise $\frac{\delta\phi^{N_i,sd}_{2,exact}}{\delta\phi^{N_i,pk}_{2,exact}}$ [a.u.]
	Amplitude	Phase	Amplitude	Phase	Amplitude	Amplitude
N1	$2.78 \cdot 10^{-5}$	-3.21	$9.10 \cdot 10^{-6}$	-3.21	0.52	0.60
N2	$8.75 \cdot 10^{-5}$	-3.12	$1.81 \cdot 10^{-5}$	-0.06	1.65	1.19
N3	$2.76 \cdot 10^{-5}$	-3.20	$7.66 \cdot 10^{-6}$	-3.20	0.52	0.50
N4	$6.21 \cdot 10^{-6}$	-0.23	$3.04 \cdot 10^{-7}$	-1.34	0.12	0.02

Table 10 Point kinetic component calculated from normalized neutron noise (BOC)

Region	Vibrating fuel assembly	Reactivity noise from ex-core detectors $\delta\phi^{pk}_{\det}$ [a.u.]		Reactivity noise (true) $\delta\phi^{pk}_{exact}$ [a.u.]	
		Amplitude	Phase	Amplitude	Phase
Core centre	J9	$1.11\cdot10^{-5}$	-0.26	$1.97\cdot10^{-5}$	-0.16
Middle of core	K11	$7.60\cdot10^{-6}$	-2.97	$1.01\cdot10^{-5}$	-0.16
Periphery of core	L14	$1.56\cdot10^{-5}$	-0.16	$1.52\cdot10^{-5}$	-0.16

Table 11 Point kinetic component calculated from normalized neutron noise (MOC)

Region	Vibrating fuel assembly	Reactivity noise from ex-core detectors $\delta\phi^{pk}_{\det}$ [a.u.]		Reactivity noise (true) $\delta\phi^{pk}_{exact}$ [a.u.]	
		Amplitude	Phase	Amplitude	Phase
Core centre	J9	$5.13\cdot10^{-6}$	-3.22	$1.36\cdot10^{-6}$	-3.33
Middle of core	K11	$2.26\cdot10^{-5}$	-3.21	$6.00\cdot10^{-6}$	-3.33
Periphery of core	L14	$2.41\cdot10^{-5}$	-0.20	$2.50\cdot10^{-5}$	-0.19

Table 12 Point kinetic component calculated from normalized neutron noise (EOC)

Region	Vibrating fuel assembly	Reactivity noise from ex-core detectors $\delta\phi^{pk}_{\det}$ [a.u.]		Reactivity noise (true) $\delta\phi^{pk}_{exact}$ [a.u.]	
		Amplitude	Phase	Amplitude	Phase
Core centre	J9	$6.98\cdot10^{-6}$	-3.28	$3.51\cdot10^{-6}$	-3.37
Middle of core	K11	$3.23\cdot10^{-5}$	-3.26	$1.43\cdot10^{-5}$	-3.37
Periphery of core	L14	$3.72\cdot10^{-5}$	-0.25	$3.96\cdot10^{-5}$	-0.23

Table 13 Point kinetic component calculated from non-normalized fast neutron noise (BOC)

Region	Vibrating fuel assembly	Reactivity noise from ex-core detectors $\delta\phi^{pk}_{det}$ [a.u.]		Reactivity noise (true) $\delta\phi^{pk}_{exact}$ [a.u.]	
		Amplitude	Phase	Amplitude	Phase
Core centre	J9	$3.79 \cdot 10^{-7}$	-0.27	$6.77 \cdot 10^{-7}$	-0.16
Middle of core	K11	$2.61 \cdot 10^{-7}$	-2.97	$3.48 \cdot 10^{-7}$	-0.16
Periphery of core	L14	$5.33 \cdot 10^{-7}$	-0.16	$5.22 \cdot 10^{-7}$	-0.16

Table 14 Point kinetic component calculated from non-normalized fast neutron noise (MOC)

Region	Vibrating fuel assembly	Reactivity noise from ex-core detectors $\delta\phi^{pk}_{det}$ [a.u.]		Reactivity noise (true) $\delta\phi^{pk}_{exact}$ [a.u.]	
		Amplitude	Phase	Amplitude	Phase
Core centre	J9	$2.29 \cdot 10^{-7}$	-3.22	$6.07 \cdot 10^{-8}$	-3.33
Middle of core	K11	$1.01 \cdot 10^{-6}$	-3.02	$2.67 \cdot 10^{-7}$	-3.33
Periphery of core	L14	$1.07 \cdot 10^{-6}$	-0.20	$1.11 \cdot 10^{-6}$	-0.19

Table 15 Point kinetic component calculated from non-normalized fast neutron noise (EOC)

Region	Vibrating fuel assembly	Reactivity noise from ex-core detectors $\delta\phi^{pk}_{det}$ [a.u.]		Reactivity noise (true) $\delta\phi^{pk}_{exact}$ [a.u.]	
		Amplitude	Phase	Amplitude	Phase
Core centre	J9	$3.53 \cdot 10^{-7}$	-3.27	$1.77 \cdot 10^{-7}$	-3.37
Middle of core	K11	$1.63 \cdot 10^{-6}$	-3.25	$7.25 \cdot 10^{-7}$	-3.37

Periphery of core	L14	$1.88 \cdot 10^{-6}$	-0.24	$2.00 \cdot 10^{-6}$	-0.23

Table 16 Point kinetic component calculated from non-normalized thermal neutron noise (BOC)

Region	Vibrating fuel assembly	Reactivity noise from ex-core detectors $\delta\phi^{pk}_{\det}$ [a.u.]		Reactivity noise (true) $\delta\phi^{pk}_{exact}$ [a.u.]	
		Amplitude	Phase	Amplitude	Phase
Core centre	J9	$2.47 \cdot 10^{-7}$	-0.27	$4.41 \cdot 10^{-7}$	-0.16
Middle of core	K11	$2.61 \cdot 10^{-7}$	-2.97	$3.27 \cdot 10^{-7}$	-0.16
Periphery of core	L14	$5.33 \cdot 10^{-7}$	-0.16	$3.40 \cdot 10^{-7}$	-0.16

Table 17 Point kinetic component calculated from non-normalized thermal neutron noise (MOC)

Region	Vibrating fuel assembly	Reactivity noise from ex-core detectors $\delta\phi^{pk}_{\det}$ [a.u.]		Reactivity noise (true) $\delta\phi^{pk}_{exact}$ [a.u.]	
		Amplitude	Phase	Amplitude	Phase
Core centre	J9	$2.31 \cdot 10^{-7}$	-3.22	$6.10 \cdot 10^{-8}$	-3.33
Middle of core	K11	$1.02 \cdot 10^{-6}$	-3.21	$2.69 \cdot 10^{-7}$	-3.33
Periphery of core	L14	$1.08 \cdot 10^{-6}$	-0.20	$1.12 \cdot 10^{-6}$	-0.19

Table 18 Point kinetic component calculated from non-normalized thermal neutron noise (EOC)

Region	Vibrating fuel assembly	Reactivity noise from ex-core detectors $\delta\phi^{pk}_{\det}$ [a.u.]		Reactivity noise (true) $\delta\phi^{pk}_{exact}$ [a.u.]	
		Amplitude	Phase	Amplitude	Phase

Core centre	J9	$3.53 \cdot 10^{-7}$	-3.27	$1.77 \cdot 10^{-7}$	-3.37
Middle of core	K11	$1.63 \cdot 10^{-6}$	-3.25	$7.25 \cdot 10^{-7}$	-3.37
Periphery of core	L14	$1.88 \cdot 10^{-6}$	-0.24	$2.00 \cdot 10^{-6}$	-0.23

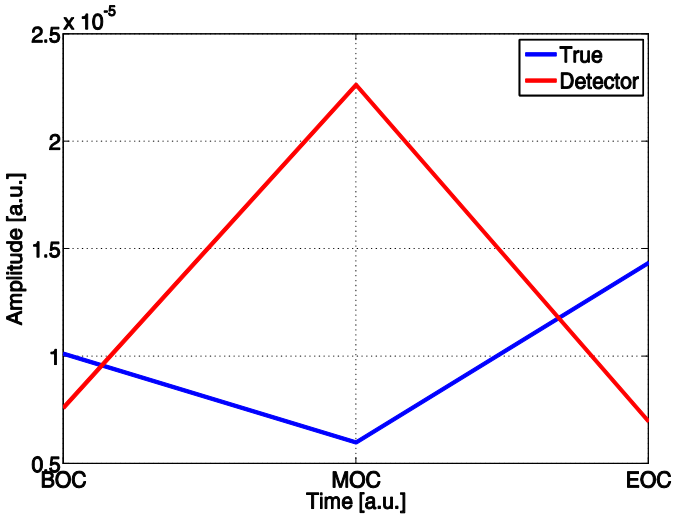

Fig. 23 Time evolution of the amplitude of the point-kinetic component of the simulated thermal (normalized to the static flux) neutron noise induced by fuel assembly vibrations (FA K11): the true one (blue line) and the one calculated from four ex-core detector signals (red line).

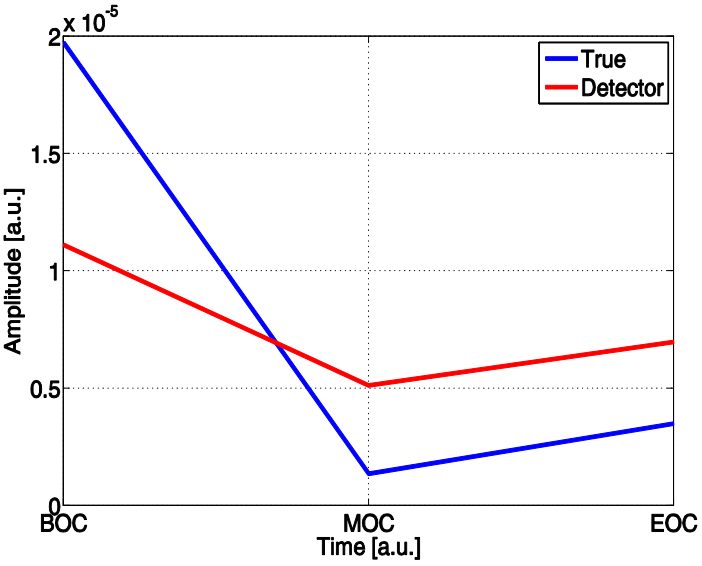

Fig. 24 Time evolution of the amplitude of the point-kinetic component of the simulated thermal (normalized to the static flux) neutron noise induced by fuel assembly vibrations (FA J9): the true one (blue line) and the one calculated from four ex-core detector signals (red line).

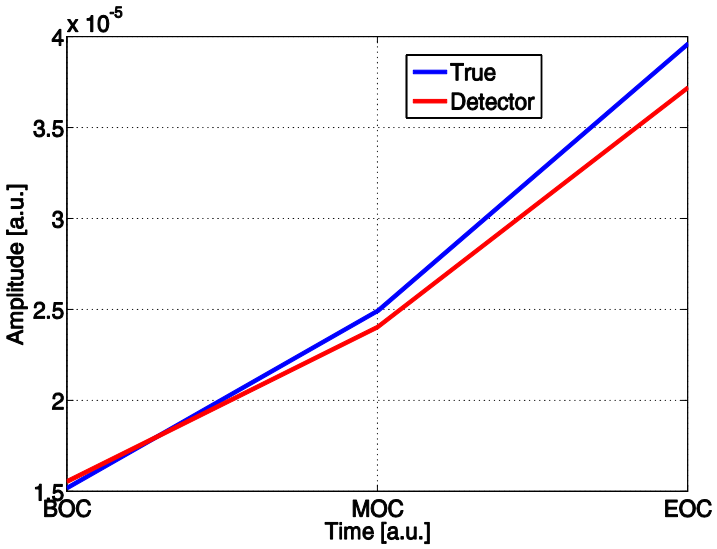

Fig. 25 Time evolution of the amplitude of the point-kinetic component of the simulated thermal (normalized to the static flux) neutron noise induced by fuel assembly vibrations (FA J9): the true one (blue line) and the one calculated from four ex-core detector signals (red line).

4.4. Conclusions

The noise induced by fuel assembly vibrations has been calculated in space and frequency domain using two-group diffusion core simulator CORE SIM. The analysis has been done for three locations of fuel assemblies, i.e. in the core centre, at the middle of core radius and the core periphery. Thereafter the point kinetic component has be evaluated from 4 selected ex-core detector positions (corresponding to the position of ex-core detector in Ringhals-3 core) and compared with the exact reactivity component calculated via adjoint static flux. The relative contribution of both reactivity and space dependent components in the total noise has been also performed. The calculations have been made for both thermal and fast neutron noise whereas only the first one is of a main interest due to CORE SIM limitations. These results clearly show that even though the contribution of the point kinetic into the total noise is significant, its evaluation from only four ex-core detector underestimate the reactivity component almost twice with the respect to the true value of the reactivity component. In addition, the contribution of the space-dependent noise in the measured noise is still significant and thus can not be neglected. Moreover, due to some interference effects between the space-dependent and point-kinetic components, the latter one seems to be suppressed much as compared to its original value. The analysis of the point kinetic component within a fuel cycle time shows that the time evolution of the reactivity component calculated from ex-core detector signals follows the true behaviour only for the case of peripheral fuel assembly vibrations. Otherwise, the true

behaviour of point-kinetic time evolution is not monotonic and can not be evaluated from 4 ex-core detector signals.

As a result, the evaluation of the reactivity component from four ex-core detectors can not be considered as to be completely reliable and appropriate. Therefore further investigation and improvement of the model are required in order to obtain more conclusive results and will be undertaken in the continuation. As an additional task, one can also develop and implement a more realistic model for simulating the neutron noise induced by fuel assembly vibrations and measured by ex-core detectors. For this purpose, one can convert the frequency dependent ex-core signals generated by CORE SIM into time domain, add some white noise and transform the result back into frequency domain. Such a simulation will provide more realistic spectra of the ex-core signals for the analysis.

Another point which has also been performed during this year project (but not shown in the report) concerns the simulation of the noise induced by core barrel vibrations. There, the results were not conclusive due to the observed unrealistic monotonic increase of the noise within one cycle period. Therefore, further improvement of the model should be undertaken in the continuation.

As a final step, both models (for the core barrel and fuel assembly vibrations) can be combined together, i.e. add the noise induced by beam mode vibration to the noise due to fuel assembly vibrations in order to obtain better simulation of real ex-core detector signals. Such a work is planned to be performed in the future.

5. A BASIC STUDY IN NEUTRON NOISE THEORY WHICH COULD PROVIDE SOME INDERECT SUPPORT FOR THE DETERMINATION OF THE VOID FRACTION FROM NEUTRON NOISE MEASUREMENTS.

5.1. Introduction

For natural reasons, the occurrence and properties of both zero power and power reactor noise was exclusively studied and considered in multiplying media (reactor cores). One obvious reason is that from the practical point of view, the problem is only interesting in such systems. Since, as a rule, in zero power systems no perturbation of the medium occurs, the only reason for the non-trivial (non-Poissonian) statistics of the neutron distribution, or that of the number of detections, is the branching process, i.e. the correlations between the neutrons born in the same fission. The information that can be gathered from the deviation from Poisson statistics (the "Y" function of the variance to mean formula which expresses the excess above unity) is related to the nuclear properties of the stationary subcritical system, primarily its subcritical reactivity.

In power reactors, the main reason for the neutron noise is the perturbations of the reactor material (due to boiling of the coolant, vibrations of fuel assemblies and control rods etc.). The zero power noise, due to the branching process is also present, but its amplitude is negligible compared to the noise induced by the perturbations of the system. Hence it is neglected in the treatment, which is based on a formalism (the Langevin equation) which cannot account for the fluctuations arising from the branching process. The non-trivial statistics of the neutron noise, or the correlations between the signals of two detectors, are primarily due to the fact that the perturbation influences all neutrons within the control volume of the perturbation. Although it is obvious that the branching is not responsible for the power reactor noise, it is still implicitly interpreted as if it played a role. This is because perturbations of the above type only occur in power producing systems which obviously utilize the fission process.

The objective of this Section is to draw attention to the fact that branching (fission) is not necessary in order to generate non-trivial neutron fluctuations both in zero power systems and high power systems, as long as there are perturbations in the system. Actually a system without fission is a medium in which neutrons can only be scattered and absorbed, and hence to maintain a neutron flux, a neutron source must be present. Thus, there is no principal difference between the "zero power" and the "power reactor" cases what regards the systems themselves. The difference is purely based on the neutron flux level, which will determine the detection process, and hence also the underlying theoretical description. Due to this fact, a clear analogue to the zero power and power reactor cases will be seen. At low neutron levels, such as a water tank with a weak neutron source, one will detect individual pulses, and the description of such a process is based on the master equation for the probability distribution of the number of neutrons or number of detections. In a system with a high neutron flux (such as a strong spallation source embedded in a

moderator, or in the reflector of a medium or high power reactor), it will be possible to use the detectors in the current mode, and apply the Langevin equation for the description of the noise.

The incentive for discussing this subject is twofold. One is the pure scientific benefit of understanding the correlation-creating role of the perturbations that is not related to the fission process and fission chains. It is hence expected to lead to a novel, deeper understanding of the link between zero power reactor noise and power reactor noise. The second reason is more pragmatic. It might expedite the study of two-phase flow diagnostic methods by simplifying the problem by replacing a critical system in which neutronics and thermal hydraulics are coupled in a two-way manner, to the case of a two-phase flow in an external neutron field. This is especially interesting for realistic Monte-Carlo simulations of the neutron noise diagnostics of two-phase flow, where treatment of the fission process in a time-varying medium is the principal problem [24].

The investigation of the role of the perturbations in non-multiplying systems can be tackled both theoretically and experimentally. The theoretical and the experimental investigations should concern both the zero power and the power reactor cases. During the reporting period no experiments were performed, due to technical difficulties at our collaboration partners, the EPFL Lausanne, where the experiments were planned to be made. Hence this section will concentrate on the theoretical basis and the design of an experiment. It can be added that from the experimental point of view, the zero power noise case would be the more interesting. This is because the zero power noise in a perturbed medium is rather difficult to treat with the master equation technique, and only indirect, although clear, indications can be derived in model cases that lack space dependence. A zero power reactor experiment would therefore be very illuminating and useful. Regarding the power reactor case, the theoretical treatment is simpler, and models a realistic system far better, by allowing for space dependence.

In the following some theoretical considerations are given, for the zero power and the power reactor cases separately, and finally the outline of an experimental arrangement, hopefully being performed in the next Stage, will be given.

5.2. Zero power noise

First it will be shown that in the absence of fission, with a neutron source of Poisson character (simple radioactive source, emitting one neutron at a time), the number of neutrons in a stationary (static) system will follow pure Poisson statistics. The usual assumptions will be used as in the case with zero power noise problems (see Refs [24] and [25]) of having an infinite homogeneous medium in which an infinite homogeneous source is embedded. For generality, a (deterministic) time-dependence of the source is allowed. The emitted neutrons will be absorbed with a constant intensity $S(t)$. The master equation for the number of neutrons in the system will then read as

$$\frac{dP(N,t)}{dt} = \lambda_a P(N+1,t)(N+1) + S(t)P(N-1,t) - P(N,t)[\lambda_a N + S] \tag{50}$$

Introducing the generating function

$$G(x,t) = \sum_N x^N P(N,t) \tag{51}$$

Eq. (50) will be simplified to

$$\frac{\partial G(x,t)}{\partial t} = \lambda_a (1-x)\frac{\partial G(x,t)}{\partial x} + (x-1)S(t)G(x,t) \tag{52}$$

From this it follows for the expectation of the neutron number that

$$\frac{d\langle N(t)\rangle}{dt} = -\lambda_a \langle N(t)\rangle + S(t) \tag{53}$$

With this it is seen that the full solution of (52) is obtained as

$$G(x,t) = e^{(x-1)\langle N(t)\rangle} \tag{54}$$

since substituting (54) into (52) will lead to (53). Eq. (54) is, on the other hand, the generating function of the Poisson distribution

$$P(N,t) = \frac{e^{-\langle N(t)\rangle}\ \langle N(t)\rangle^N}{N!} \tag{55}$$

The dependence on the source intensity is embedded in the expectation $\langle N \rangle$ since, as it is seen from (53), in the stationary case one has

$$\langle N \rangle = \frac{S}{\lambda_a}$$

In both cases, the variance to mean equals to unity:

$$\frac{\sigma_N^2}{\langle N \rangle} = 1 \tag{56}$$

which is independent from the source strength.

It is thus seen that the number of particles in a non-multiplying medium (i.e. one in which branching does not occur) follows Poisson statistics even with a (deterministically) time-varying source intensity. (If the source intensity is a random process, as in some of the cases of pulsed ADS experiments, the statement is not true). This means that making a measurement in a water tank with a neutron source, due to the Poisson statistics of the neutron number, a Feymnan-alpha measurement would yield a zero Y value, since

$$\frac{\sigma_Z^2}{\langle Z \rangle} = 1 + Y \tag{57}$$

Note, however, that in the above, Z is the number of *detections* made during a time period, which is not identical with the number of neutrons in the system. However, it is also easy to see from the classical Feymnan-alpha formulae that the Y function is zero in a non-multiplying system, since it is proportional to the second factorial moment of the number of neutrons from a fission (or any reaction), i.e. to. $\langle \nu(\nu-1) \rangle = 0.$

The reason we chose to derive the statistics of the neutron number is twofold. Partly, Eq. (55) gives a solution for the full statistics (any order moment) of the distribution of the neutron number, whereas the Feynman-alpha formula only gives the second moment, hence it is not as general as a full distribution. Second, for the time-varying case (to be treated soon), the existing formulae refer only to the number of neutrons in the system, but not to the number of detections during a time period. To make a comparison between the stationary case and the time-varying system, we need therefore the statistics of the number of neutrons.

Also, since the neutrons emitted from the source are independent, and hence remain independent all the time before they get absorbed, the counts from two detectors in such a system would be independent. That means that if Z_1 and Z_2 are the counts from two detectors, the covariance between the counts will be zero:

$$\mathrm{Cov}(Z_1, Z_2) = \langle Z_1 Z_2 \rangle - \langle Z_1 \rangle \langle Z_2 \rangle = 0. \tag{58}$$

5.2.1. Zero power noise in a time-varying system

The treatment of a time-varying system with master equations represents a case that has the potential (when applied to multiplying systems) to contain both the zero-power noise (the non-trivial fluctuations due to branching) as well as the power reactor noise (the neutron fluctuations due to the perturbations of the system). However, such a treatment constitutes a formidable task. There has only been one study performed so far in regarding neutron noise in a time-varying medium (Refs [25]-[27]). The study was made in a multiplying medium, but the case for a non-multiplying medium can be extracted from the results. Here we will briefly describe the model and give the final results, showing the deviation of the variance to mean of the neutron number from unity, due to the fluctuations of the system. It will be based on results from [27], which is the best suited to our purposes.

As in the static case, the medium is homogeneous and infinite, as well as the source. The time variations of the system will constitute a binary process: the intensity of the absorption will jump between two discrete states of the system, denoted by λ_1 and λ_2. The jump process is a pure Markovian one with an exponential distribution of the time to both

directions with the same intensity γ. That is, the probability during time dt of jumping from state λ_1 to λ_2, or to the opposite direction, will be equal to γdt.

As explained in [25]-[27], with the master equation approach, only discrete changes of the system state can be treated, out of which the above binary case is the simplest. The reason is that in the derivation of the master equation, the probabilities of mutually exclusive events need to be summed up, which therefore must be countable. This means that the continuous variations of the system, as in reality, and which can easily be handled by the Langevin formalism of the power reactor noise, cannot be handled by the master equation approach. The result is that the model used to illustrate the effect of the temporal variations of the medium is rather crude; it does not have a space dependence, and its time dependence is also discrete. Hence, although the results still clearly indicate the deviation of the statistics of the neutron number from the Poissonian one, they cannot quantitatively predict the magnitude of the deviation, or the magnitude of the covariance between two detector counts, with a space-dependent perturbation. This underlines the interest in performing an experiment along the lines outlined in the forthcoming.

To show the deviation of the variance to mean from unity, we will follow the procedure described in [27]. We shall assume that the system performs small fluctuations around a reference state λ, such that $\lambda_1 = \lambda + \delta\lambda$ and $\lambda_2 = \lambda - \delta\lambda$. From the results in [85], for this case one obtains the following result for the variance to mean of the number of neutrons in the system for the lowest order terms of the perturbation:

$$\frac{\sigma_N^2}{\langle N \rangle} = 1 + \left[\left(1 - 2\frac{\gamma}{\lambda} + 4\frac{\gamma^2}{\lambda^2}\right) + \langle N \rangle \left(1 - 2\frac{\gamma}{\lambda}\right)\right]\left(\frac{\delta\lambda}{\lambda}\right)^2 + \cdots \tag{59}$$

It is clearly seen that the variance to mean deviates from unity. It was also shown in [27] that the second term in the square brackets corresponds to what one would obtain from a traditional Langevin treatment of the perturbation $\delta\lambda$. Eq. (1.12) also means that a corresponding Feynman-alpha measurement would result in Y values larger than zero. Correspondingly, one can also deduct, although this is a rather indirect conclusion, that the covariance of the detector counts between two detectors would be non-zero.

5.3. Power reactor noise

This case will be treated with the standard Langevin formalism. The treatment follows the same lines as the usual one for multiplying systems with many similarities and some obvious differences.

Assume a one-dimensional slab reactor lying between $x \in (-a, a)$, and a static Dirac-delta neutron source in the middle. Actually, as it will be seen later, the position of the source influences only the shape of the static flux, but has no influence on the induced noise whatsoever. With these assumptions the static equation will read as

$$D\phi_0''(x) - \Sigma_a \phi_0(x) + S_0 \delta(x) = 0 \tag{60}$$

with the vacuum boundary conditions

$$\phi_0(\pm a) = 0. \tag{61}$$

With the introduction of the diffusion length L such that $L^2 = D / \Sigma_a$, the static equation has the form

$$\phi_0''(x) - \frac{\phi_0(x)}{L^2} + \frac{S_0}{D}\delta(x) = 0 \tag{62}$$

An illustration of the static flux is given in *Fig. 26.*

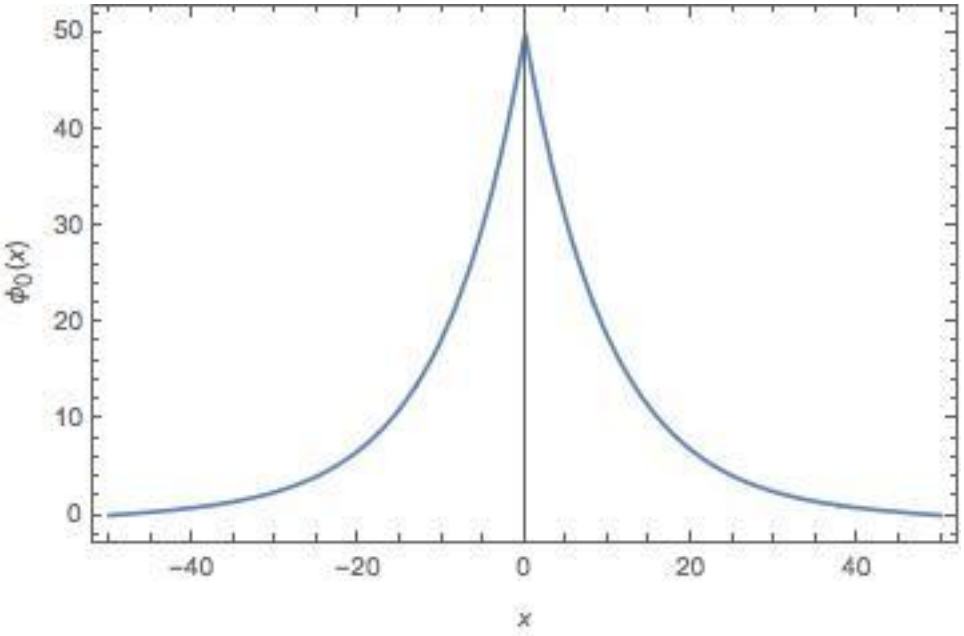

Fig. 26 The space dependence of the static flux with a Dirac-delta function neutron source at x=0.

The time-dependent equation is simple since there are no delayed neutrons, hence there is only one single equation which reads as

$$\frac{1}{v}\frac{\partial \phi(x,t)}{\partial t} = D\phi''(x,t) - \Sigma_a(x,t)\phi(x,t) + S_0\delta(x) \tag{63}$$

Assuming

$$\Sigma_a(x,t) = \Sigma_a + \delta\Sigma_a(x,t) \tag{64}$$

and

$$\phi(x,t) = \phi_0(x) + \delta\phi(x,t), \tag{65}$$

after the usual steps of linearization, subtracting the static equations and temporal Fourier-transform, one obtains

$$\delta\phi''(x,\omega) - \frac{1}{L^2(\omega)}\delta\phi(x,\omega) = \frac{\delta\Sigma_a(x,\omega)\phi_0(x)}{D} \tag{66}$$

where

$$L^2(\omega) = \frac{D}{\Sigma_a(\omega)} = \frac{D}{\Sigma_a + \frac{i\omega}{v}} \tag{67}$$

As usual, Eq. (66) can be solved with the Green's function technique. The equation for the Green's function reads as

$$G''(x,x_{p,}\omega) - \frac{1}{L^2(\omega)}\delta G(x,x_p,\omega) = \delta(x-x_p) \tag{68}$$

This is a complete analogue of the usual noise equation for multiplying systems, with $-1/L^2(\omega)$ replacing $B^2(\omega)$. Correspondingly, the solution is given as

$$G(x,x_p,\omega) = \frac{L(\omega)}{\sinh\left(\frac{2a}{L(\omega)}\right)} \begin{cases} \sinh\left(\frac{a+x}{L(\omega)}\right)\sinh\left(\frac{a-x_p}{L(\omega)}\right); & x < x_p \\ \sinh\left(\frac{a-x}{L(\omega)}\right)\sinh\left(\frac{a+x_p}{L(\omega)}\right); & x \geq x_p \end{cases} \tag{69}$$

An illustration of the amplitude of the noise for $x_p = 25$ and frequency $\omega = 10$ rad/s is shown in Fig. 26. As is seen from both the Figure and from Eq. (69), the presence of the neutron source has no influence on the shape of the noise; the discontinuous derivative of the static flux at the source position $x = 0$ does not appear in the induced neutron noise (unless one has $x_p = 0$). Since there are no fission chains present, the noise has a short relaxation length around the perturbation. One can say that the noise "field-of-view" is comparable with the diffusion length $L(\omega)$. Up to frequencies at the upper end of the usual plateau of the transfer function of multiplying cores, one has $L(\omega) \approx L$.

The above properties of the Green's function show considerable resemblance to the local component of the noise in multiplying cores. The difference is that in multiplying systems the local component can only be calculated in two-group theory; in one-group theory the dominating spatial relaxation length (the eigenvalue of the diffusion equation) is related to the long-range prompt neutron chains. The reason one can obtain a term similar to the local component of multiplying cores is that the fission chains are missing here, so

the relaxation length is determined by the thermal diffusion length (just as the range of the local component in two-group diffusion theory is related to the thermal diffusion length). Quantitatively, in homogenised models of multiplying systems, the diffusion length is shorter than in a pure moderator, due to neutron absorption in the fuel.

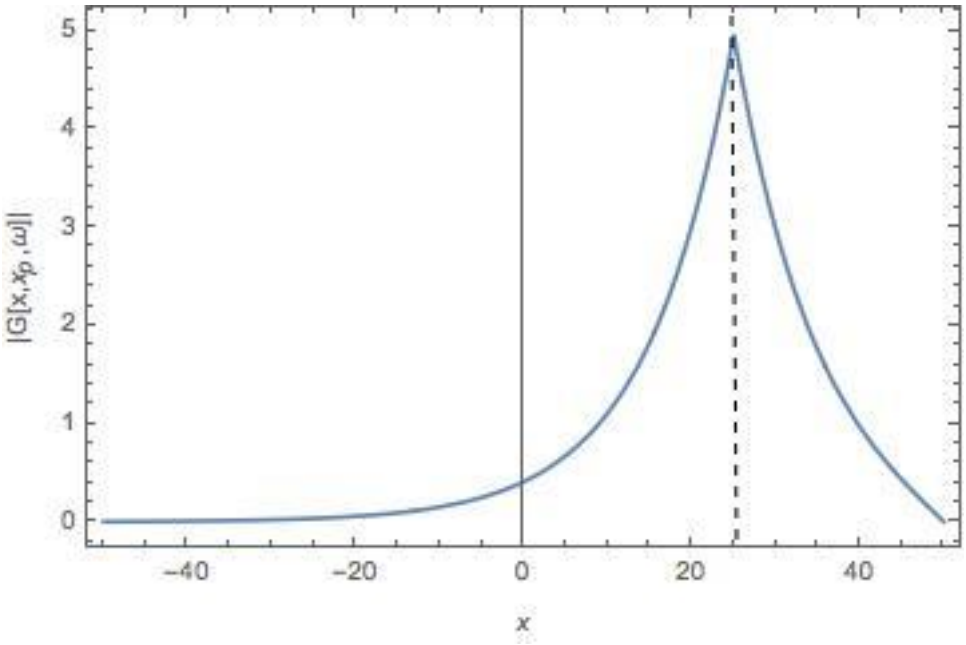

Fig. 27. The space dependence of the amplitude of the Green's function for a perturbation position x_p = 25 cm and frequency 10 rad/s.

These simplified calculations above show that the "detector field-of-view" in such systems is short. Hence, in practice, correlations between two detectors can only be found between detectors that are placed at a distance comparable or less, that the diffusion length, from both the source and from each other. This conclusion can, by generalization and induction, also be transferred to the pulse counting methods of zero power noise, where space-dependent calculations cannot be performed. It is also seen that what regards the power reactor noise induced by fluctuations of the medium, it does not play a role whether the existing neutron flux is generated by a self-maintained chain reaction, or by an external neutron source. The difference is only in the relaxation length of the neutron noise around a localized perturbation, which, for obvious reasons, is much shorter in a non-multiplying medium than in a multiplying medium.

5.4. The zero power noise experiment

The aim of the experiment is to prove that a sufficient condition of the existence of correlated, non-trivial neutron fluctuations is the fluctuation of the medium, even in the absence of fission. To this end an experiment is proposed to be performed with a neutron source in a water tank and at least two neutron detectors, with introducing bubbles in the water between the source and the detectors.

5.4.1. Experimental setup

The experiment would require to put a strong neutron source of simple Poisson statistics (i.e. **not** a Cf-252 which emits several neutrons at a time and which has therefore a compound Poisson statistics) and then inducing perturbations, i.e. the effect of change of moderation, triggered for example by passing bubbles. The purpose is to show that the statistics of one detector deviates from the Poisson one, or, expressed in the terms of the Feynman-alpha formula, the variance to mean exceeds unity. Another possibility is to consider the correlations between two detectors. Without perturbation, the covariance of the counts of two detectors is zero (within experimental uncertainties, of course). In the presence of the perturbation, the covariance is larger than zero; in experimental terms it should be significantly larger than without perturbation.

The neutron noise analysis setup was originally planned to be installed in the CARROUSEL facility of EPFL Lausanne. This facility already contains a holder for a Pu-BE source. A holder for the two detectors needs be designed, as well as a way to generate bubbles. Data acquisition and post-processing should be developed based on the existing neutron noise experiment on the zero power facility CROCUS [28].

In terms of bubbles generation, no channel to guide the bubbles is needed, some bubbles should be able to perturb both detectors signal. There is no need to characterize the bubbles injected in CARROUSEL, i.e. measure the void fraction or void velocity.

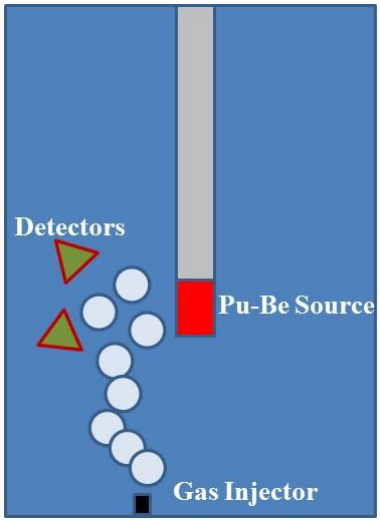

Fig. 28. Layout of the zero power noise experiment

5.4.2. The analysis

To have sufficiently good statistics, a strong neutron source and large detectors should be used. The detectors should be sensitive to thermal neutrons since the local component of the noise is stronger in the thermal range. He-3, BF3 detectors or large U-235 fission chambers available at EPFL (coming from PROTEUS inventory) could be used.

At the low neutron levels of this experiment, the measurement will consist of pulse counting, exactly as in the Feynman- or Rossi-alpha measurements. The measurement is

suggested to be performed in list mode, i.e. registering the times of each count. If this is not possible, then a shift register mode is fine too, or doing the measurement as in the Feynman-alpha, measuring the counts during a time period, making several measurements with that period in order to calculate the mean and the variance, and then repeating it with changing the length of the period. Ultimately, one single long time measurement would also do: measuring several times, one could calculate the correlation coefficient

$$\mathrm{Cov}(Z_1, Z_2) = \langle Z_1 Z_2 \rangle - \langle Z_1 \rangle \langle Z_2 \rangle \tag{70}$$

where Z_1 is the count in detector #1 and Z_2 is the same for detector #2. For the case without bubbles, this quantity is zero, and with bubbles it will deviate from zero. One can also perform a Rossi- or Feymnan measurement; without bubbles, both measurements will yield a result which is constant (independent of time) (for the Rossi-alpha = 0, and for the Feymnan-Y also zero if the unity is deducted from the variance to mean). With bubbles, the Rossi-alpha will have the exponential decay and the Feymnan-alpha the rising character.

5.5. Conclusions

It was shown that branching, represented by the fission process in a multiplying medium, is not necessary for the existence of either zero power noise or power reactor noise. This recognition makes studying the properties of the neutron noise, induced by e.g. two-phase flow in a neutron field, simpler in that the coupling of the fluctuations of the medium back to the neutron generating fission process do not need to be taken into account. From the point of view of the zero power noise, this recognition has some relevance at the basic research level. A zero power noise experiment would have a pure scientific value and it will be performed either in Chalmers or at a foreign laboratory in the not too distant future.

6. A PRELIMINARY STUDY OF THE POSSIBILITY OF MODELLING 3-DIMENSIONAL FUEL ASSEMBLY VIBRATIONS IN A REALISTIC PWR SYSTEM WITH THE CORE SIM SIMULATOR.

6.1. Introduction

In this section some results on a preliminary study of the possibility of modelling 3-dimensional fuel assembly vibrations in a realistic PWR system with the CORE SIM simulator will be presented and discussed. Some results on the modelling of the neutron noise induced by two-dimensional (radial) fuel assembly vibrations have already been reported earlier in [20]-[21]. There the main purpose with the simulation of fuel assembly vibrations was to get better understanding and insight into the origin of 8 Hz peak observed in the ex-core spectra of past measurements taken at Ringhals 4. After thorough investigations it turned out that this peak which amplitude increases within a cycle and corresponds to the beam mode of core barrel vibrations, consists of two closely seated in frequency peaks. Later on, it was suggested that the first peak (closer to 7 Hz) maintaining constant amplitude is induced by the core barrel vibrations. The second peak closer to 8 Hz is due to the individual fuel assembly vibrations and its amplitude can increase monotonically during the cycle. The latter increase in the vibrations amplitude was addressed to the change of boron concentrations and burn-up effects by Sweeney [29]. Thus, the purpose of the 2D fuel assembly vibrations was to validate such a hypothesis. Unfortunately the results of such a study were not conclusive since depending on the location in the core, both the increase and decrease in the vibration amplitude were observed. More details on this topic can be found in [20]-[21]. The main goal with a present simulation as compared to the previous wok is to correctly simulate the noise induced by 3D fuel assembly vibrations and investigate how it affects the induced ex-core response. Such a simulation is not straight forward and requires a number of intermediate steps which are listed below.

Due to the fact that the computational mesh grid of the existing core simulators is too coarse as compared to the displacement of the fuel assemblies (the node size is around 15 cm whereas the fuel assembly displacement is in the millimetre range), the direct simulation of the fuel vibrations with such tools seems to be a complicated task and might lead to erroneous results. One way to handle such a problem is to use dynamic adjoint noise equations where the inhomogeneous part of the equation is defined by the detector cross sections and the variables of the solutions are the perturbation coordinates. In such a case in order to calculate the induced noise is determined by the spatial derivatives of the dynamic adjoint Greens function and static flux at the position of the vibrating component.

Another possibility is to use forward noise equations with finer mesh and calculate the derivative of the Greens functions by moving the inhomogeneous part of the equation with one node. Such a method can be used for the cases where refinements of the mesh does not lead to excessive memory problems and long simulation times such as in the case one

dimensional vibration. Yet another possibility which is utilized in the present study, does not require to calculate any derivatives at all. Instead one directly solved the noise equations in space and frequency numerically with specified noise source. Such an approach has already been tested for simulating one-dimensional core barrel vibrations in [14] and will be adopted and extended to three-dimensions in the present study. In order to specify the noise source in appropriate manner, the changes in cross sections (both amplitude and phase) due to fuel vibrations separately are calculated on a separate fixed grid fine mesh computational tool and then use it as a noise source for the core simulator with a coarser mesh. In addition, compared to the earlier studies where only radial vibrations of the fuel assemblies were of a main interest, the axial vibrations of the fuel assemblies are also properly taken into account in such a study by specifying static flux profile for the noise source in axial direction. Some preliminary results of such estimation are summarized below. In the case of positive results, the analysis might be continued in the future.

6.2. Calculation of the noise induced by 3D fuel assembly vibrations.

As was mentioned earlier, to calculate the spatial distribution of the neutron noise due to fuel assembly vibrations in frequency domain, a numerical core simulator called CORE SIM and developed at Chalmers University of Technology will be used [22]. This numerical tool is based on two-group diffusion theory and allows computing the neutron noise induced by varies types of spatially distributed /localized sources in three-dimensions of any heterogeneous system in first order perturbation approximation.

In Stage 11 [13] the 2-dimensional version of CORE SIM tool for handling heterogeneous systems was modified to simulate the noise induced by core barrel vibrations. In such a case only large displacements could be treated. In Stage 12 [14], the tool was modified again in order to be able to treat sub-millimetre node size corresponding to the realistic core barrel displacements.

Below we give a brief description of the models utilized in CORE SIM for the steady state and dynamic (noise) calculations. Since in the simulation of fuel assembly vibrations, two different meshes have to be used, namely fine mesh for the vibrating fuel assembly and coarse mesh for the rest of the reactor core, there are two versions (blocks) of CORE SIM used in the present calculations, respectively and thus described below.

6.2.1. Steady state calculations for coarse mesh CORE SIM module

In the case of coarse mesh model applied for the entire reactor core (except for the area occupies by vibrating fuel assembly), there are no any external source presented in the system. To obtain the two-group spatial steady-state solution for such a system, the system should be critical and therefore is described by the following matrix equations:

$$\begin{bmatrix} \nabla^{CM} \overline{\overline{D}}^{CM}(\bar{r}) \nabla^{CM} + \overline{\overline{\Sigma}}^{CM}_{sta}(\bar{r}) \end{bmatrix} \times \begin{bmatrix} \phi^{CM}_{1,0}(\bar{r}) \\ \phi^{CM}_{2,0}(\bar{r}) \end{bmatrix} = \frac{1}{k_{eff}} \overline{\overline{F}}^{CM}(\bar{r}) \times \begin{bmatrix} \phi^{CM}_{1,0}(\bar{r}) \\ \phi^{CM}_{2,0}(\bar{r}) \end{bmatrix}, \tag{71}$$

$$\overline{\overline{D}}^{CM}(\bar{r}) = \begin{bmatrix} D^{CM}_{1,0}(\bar{r}) & 0 \\ 0 & D^{CM}_{2,0}(\bar{r}) \end{bmatrix} \tag{72}$$

$$\overline{\overline{\Sigma}}^{CM}_{sta}(\bar{r}) = \begin{bmatrix} -\Sigma^{CM}_{1,0}(\bar{r}) & \frac{\nu \Sigma^{CM}_{f,2,0}(\bar{r})}{k_{eff}} \\ \Sigma^{CM}_{rem,0}(\bar{r}) & -\Sigma^{CM}_{a,2,0}(\bar{r}) \end{bmatrix} \tag{73}$$

$$\Sigma^{CM}_{1,0}(\bar{r}) = \Sigma^{CM}_{a,1,0}(\bar{r}) + \Sigma^{CM}_{rem,0}(\bar{r}) - \frac{\nu \Sigma^{CM}_{f,1,0}(\bar{r})}{k_{eff}} \tag{74}$$

and the respective Marshak boundary conditions (zero incoming current at the boundaries):

$$\bar{J}^{CM}_{g,0}(\bar{r}^{CM}_{B}) \bullet \bar{n}^{CM} = \frac{1}{2} \phi^{CM}_{g,0}(\bar{r}^{CM}_{B}), \tag{75}$$

In the above, $g = 1,2$, $\phi^{CM}_{g,0}(\bar{r})$ stands for the static fast and thermal flux, respectively, $\Sigma^{CM}_{\alpha,g,0}(\bar{r})$ denotes the steady-state macroscopic cross-section of type α, $\alpha = a, f, rem$, $\bar{r}^{CM}_{B}$ represents a spatial point on the boundary with $\bar{n}$ being an outwards unit normal vector and $\bar{J}^{CM}_{g,0}(\bar{r}_{B})$ and $\phi^{CM}_{g,0}(\bar{r}_{B})$ are the net current and the scalar neutron flux taken at the boundary.

After the discretisation procedure with finite differences, Eq. (71) reads in matrix form as:

$$\overline{\overline{M}}^{CM}_{sta} \times \begin{bmatrix} \bar{\phi}^{CM}_{1,0} \\ \bar{\phi}^{CM}_{2,0} \end{bmatrix} = \frac{1}{k_{eff}} \overline{\overline{F}}^{CM} \times \begin{bmatrix} \bar{\phi}^{CM}_{1,0} \\ \bar{\phi}^{CM}_{2,0} \end{bmatrix}, \tag{76}$$

where $\bar{\phi}^{CM}_{1,0}$ and $\bar{\phi}^{CM}_{2,0}$ are columns vectors describing the fast and the thermal spatially-discretized static fluxes, respectively. Assuming that the reactor core is discretized in total into N^{CM} - nodes, $\bar{\phi}^{CM}_{1,0}$ and $\bar{\phi}^{CM}_{2,0}$ then represent $2N^{CM}$ column vectors whereas $\overline{\overline{M}}^{CM}_{sta}$ and $\overline{\overline{F}}^{CM}$ representing the loss and production operators, become $2N^{CM} \times 2N^{CM}$ matrixes. Eq. (76) is then can be reformulated as eigenvalue problem as:

$$\overline{\overline{A}}^{CM} \times \bar{x}^{CM} = k_{eff} \bar{x}^{CM}, \tag{77}$$

with

$$\overline{\overline{A}}^{CM} = \overline{\overline{M}}_{sta}^{CM^{-1}} \times \overline{\overline{F}}^{CM} \tag{78}$$

and

$$\overline{x}^{CM} = \begin{bmatrix} \overline{\phi}_{1,0}^{CM} \\ \overline{\phi}_{2,0}^{CM} \end{bmatrix} \tag{79}$$

As one case see from Eq. (77), the calculation of the static fluxes requires the inversion of the matrix $\overline{\overline{M}}_{sta}^{CM}$ of a very large size. The direct inversion of such a matrix is both CPU and memory expensive as well as does not allow to reach the necessary node size in the sub-millimetre range. Therefore, in order to preserve the sparsity of the matrix $\overline{\overline{M}}_{sta}^{CM}$ an approximate Minimum Degree ordering as well as $LU \quad PQ$ decomposition of $\overline{\overline{M}}_{sta}^{CM}$ has been carried out. As a result, Eq. (77) reads as:

$$\overline{\overline{Q}}_{sta}^{CM} \times \left\{ \overline{\overline{U}}_{sta}^{CM} \setminus \left[\overline{\overline{L}}_{sta}^{CM} \setminus \left(\overline{\overline{P}}_{sta}^{CM} \times \overline{\overline{F}}^{CM} \times \overline{x}^{CM} \right) \right] \right\} = k_{eff} \overline{x}^{CM} \tag{80}$$

since $\overline{\overline{P}}_{sta}^{CM,H} \times \overline{\overline{P}}_{sta}^{CM} = I = \overline{\overline{Q}}_{sta}^{CM,H} \times \overline{\overline{Q}}_{sta}^{CM}$. Eq. (77) can then be solved by Arnoldi power iteration method. For more details one refers to [22].

6.2.2. Steady state calculations for fine mesh CORE SIM module

For the fine mesh static solution describing the spatial distribution of the neutrons in two energy groups within a range of vibrating fuel assembly, the problem with a presence of internal neutron source should be considered. This appearance of the internal source in the fine mesh problem is the result of the specific boundary conditions which are imposed on the fine mesh system (as it has already been mentioned in the introduction), namely reflected boundary conditions (zero net current at the boundaries). In order to satisfy such boundary conditions, one needs to modify streaming term in the original and discretized equations. Such a streaming term is then designated with a superscript “MOD” in the further equations below. Thus, the following set of equations can be written:

$$\left[\left[\nabla^{FM} \overline{\overline{D}}^{FM}(\overline{r}) \nabla^{FM} \right]^{MOD} + \overline{\overline{\Sigma}}_{sta}^{FM}(\overline{r}) - \overline{\overline{F}}^{FM}(\overline{r}) \right] \times \begin{bmatrix} \phi_{1,0}^{FM}(\overline{r}) \\ \phi_{2,0}^{FM}(\overline{r}) \end{bmatrix} = -\overline{S}_0^{\text{int},FM}(\overline{r}), \tag{81}$$

and the corresponding reflected boundary (zero net current at the boundaries) conditions:

$$\overline{J}_{g,0}^{FM}(\overline{r}_B^{FM}) = 0, \tag{82}$$

where $\bar{\bar{S}}_0^{\text{int},FM}(\bar{r}) = \begin{bmatrix} S_{1,0}^{\text{int},FM}(\bar{r}) \\ S_{2,0}^{\text{int},FM}(\bar{r}) \end{bmatrix}$ stands for external fast and thermal noise sources, respectively.

After the discretisation procedure with finite differences, Eq. (81) reads in matrix form as:

$$\bar{\bar{M}}_{sta}^{FM} \times \begin{bmatrix} \bar{\phi}_{1,0}^{FM} \\ \bar{\phi}_{2,0}^{FM} \end{bmatrix} = \bar{\bar{S}}_0^{\text{int},FM}, \tag{83}$$

where the vector $\bar{\bar{S}}_0^{\text{int},FM}$ represents the $2N^{FM}$ column vector for internal fast and thermal noise sources, respectively. Similarly to the static case of the coarse mesh system, the calculation of the static flux via Eq. (83) requires the inversion of the matrix $\bar{\bar{M}}_{sta}^{FM}$ of a very large size which is again carried out via an approximate Minimum Degree ordering as well as LU PQ decomposition of $\bar{\bar{M}}_{sta}^{FM}$. As a result, Eq. (83) then reads as:

$$\bar{\bar{L}}_{sta}^{FM} \times \bar{\bar{U}}_{sta}^{FM} = \bar{\bar{P}}_{sta}^{FM} \times \bar{\bar{M}}_{sta}^{FM} \times \bar{\bar{Q}}_{sta}^{FM}. \tag{84}$$

and for the static solution, one gets:

$$\bar{\phi}_0^{FM} = \bar{\bar{Q}}_{sta}^{FM} \times \left\{ \bar{\bar{U}}_{sta}^{FM} \setminus \left[\bar{\bar{L}}_{sta}^{FM} \setminus \left(\bar{\bar{P}}_{sta}^{FM} \times \bar{\bar{S}}_0^{ext,FM} \right) \right] \right\} \tag{85}$$

since $\bar{\bar{P}}_{sta}^{FM,H} \times \bar{\bar{P}}_{sta}^{FM} = I = \bar{\bar{Q}}_{sta}^{FM,H} \times \bar{\bar{Q}}_{sta}^{FM}$.

6.2.3. Noise calculations for coarse mesh CORE SIM module

The corresponding dynamic (noise) equations solved by coarse mesh CORE SIM module for the two-group noise in space and frequency are summarized below (for more details the interested reader is referred to [22]):

$$\begin{bmatrix} \nabla^{CM} \bar{\bar{D}}^{CM}(\bar{r}) \nabla^{CM} + \bar{\bar{\Sigma}}_{dyn}^{CM}(\bar{r},\omega) \end{bmatrix} \times \begin{bmatrix} \delta\phi_1^{CM}(\bar{r},\omega) \\ \delta\phi_2^{CM}(\bar{r},\omega) \end{bmatrix} = \bar{\delta S}^{ext,CM}(\bar{r},\omega) \tag{86}$$

$$\overline{\delta S}^{CM}(\overline{r},\omega) = \overline{\phi}^{CM}_{rem}(\overline{r})\delta\sum\nolimits^{CM}_{rem}(\overline{r},\omega) + \overline{\overline{\phi}}^{CM}_{a}(\overline{r})\begin{bmatrix}\delta\sum\nolimits^{CM}_{a,1}(\overline{r},\omega)\\ \delta\sum\nolimits^{CM}_{a,2}(\overline{r},\omega)\end{bmatrix} + \overline{\overline{\phi}}^{CM}_{f}(\overline{r})\begin{bmatrix}\delta\nu\sum\nolimits^{CM}_{f,1}(\overline{r},\omega)\\ \delta\nu\sum\nolimits^{CM}_{f,2}(\overline{r},\omega)\end{bmatrix}$$

(87)

$$\overline{\overline{\sum}}^{CM}_{dyn}(\overline{r},\omega) = \begin{bmatrix} -\sum\nolimits^{CM}_{1}(\overline{r},\omega) & \dfrac{\nu\sum\nolimits^{CM}_{f,2,0}(\overline{r})}{k_{eff}}\left(1-\dfrac{i^{\omega}\beta_{eff}}{i^{\omega}+\lambda}\right) \\ \sum\nolimits^{CM}_{rem,0}(\overline{r}) & -\left(\sum\nolimits^{CM}_{a,2,0}(\overline{r})+\dfrac{i^{\omega}}{\upsilon_{2}}\right)\end{bmatrix} \tag{88}$$

$$\overline{\overline{\phi}}^{CM}_{rem}(\overline{r}) = \begin{bmatrix}\phi^{CM}_{1,0}(\overline{r})\\ -\phi^{CM}_{1,0}(\overline{r})\end{bmatrix} \tag{89}$$

$$\overline{\overline{\phi}}^{CM}_{a}(\overline{r}) = \begin{bmatrix}\phi^{CM}_{1,0}(\overline{r}) & 0\\ 0 & \phi^{CM}_{2,0}(\overline{r})\end{bmatrix} \tag{90}$$

$$\overline{\overline{\phi}}^{CM}_{f}(\overline{r},\omega) = \begin{bmatrix} -\phi^{CM}_{1,0}(\overline{r})\left(1-\dfrac{i^{\omega}\beta_{eff}}{i^{\omega}+\lambda}\right) & -\phi^{CM}_{2,0}(\overline{r})\left(1-\dfrac{i^{\omega}\beta_{eff}}{i^{\omega}+\lambda}\right)\\ 0 & 0\end{bmatrix} \tag{91}$$

$$\sum\nolimits^{CM}_{1}(\overline{r},\omega) = \sum\nolimits^{CM}_{a,1,0}(\overline{r}) + \frac{i^{\omega}}{\upsilon_{1}} + \sum\nolimits^{CM}_{rem,0}(\overline{r}) - \frac{\nu\sum\nolimits^{CM}_{f,1,0}(\overline{r})}{k_{eff}}\left(1-\frac{i^{\omega}\beta_{eff}}{i^{\omega}+\lambda}\right) \tag{92}$$

and the respective Marshak boundary conditions (zero incoming noise current at the boundaries):

$$\delta\overline{\boldsymbol{J}}^{CM}_{g,0}(\overline{\boldsymbol{r}}^{CM}_{B},\omega)\bullet\overline{\boldsymbol{n}}^{CM} = \frac{1}{2}\delta\phi^{CM}_{g,0}(\overline{\boldsymbol{r}}^{CM}_{B},\omega), \tag{93}$$

In the above, $\delta\phi^{CM}_{g}(\overline{\boldsymbol{r}},\omega)$ stands for the neutron noise induced by fluctuations $\delta\sum\nolimits^{CM}_{\alpha,g}(\overline{\boldsymbol{r}},\omega)$ in the macroscopic cross-sections of type α, $\delta\overline{\boldsymbol{J}}^{CM}_{g,0}(\overline{\boldsymbol{r}}_{B},\omega)$ and $\delta\phi^{CM}_{g,0}(\overline{\boldsymbol{r}}_{B},\omega)$ are the noise in the net current and the noise in the scalar neutron flux taken at the boundary..

After the discretisation procedure with finite differences, Eq. (86) reads in matrix form as:

$$\overline{\overline{\boldsymbol{M}}}^{CM}_{dyn}\times\overline{\delta\phi}^{CM} = \overline{\delta\boldsymbol{S}}^{ext,CM}, \tag{94}$$

where $\overline{\delta\phi}^{CM}$ is column vector describing the fast and the thermal noise in the core and column vector $\overline{\delta\boldsymbol{S}}^{ext,CM}$ stands for external fast and thermal noise sources, respectively. Following the same procedure as before, we assume that the reactor core is discretized in

total into N^{CM} - nodes and therefore $\overline{\delta\phi}^{CM}$ and $\overline{\delta S}^{CM}$ then represent $2N^{CM}$ column vectors whereas $\overline{\overline{M}}^{CM}_{dyn}$ becomes a $2N^{CM} \times 2N^{CM}$ matrix.

Similarly to the static case, one can see from Eq. (94) that the calculation of the induced noise requires the inversion of the matrix $\overline{\overline{M}}^{CM}_{dyn}$ of a very large size. The direct inversion of such a matrix is both CPU and memory expensive as well as does not allow reaching the necessary node size in the sub-millimetre range. Therefore, in order to preserve the sparsity of the matrix $\overline{\overline{M}}^{CM}_{dyn}$ an approximate Minimum Degree ordering as well as LU PQ decomposition of $\overline{\overline{M}}^{CM}_{dyn}$ has been carried out. As a result, Eq. (94) reads as:

$$\overline{\overline{L}}^{CM}_{dyn} \times \overline{\overline{U}}^{CM}_{dyn} = \overline{\overline{P}}^{CM}_{dyn} \times \overline{\overline{M}}^{CM}_{dyn} \times \overline{\overline{Q}}^{CM}_{dyn}. \tag{95}$$

The neutron noise is then given as:

$$\overline{\delta\phi}^{CM} = \overline{\overline{Q}}^{CM}_{dyn} \times \left\{ \overline{\overline{U}}^{CM}_{dyn} \setminus \left[\overline{\overline{L}}^{CM}_{dyn} \setminus \left(\overline{\overline{P}}^{CM}_{dyn} \times \overline{\delta S}^{ext,CM}_{dyn} \right) \right] \right\} \tag{96}$$

since $\overline{\overline{P}}^{CM,H}_{dyn} \times \overline{\overline{P}}^{CM}_{dyn} = I = \overline{\overline{Q}}^{CM,H}_{dyn} \times \overline{\overline{Q}}^{CM}_{dyn}$.

6.2.4. Noise calculations for fine mesh CORE SIM module

Further, the dynamical two-group (noise) solution in space and frequency domain for the fine mesh system is considered below. For obvious reasons, such a problem should be formulated as a problem with a presence of both internal and external neutron noise source. The occurrence of the internal source in the fine mesh problem can be justified (similarly to the static case) by the specific boundary conditions which are imposed on the fine mesh system, namely reflected boundary conditions (zero net current at the boundaries). In order to fulfil such boundary conditions, the corresponding streaming term in the original and discretized equations should be modified which then is designated with a superscript "MOD" in the further equations below. The corresponding equations for the noise read as:

$$\left[\nabla^{FM} \overline{\overline{D}}^{FM}(\overline{r}) \nabla^{FM} \right]^{MOD} + \overline{\overline{\Sigma}}^{FM}_{dyn}(\overline{r},\omega) \times \begin{bmatrix} \delta\phi_1^{FM}(\overline{r},\omega) \\ \delta\phi_2^{FM}(\overline{r},\omega) \end{bmatrix} = \overline{\delta S}^{\mathrm{int},FM}(\overline{r},\omega) + \overline{\delta S}^{ext,FM}(\overline{r},\omega) \tag{97}$$

$$\overline{\delta S}^{ext,FM}(\overline{r},\omega) = \overline{\phi}^{FM}_{rem}(\overline{r})\delta\sum\nolimits^{FM}_{rem}(\overline{r},\omega) + \overline{\overline{\phi}}^{FM}_{a}(\overline{r})\begin{bmatrix}\delta\sum\nolimits^{FM}_{a,1}(\overline{r},\omega)\\ \delta\sum\nolimits^{FM}_{a,2}(\overline{r},\omega)\end{bmatrix} + \overline{\overline{\phi}}^{FM}_{f}(\overline{r})\begin{bmatrix}\delta\nu\sum\nolimits^{FM}_{f,1}(\overline{r},\omega)\\ \delta\nu\sum\nolimits^{FM}_{f,2}(\overline{r},\omega)\end{bmatrix}$$

(98)

$$\overline{\overline{\sum}}^{FM}_{dyn}(\overline{r},\omega) = \begin{bmatrix} -\sum\nolimits^{FM}_{1}(\overline{r},\omega) & \dfrac{\nu\sum\nolimits^{FM}_{f,2,0}(\overline{r})}{k_{eff}}\left(1-\dfrac{i^{\omega}\beta_{eff}}{i^{\omega}+\lambda}\right) \\ \sum\nolimits^{FM}_{rem,0}(\overline{r}) & -\left(\sum\nolimits^{FM}_{a,2,0}(\overline{r})+\dfrac{i^{\omega}}{\upsilon_{2}}\right)\end{bmatrix} \tag{99}$$

$$\overline{\overline{\phi}}^{FM}_{rem}(\overline{r}) = \begin{bmatrix}\phi^{FM}_{1,0}(\overline{r})\\ -\phi^{FM}_{1,0}(\overline{r})\end{bmatrix} \tag{100}$$

$$\overline{\overline{\phi}}^{FM}_{a}(\overline{r}) = \begin{bmatrix}\phi^{FM}_{1,0}(\overline{r}) & 0\\ 0 & \phi^{FM}_{2,0}(\overline{r})\end{bmatrix} \tag{101}$$

$$\overline{\overline{\phi}}^{FM}_{f}(\overline{r},\omega) = \begin{bmatrix} -\phi^{FM}_{1,0}(\overline{r})\left(1-\dfrac{i^{\omega}\beta_{eff}}{i^{\omega}+\lambda}\right) & -\phi^{FM}_{2,0}(\overline{r})\left(1-\dfrac{i^{\omega}\beta_{eff}}{i^{\omega}+\lambda}\right)\\ 0 & 0\end{bmatrix} \tag{102}$$

$$\sum\nolimits^{FM}_{1}(\overline{r},\omega) = \sum\nolimits^{FM}_{a,1,0}(\overline{r}) + \frac{i^{\omega}}{\upsilon_{1}} + \sum\nolimits^{FM}_{rem,0}(\overline{r}) - \frac{\nu\sum\nolimits^{FM}_{f,1,0}(\overline{r})}{k_{eff}}\left(1-\frac{i^{\omega}\beta_{eff}}{i^{\omega}+\lambda}\right) \tag{103}$$

and the corresponding reflected boundary (zero noise in the net current at the boundaries) conditions:

$$\delta\overline{\boldsymbol{J}}^{\boldsymbol{FM}}_{\boldsymbol{g},0}(\overline{\boldsymbol{r}}^{\boldsymbol{FM}}_{\boldsymbol{B}}) = 0, \tag{104}$$

Following the same discretisation procedure as before, the discretised form of Eq. (97) can be written as:

$$\overline{\overline{\boldsymbol{M}}}^{\boldsymbol{FM}}_{\boldsymbol{dyn}} \times \overline{\delta\phi}^{\boldsymbol{FM}} = \overline{\delta\boldsymbol{S}}^{\mathrm{int},\boldsymbol{FM}} + \overline{\delta\boldsymbol{S}}^{\boldsymbol{ext},\boldsymbol{FM}} \equiv \overline{\delta\boldsymbol{S}}^{\boldsymbol{tot},\boldsymbol{FM}}, \tag{105}$$

where the column vector $\overline{\delta\boldsymbol{S}}^{\mathrm{int},\boldsymbol{FM}}$ stands for the external fast and thermal noise sources, respectively due to the specific boundary conditions (zero net current at the boundaries) imposed for the fine mesh system. Following the same procedure as before, we assume that the reactor core is discretized in total into $\boldsymbol{N}^{FM}$ - nodes and therefore $\overline{\delta\phi}^{\boldsymbol{FM}}$, $\overline{\delta\boldsymbol{S}}^{\boldsymbol{ext},\boldsymbol{FM}}$ and $\overline{\delta\boldsymbol{S}}^{\mathrm{int},\boldsymbol{FM}}$ then represent $2\boldsymbol{N}^{FM}$ column vectors whereas $\overline{\overline{\boldsymbol{M}}}^{\boldsymbol{FM}}_{\boldsymbol{dyn}}$ becomes a $2\boldsymbol{N}^{FM} \times 2\boldsymbol{N}^{FM}$ matrix.

Similarly to the static case, $\overline{\overline{M}}^{FM}_{dyn}$ represents a matrix of a very large size which is difficult to invert directly. Therefore, to preserve the sparsity of the matrix $\overline{\overline{M}}^{FM}_{dyn}$ an approximate Minimum Degree ordering as well as $L\,U \quad P\,Q$ decomposition of $\overline{\overline{M}}^{FM}_{dyn}$ has been performed. Then, Eq. (105) reads as:

$$\overline{\overline{L}}^{FM}_{dyn} \times \overline{\overline{U}}^{FM}_{dyn} = \overline{\overline{P}}^{FM}_{dyn} \times \overline{\overline{M}}^{FM}_{dyn} \times \overline{\overline{Q}}^{FM}_{dyn}. \tag{106}$$

The dynamic solution can then be written as:

$$\overline{\delta\phi}^{FM} = \overline{\overline{Q}}^{FM}_{dyn} \times \left\{ \overline{\overline{U}}^{FM}_{dyn} \setminus \left[\overline{\overline{L}}^{FM}_{dyn} \setminus \left(\overline{\overline{P}}^{FM}_{dyn} \times \overline{\delta S}^{tot,FM}_{dyn} \right) \right] \right\} \tag{107}$$

since $\overline{\overline{P}}^{FM,H}_{dyn} \times \overline{\overline{P}}^{FM}_{dyn} = I = \overline{\overline{Q}}^{FM,H}_{dyn} \times \overline{\overline{Q}}^{FM}_{dyn}$.

6.3. Homogenization procedure at fine mesh level

As was mentioned before the calculation of the noise induced by fuel assembly vibrations in the presented model requires the coupling between two different meshes corresponding toe two different system: the fine mesh system (the area within the vibrating fuel assembly) and the coarse mesh system (the rest of the reactor core). In order to correctly perform such a coupling as well as to obtain a full consistence between group constants belonging to two different meshes, some additional conditions imposed on the neutron flux should be fulfilled, namely the actual reaction rates per coarse mesh node should be preserved. For this purpose, the following node-averaged data are defined:

- Spatial homogenization of the static fluxes:

$$\phi^{CM}_{g,0,n} = \frac{1}{V^{CM}_n} \int_{V^{CM}_n} \phi^{FM}_{g,0,n}(\overline{r})\,d\overline{r} \approx \frac{\sum_{m=1}^{N^{FM}_n} \phi^{FM}_{g,0,n,m}}{N^{FM}_n} \tag{108}$$

where $\phi^{CM}_{g,0n}$ represents coarse mesh discretized static flux of group g corresponding to n node, $\phi^{FM}_{g,0,n}(\overline{r})$ and $\phi^{FM}_{g,0,n,m}$ represents the fine mesh static flux of group g corresponding to the n coarse mesh node and its discretized form (corresponding to m fine mesh node of the same coarse mesh node) respectively , V^{CM}_n is the total volume of coarse mesh node, N^{FM}_n is the total number of the fine mesh nodes in which one coarse mesh n node was discretized to.

- Spatial homogenization of the static cross sections:

$$\sum_{\alpha,g,0,n}^{CM} = \frac{\frac{1}{V_n^{CM}} \int_{V_n^{CM}} \sum_{\alpha,g,0,n}^{FM}(\bar{r})\phi_{g,0,n}^{FM}(\bar{r})d\bar{r}}{\phi_{g,0,n}^{CM}} \tag{109}$$

where $\sum_{\alpha,g,0,n}^{CM}$ represents coarse mesh static cross section of type α in group g corresponding to n node, $\sum_{\alpha,g,0,n}^{FM}(\bar{r})$ represents fine mesh static cross section of type α in energy group g corresponding to n coarse mesh node,

- Spatial homogenization of the neutron noise:

$$\delta\phi_{g,n}^{CM}(\omega) = \frac{1}{V_n^{CM}} \int_{V_n^{CM}} \delta\phi_{g,n}^{FM}(\bar{r},\omega)d\bar{r} \approx \frac{\sum_{m=1}^{N_n^{FM}} \delta\phi_{g,n,m}^{FM}(\omega)}{N_n^{FM}} \tag{110}$$

where $\delta\phi_{g,n}^{CM}(\omega)$ represents the coarse mesh discretized neutron noise of group g corresponding to n node, $\delta\phi_{g,n}^{FM}(\bar{r},\omega)$ and $\delta\phi_{g,n,m}^{FM}(\omega)$ represents the fine mesh neutron noise of group g corresponding to the n coarse mesh node and its discretized form (corresponding to m fine mesh node of the same coarse mesh node) respectively;

- Spatial homogenization of the static cross sections (for the nodes corresponding to the vibrating fuel assemblies):

$$\sum_{\alpha,g,0,n}^{CM} = \frac{\frac{1}{V_n^{CM}} \int_{V_n^{CM}} \sum_{\alpha,g,0,n}^{FM}(\bar{r})\delta\phi_{g,n}^{FM}(\bar{r},\omega)d\bar{r}}{\delta\phi_{g,n}^{CM}} \tag{111}$$

- Spatial homogenization of dynamic cross sections (fluctuations, for the nodes corresponding to the vibrating fuel assemblies):

$$\delta\sum_{\alpha,g,n}^{CM}(\omega) = \frac{\frac{1}{V_n^{CM}} \int_{V_n^{CM}} \delta\sum_{\alpha,g,n}^{FM}(\bar{r},\omega)\phi_{g,0,n}^{FM}(\bar{r})d\bar{r}}{\phi_{g,0,n}^{CM}} \tag{112}$$

where $\delta\sum_{\alpha,g,n}^{CM}(\omega)$ represents a fluctuation in the coarse mesh cross section of type α in group g corresponding to n node, $\delta\sum_{\alpha,g,n}^{FM}(\bar{r},\omega)$ represents a fluctuation in the fine mesh cross section of type α in energy group g corresponding to n coarse mesh node.

The above-defined node-averaged data are defined only for the nodes corresponding to the vibrating fuel assemblies.

6.4. Modelling of the three-dimensional fuel assembly vibrations.

As was mentioned in the previous section, in the present study to model fuel assembly vibrations we adopt the model which had been used earlier to simulate the noise induced by the beam mode of core barrel vibrations in one dimensional two-group reflected system [14]. First, the brief overview of such a model will be given below. Then, the latter model is modified and extended to a 3 dimensional heterogeneous system representing a realistic PWR.

In such a one-dimensional system, the static space dependence of the macroscopic cross-sections of type α in energy group g can be written in following analytical form for $x \geq 0$:

$$\Sigma_{\alpha,g}(x) = \left[1 - H(x-b)\right]\Sigma^{c}_{\alpha,g} + H(x-b)\Sigma^{r}_{\alpha,g}, \tag{113}$$

where b denotes equilibrium position of the interface boundary between active part of the core and the reflector, superscripts c and r designate the core and the reflector regions, respectively and H stands for the Heaviside function.

For visualization, the schematic illustration of the one-dimensional reactor core with the corresponding boundaries is given in Fig. In the case of the beam mode motion, the boundaries $x = \pm b$ between the core and the reflectors start to move in the same direction and can be resented as $b_{-}(t) = -b + \varepsilon(t)$ for $x < 0$ and $b_{+}(t) = b + \varepsilon(t)$ for $x \geq 0$. After one term Taylor expansion, subtraction of the static equation (113) and Fourier transform, for frequency and space dependent fluctuations in macroscopic cross-sections of

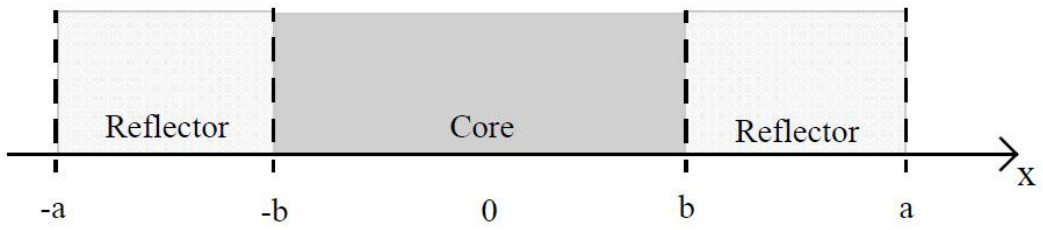

Fig. 29 One-dimensional two-region reactor model used for explaining the modelling of the beam mode vibrations with the neutron noise simulator.

type α in energy one obtains:

$$\delta\Sigma_{\alpha,g}(x,\omega) = \varepsilon(\omega)\left[\delta(x-b) - \delta(x+b)\right]\left[\Sigma^{c}_{\alpha,g} - \Sigma^{r}_{\alpha,g}\right], \tag{114}$$

For the of three-dimensional fuel assembly vibrations the space dependence of the static macroscopic cross sections of type α in energy g group, i.e. Eq. (113) can be generalized correspondingly as:

$$\Sigma_{\alpha,g}(\bar{r}) = \Sigma^{r}_{\alpha,g}(z)\left[1 - H(y-y_1) - H(y-y_2)\right]\left[H(x-x_1) - H(x-x_2)\right] +$$

$$\sum {}^{c}_{\alpha,g}(z) \quad \boldsymbol{H}(y - y_1) - \boldsymbol{H}(y - y_2) \quad \boldsymbol{H}(x - x_1) - \boldsymbol{H}(x - x_2) \quad , \tag{115}$$

Then assuming that in the dynamical case, the movement of the vibrating fuel assemblies take place only in radial direction and are characterized by two-component displacement vector, the space-time dependent macroscopic cross-.sections of type α in energy g group of type α in energy g group read as:

$$\sum {}_{\alpha,g}(\bar{r},t) = \sum {}^{r}_{\alpha,g}(z) \; 1 - \boldsymbol{H}(y - y_1 - \varepsilon_y(z,t)) - \boldsymbol{H}(y - y_2 - \varepsilon_y(z,t)) \quad \boldsymbol{H}(x - x_1 - \varepsilon_x(z,t)) -$$

$$\boldsymbol{H}(x - x_2 - \varepsilon_x(z,t)) \quad + \sum {}^{c}_{\alpha,g}(z) \quad \boldsymbol{H}(y - y_1 - \varepsilon_y(z,t)) - \boldsymbol{H}(y - y_2 - \varepsilon_y(z,t))$$

$$\boldsymbol{H}(x - x_1 - \varepsilon_x(z,t)) - \boldsymbol{H}(x - x_2 - \varepsilon_x(z,t)) \quad . \tag{116}$$

It should be pointed out that in order to introduce the third dimension in the case of fuel assembly vibration, the so-called axial bending of the fuel assemblies were assumed. The bending of the fuel assembly can be modelled by specifying an axial dependence of radial displacement of the assembly. There several bending modes of the fuel assemblies can take place in the reactor core depending on how fuel assemblies are fixed at the bottom and the top. In the present case, we consider only the simplest bending mode, the so called fundamental mode when both ends of the fuel assembly are fixed. In this latter case, the fuel assembly vibrations are similar to the string vibrations with fixed ends. For the simplicity, the sin-shape of the axial dependence of the displacements will be used. It is also worth to mention that in the case of three-dimensional fuel assembly vibrations, the corresponding macroscopic cross section also becomes axially dependent and will be taken into account in the modelling process.

Then, expanding Eq. (116) in Taylors series around the displacement positions $\varepsilon(z,t) = \varepsilon_x(z,t), \varepsilon_y(z,t)$

$$\boldsymbol{H}(\alpha - \alpha_i - \varepsilon_\alpha(z,t)) = \boldsymbol{H}(\alpha - \alpha_i) - \varepsilon_\alpha(z,t)\delta(\alpha - \alpha_i) + \boldsymbol{O}(\varepsilon^2(z,t)) \tag{117}$$

where $\alpha = x, y$, $i = 1,2$, neglecting second order (or higher) order terms such as $\varepsilon_\alpha(z,t) \times \varepsilon_\beta(z,t)$ with $\alpha, \beta = x, y$, subtracting static equation (115), after Fourier transform, the fluctuations in the cross sections due to fuel assembly vibration in 3d read as:

$$\delta \sum {}_{\alpha,g}(\bar{r},t) = \sum {}^{r}_{\alpha,g}(z) - \sum {}^{c}_{\alpha,g}(z) \quad \boldsymbol{H}(x - x_1) - \boldsymbol{H}(x - x_2) \quad \delta(y - y_1) - \delta(y - y_2) \times$$

$$\varepsilon_y(z,t) + \boldsymbol{H}(y - y_1) - \boldsymbol{H}(y - y_2) \quad \delta(x - x_1) - \delta(x - x_2) \; \varepsilon_x(z,t) \tag{118}$$

where the axial dependence of the displacement is defined in the following form:

$$\varepsilon_{\alpha}(z,\omega) = \varepsilon_{\alpha}^{0}(\omega)\sin(\frac{\pi}{H}z), \quad (119)$$

with H standing for the height of the reactor core.

6.5. Coupling between fine mesh (FM) CORE SIM and coarse mesh (CM) CORE SIM simulators

In the equations presented in Section, $\Sigma_{\alpha,g}(r)$ and $\delta\Sigma_{\alpha,g}(r,\omega)$, $\alpha = a, f, rem$, $g = 1,2$ having the generic meaning of a static macroscopic cross-section and its fluctuations, $\phi_{g}(r)$ and $\delta\phi_{g}(r,\omega)$ having the generic meaning of the static scalar flux and its fluctuations (neutron noise) and $S_{g}(r)$ and $\delta S_{g}(r,\omega)$ having the generic meaning of a neutron source and its fluctuations (neutron noise source), the following node-averaged quantities for the node corresponding to a vibrating fuel assembly are defined:

6.6. Calculation procedure

In the current model, the neutron noise is calculated by using first order perturbation theory. Therefore, as a first step, the corresponding steady-state solution should be found. For this reason, in the next section the calculation scheme used to evaluate the static solution is discussed and followed by the description of respective dynamical calculations. As has already been underlined earlier, the present model consists of two sub models with different mesh sized: fine mesh sub model (vibrating fuel assembly) and fine mesh sub model (the rest of the core) which are strongly couple between each other. Both sub models are represented in static and dynamic calculations and discussed in more details below.

6.6.1. Steady-state calculations

In the present study, the following iterative scheme to obtain the steady-state solution for coupled fine-coarse mesh system was developed and summarised below:

- 1. First, the cross sections for vibrating fuel assemblies at the coarse mesh level are calculated via Eqs. (108)-(109) by condensing the input fine mesh cross sections with the respective two-group static flux as a weighting function (the latter is also given as an input); at this first iteration, one assumes a unit spatial distribution for the static flux at the fine mesh level whereas in all consecutive iterations, the corresponding static flux calculated at the previous iteration is used.
- 2. The spatial distribution of the static fluxes at the coarse mesh level is computed by numerically solving Eq. (80).

- 3. Then, the spatial distributions of the net currents at the coarse mesh node interfaces are estimated using Fick's law and the continuity of the currents.
- 4. Further, the spatial distribution of the noise source for the fine mesh subsystem expressed in terms of reflected boundary conditions is computed.
- 5. Next, the steady-state solution for the fine mesh subsystem is found via Eq. (85) by solving the correspond source problem.
- 6. Finally the obtained fine-mesh static fluxes are used to update the coarse mesh cross section data at the position of vibrating fuel assembly via Eqs. (108)-(109).
- 7. All the interaction steps (2-6) except for the first one are repeated until the required convergence in the corresponding fine /coarse mesh quantities (fluxes, cross-sections, sources and keff) is achieved.

The main steps of the static coarse-fine mesh iterative scheme are summarized in *Fig. 30*.

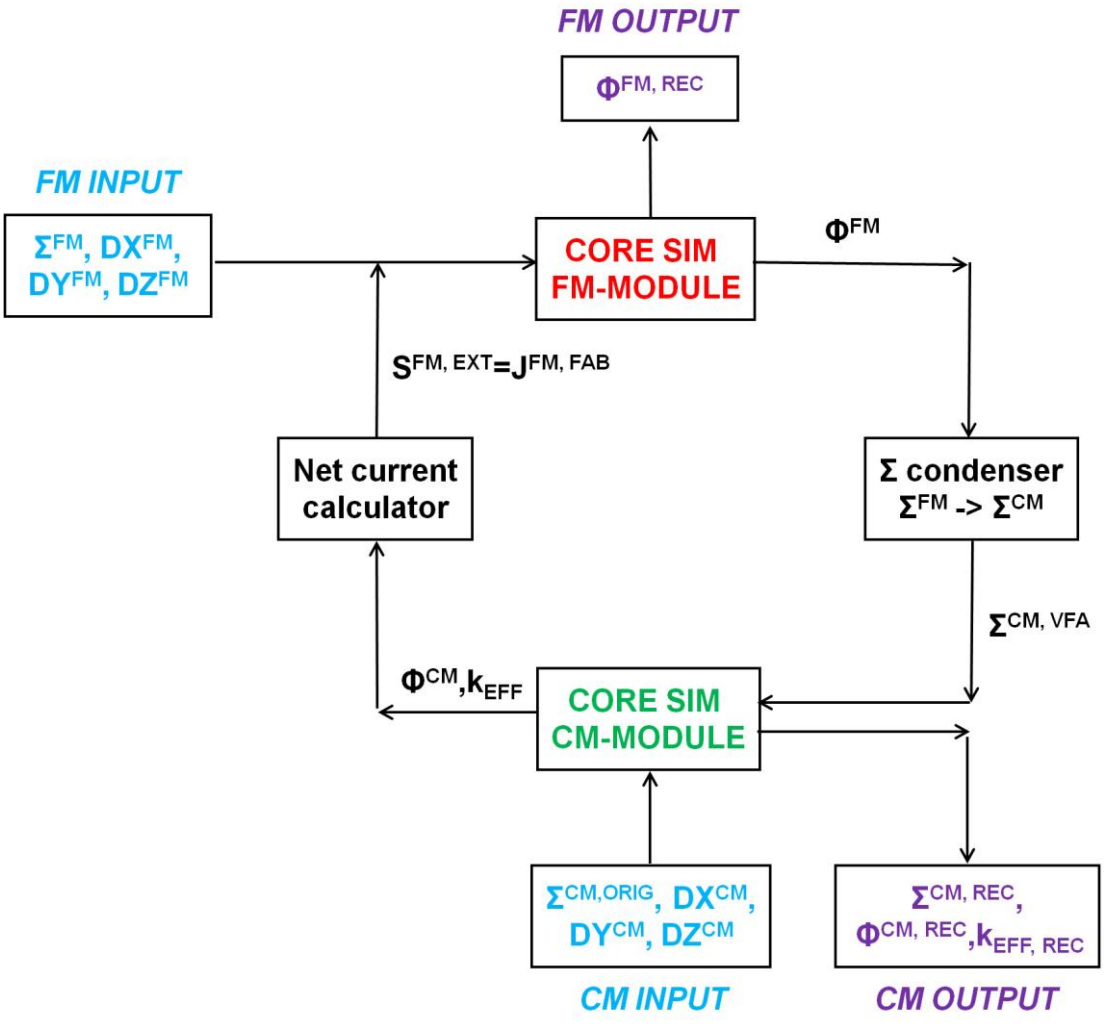

Fig. 30 Coupled CM-FM coupled steady-state calculations.

In *Fig. 30*, the iterative scheme used for the coupled coarse-fine mesh static calculations, is shown. This loop is meant to solve the static problem, assuming that the neutron fluxes at the fine mesh, the cross-sections at the fine and coarse mesh levels as well as node size for both subsystems are given. As can be seen from *Fig. 30*, this scheme contains two separate neutronic modules. The first one, designated as CORESIM CM-MODULE (where "CM" stands for Coarse Mesh) is based on Eqs.(76), (80) and calculates the spatial distributions of the coarse mesh static neutron flux (both fast and thermal) as well as k-effective. As an input for this module, the spatial distributions of the coarse mesh cross-sections and node size. The second module, called CORESIM FM-MODULE (where "FM" stands for Fine Mesh), is built on the basis of Eqs. (83), (85) and estimates the spatial distribution of the fine mesh two-group neutron flux throughout the core. As an input, one needs to provide the spatial distributions of fine mesh cross-sections, node size as well as the boundary conditions (i.e. net current at the boundaries) or the external source. The convergence criteria in the present iterative scheme was imposed on the coarse and fine mesh neutron fluxes, k-effective and coarse mesh cross-sections by requiring that the difference in any of these quantities between two consecutive iteration should be below certain values.

6.6.2. Dynamical calculations

Similarly to the static case, the following iterative scheme for solving noise equations was introduced:

- 1. First, the updated coarse mesh cross-sections for the nodes corresponding to the vibrating fuel assemblies are estimated from Eq. (111) assuming that at the first iteration all the core nodes have the same unit distribution of the fine mesh neutron noise; in the consecutive iterations, the neutron noise distribution defined at the previous iteration might be used.
- 2. Further, the coarse mesh noise source corresponding to the vibrating fuel assemblies is calculated from Eq. (112) using the information about the noise source and static two–group flux distributions at the fine mesh level as an input.
- 3. Next, the space-frequency distribution of the two group neutron noise at the coarse mesh level is estimated via Eqs. (94), (96).
- 4. Then, the space frequency distribution of the fine mesh internal noise source (noise in the net current), i.e. the boundary conditions for the fine mesh neutron noise is calculated from the coarse mesh neutron noise from the previous iteration.
- 5. Finally, the space-frequency distribution of the two-group fine mesh neutron noise is calculated via Eqs. (105), (107) and used for updating the coarse mesh cross-sections for the nodes corresponding to the vibrating fuel assemblies (if it is needed).

- 6. Steps 1, 3,4,5 are repeated until the required convergence in the fine mesh and coarse mesh neutron noise is achieved. In the case when Step 1 is not undertaken, Step 6 is automatically eliminated and the calculations are performed only once.

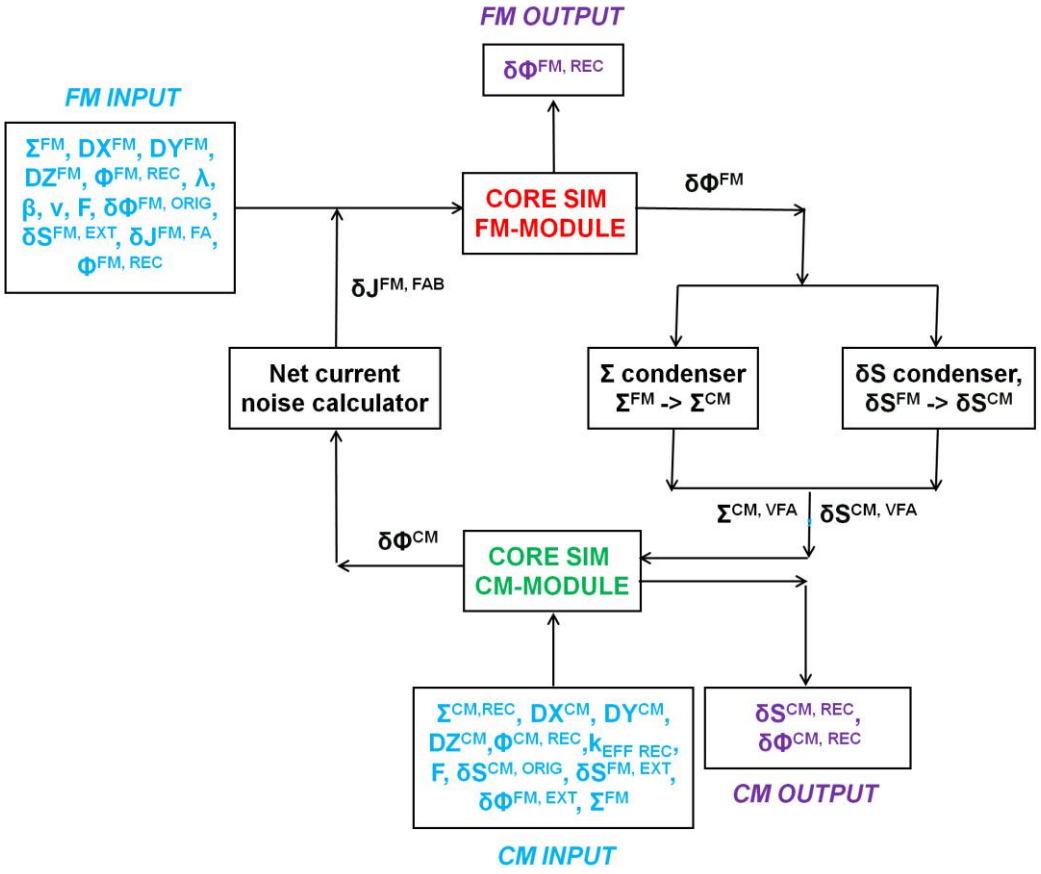

Fig. 31 Coupled CM-FM coupled noise calculations.

Here, one should point out that in the above dynamic iterative scheme, Step 1 is no necessary. There are tow reason for this. First such a step will not affect significantly the final results. The second argument refers to the fact that the use of the fine mesh neutron noise as a weighting function in Eq. (111) can not be always appropriate as well as preservation of the noise in the current is not required for the dynamic calculations (the current is never preserved in the dynamic change).

The main steps of the dynamic thermo-hydraulic iterative scheme are summarized in *Fig. 31* In *Fig. 31,* the iterative scheme used for the coarse-fine mesh noise calculations is shown. This loop is meant to solve the dynamic problem, assuming that the fine mesh neutron noise, fine mesh noise source, fine and coarse mesh static solutions, cross-sections and kinetic data is given. As can be seen from *Fig. 31,* this scheme contains two separate thermo-hydraulic modules. The first one, designated as CORESIM CM-MODULE is based

on Eqs. (94), (96) and calculates the space-frequency distributions of the coarse mesh two-group neutron noise. As an input for this module, the initial coarse mesh external noise source (calculated form fine mesh subsystem from the fine mesh external noise source and the static fluxes), coarse mesh static solution and cross-sections, kinetic parameters (node size, frequency of the vibrations, k-effective, effective fraction of delayed neutrons and decay constant for neutron precursors) are necessary. The second module, called CORE SIM FM-MODULE, is built on the basis of Eqs. (105), (107) and estimates the space-frequency distribution of the fine mesh neutron noise. As an input, one needs to provide static fine mesh fluxes and cross sections, kinetic parameters (node size, frequency of the vibrations, k-effective, effective fraction of delayed neutrons and decay constant for neutron precursors), fine mesh external noise source and fine mesh internal noise source i.e. the boundary conditions for the noise calculated from the coarse mesh dynamic solution. The convergence criteria in the present iterative scheme was imposed on the fine/coarse mesh neutron noise by requiring that the difference in any of these noise quantities between two consecutive iteration should be below certain values.

6.7. Results and discussion

In this section the results of numerical simulations performed with modified coupled coarse-fine mesh CORE SIM simulator for the case of vibrating single fuel assembly are presented and discussed. The detailed description of the eelier developed coarse-fine mesh CORE SIM can be found in the previous sections. Here, the results obtained for both the static solution as well as for the dynamic (neutron noise) are summarized. For illustration purpose, the fuel assembly located approximately in the middle of the Ringhals 3 reactor core ($I = 15, J = 15$) was selected. In the simulation, it was assumed that the fuel assembly vibrates in radial direction i.e. simultaneously in both x – and y – directions (diagonal vibrations) with the frequency of 6 Hz and equal displacements $\varepsilon_x(\omega) = \varepsilon_y(\omega) = \varepsilon(\omega)$ and thus vibration amplitudes. What regards the axial direction of fuel assembly vibrations, a sine function profile has been selected which thus resolves the axial shape of the static flux. The latter corresponds to the fundamental mode type of fuel assembly vibrations.

6.7.1. Static calculations

In *Fig. 32-Fig. 33* the radial and axial distributions of the static removal cross sections for the fine and coarse mesh subsystems respectively are given. In order to provide a more realistic simulation of fuel assembly vibrations with a realistic displacement, for the fine mesh subsystem the node size was reduced to $DX = DY = 0.25$ cm as compared to $DX = DY = 5.375$ cm in the coarse mesh system. In addition, as can be clearly seen from *Fig. 32* both the reflector/moderator and fuel regions were modelled separately in the fine mesh system.

Further, in *Fig. 34-Fig. 37* the radial axial distributions of the fast and thermal static fluxes both at the fine and coarse mesh level are demonstrated. The shape of the static flux

in the fine mesh subsystem which models only the vibrating fuel assembly is defined by the increasing flux gradient around the vibrating assembly in the coarse mesh system via the respective boundary conditions.

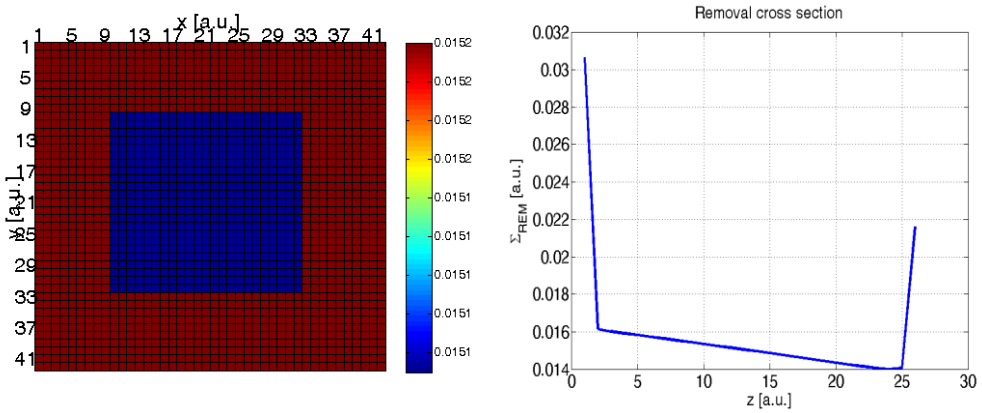

Fig. 32 Radial and axial distribution of removal cross-section (fine mesh, at the middle of the vibrating fuel assembly.

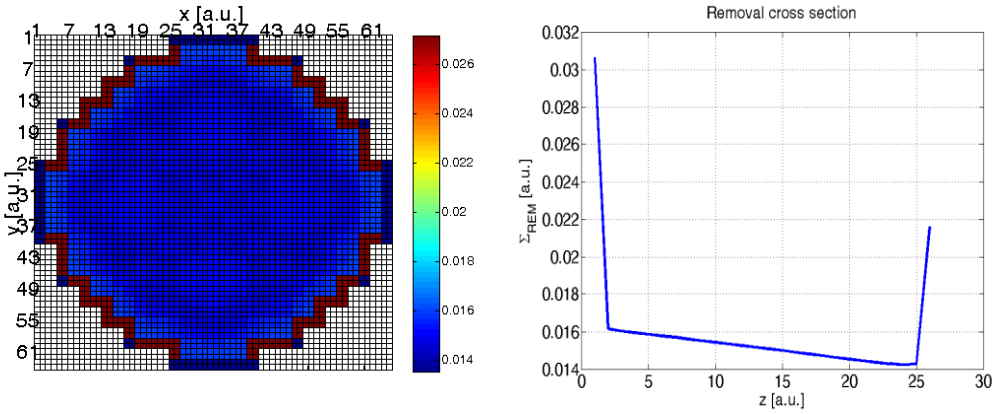

Fig. 33 Radial and axial distribution of removal cross-section (coarse mesh, at the middle of the core.

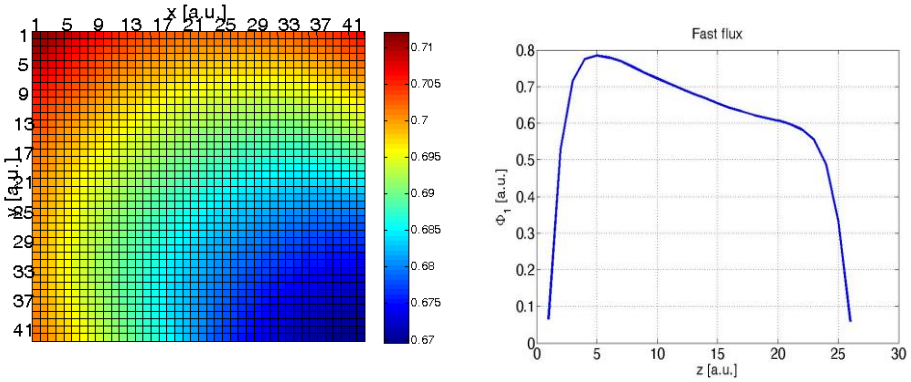

Fig. 34 Radial and axial distribution of static fast flux (fine mesh, at the middle of vibrating fuel assembly.

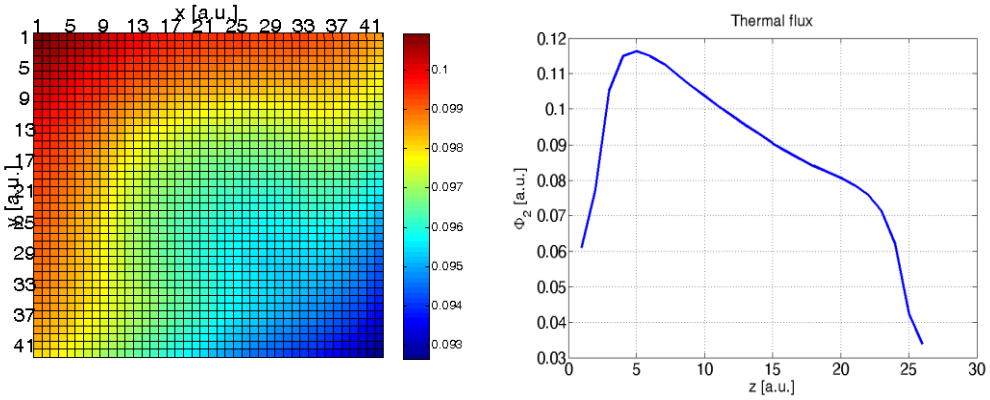

Fig. 35 Radial and axial distribution of static thermal flux (fine mesh, at the middle of vibrating fuel assembly.

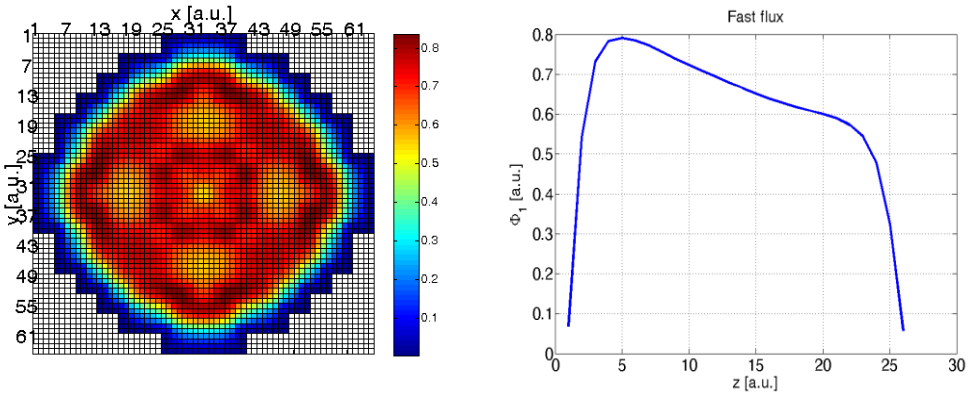

Fig. 36 Radial and axial distribution of static fast flux (coarse mesh, at the middle of the core.

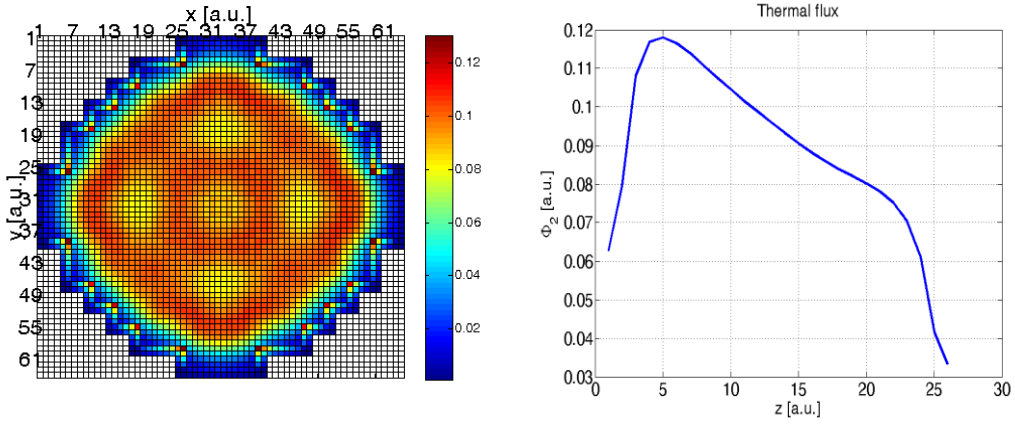

Fig. 37 Radial and axial distribution of static thermal flux (coarse mesh, at the middle of the core.

6.7.2. Dynamic calculations

In *Fig. 38-Fig. 41*, the radial and axial distributions of the amplitude and the phase of the fluctuations induced in the removal cross sections (noise source) due to fuel assembly vibrations for both the fine and coarse mesh subsystems respectively are shown. The results for the noise source at the coarse mesh level were obtained by homogenising the corresponding noise source from the fine mesh subsystem. In order to obtain the correct out-of-phase behaviour of the induced noise due to fuel assembly vibrations at the coarse mesh level after the homogenization, the mesh in the coarse mesh system was refined up to 64 node in x – x and y – directions (compared to the standard core simulator 32 nodes). From the results obtained for the phase, one can clearly notice the out-phase behaviour of the noise source around the vibrating fuel assembly.

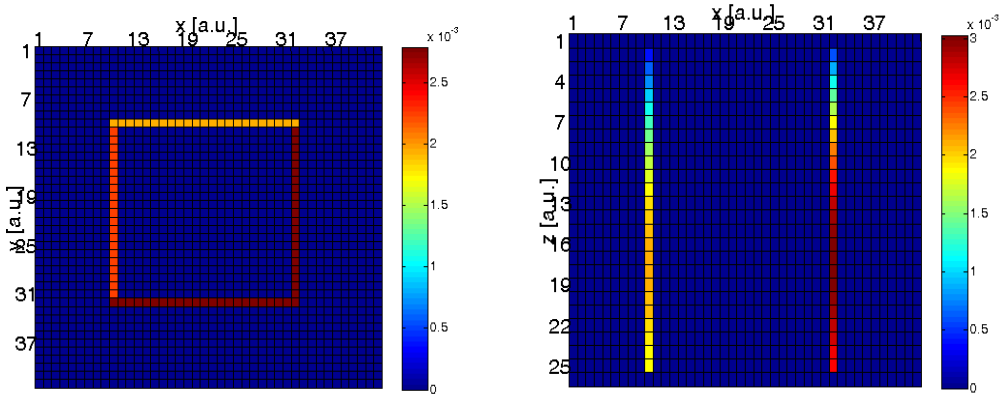

Fig. 38 Radial and axial amplitude distributions of the fluctuations in the removal cross-section (noise source, fine mesh, at the middle of the vibrating fuel assembly.

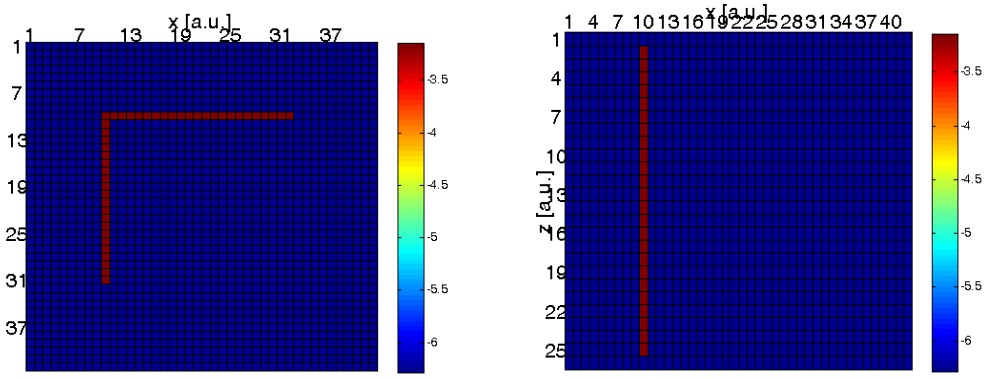

Fig. 39 Radial and axial phase distributions of the fluctuations in the removal cross-section (noise source, fine mesh, at the middle of the vibrating fuel assembly.

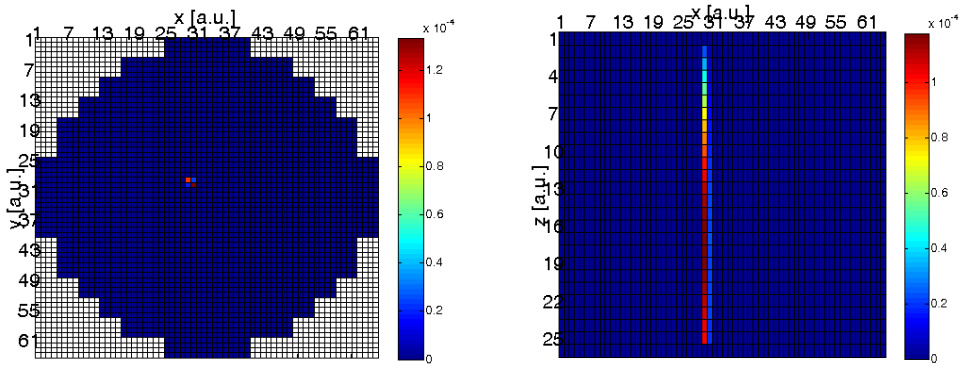

Fig. 40 Radial and axial amplitude distributions of the fluctuations in the removal cross-section (noise source, coarse mesh, at the middle of the core).

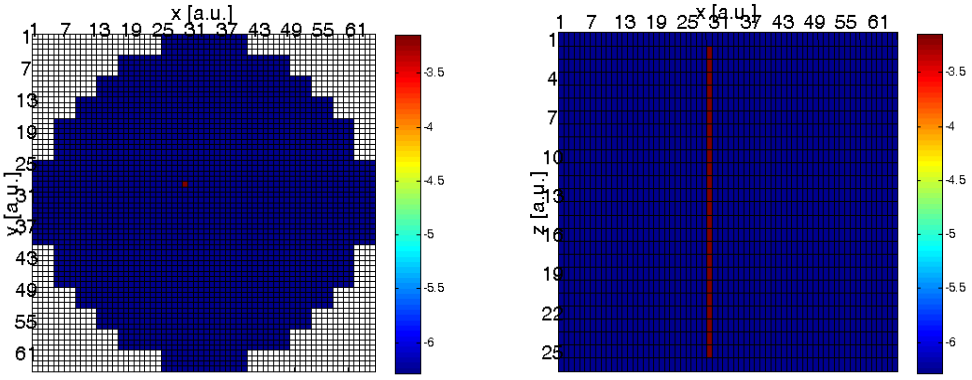

Fig. 41 Radial and axial phase distributions of the fluctuations in the removal cross-section (noise source, coarse mesh, at the middle of the core).

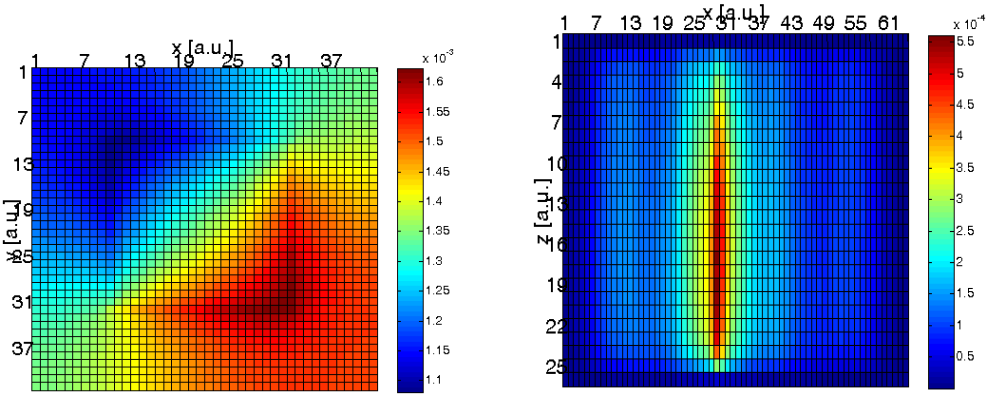

Fig. 42 Radial and axial amplitude distributions of fast noise (fine mesh, at the middle of vibrating fuel assembly.

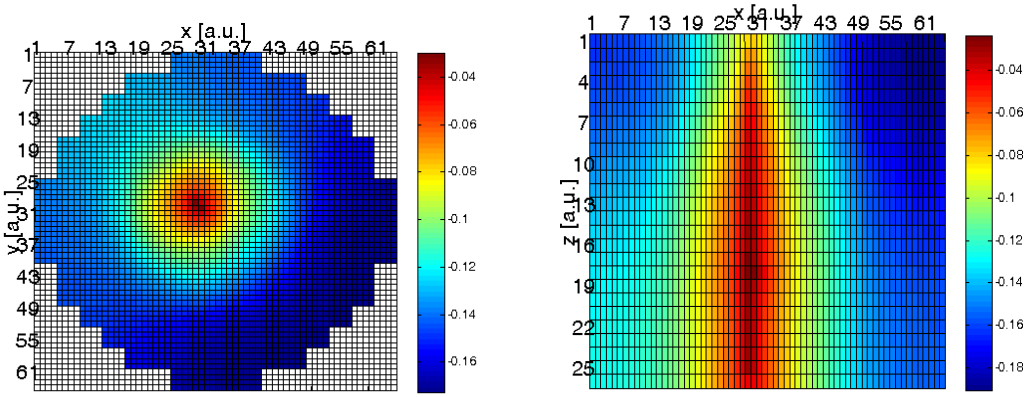

Fig. 43 Radial and axial phase distributions of fast noise (fine mesh, at the middle of vibrating fuel assembly.

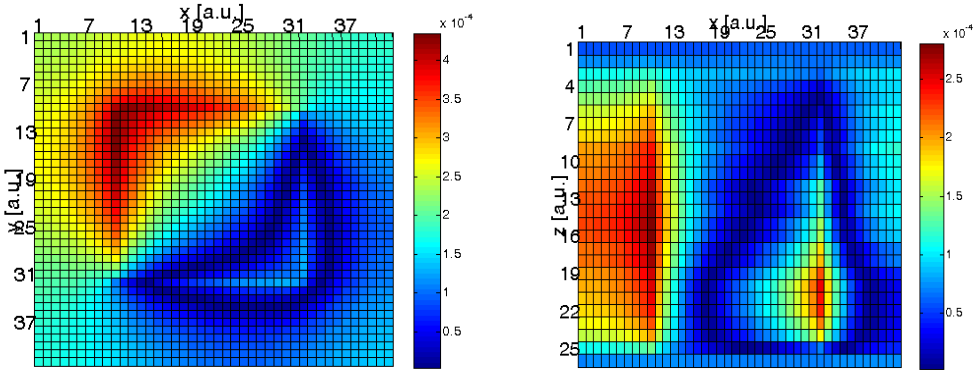

Fig. 44 Radial and axial amplitude distributions of thermal noise (fine mesh, at the middle of vibrating fuel assembly.

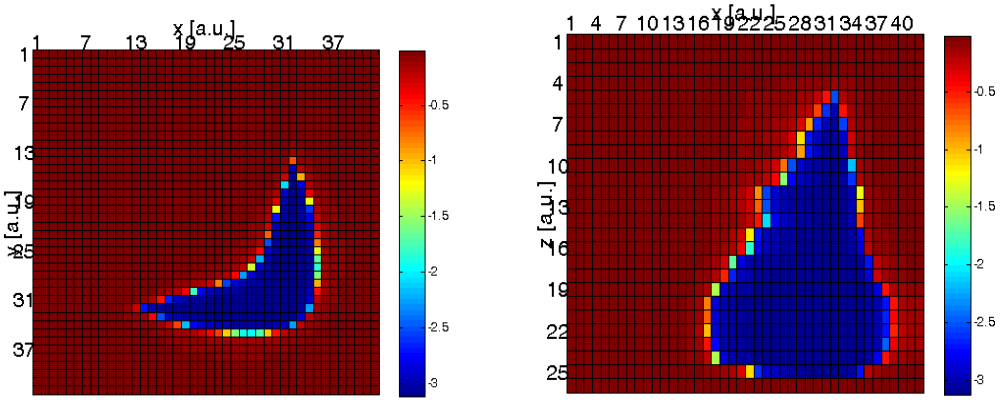

Fig. 45 Radial and axial phase distributions of thermal noise (fine mesh, at the middle of vibrating fuel assembly.

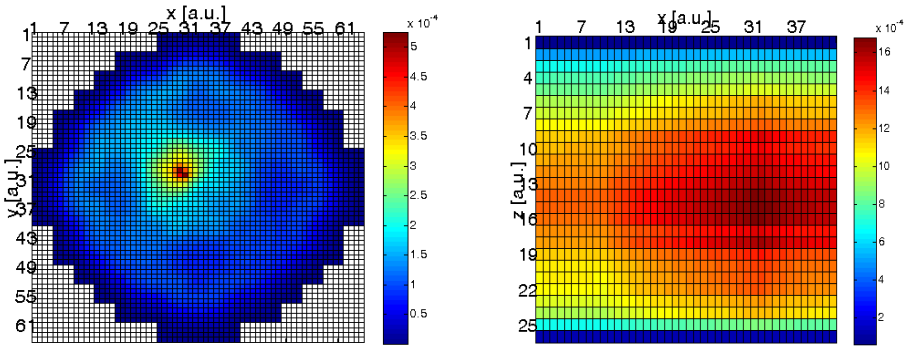

Fig. 46 Radial and axial amplitude distributions of fast noise (coarse mesh, at the middle of vibrating fuel assembly.

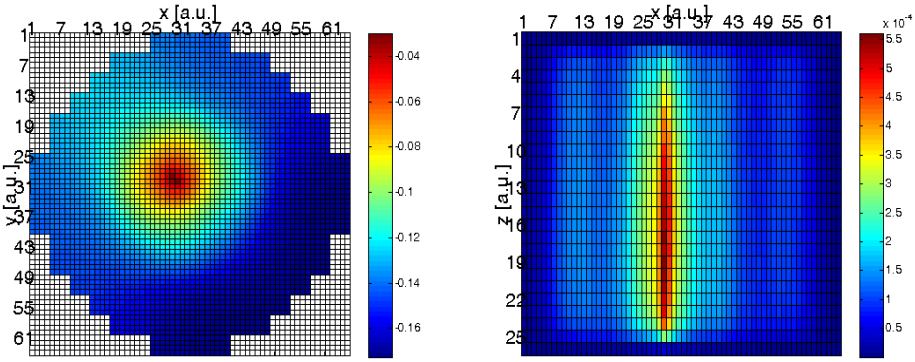

Fig. 47 Radial and axial phase distributions of fast noise (coarse mesh, at the middle of vibrating fuel assembly.

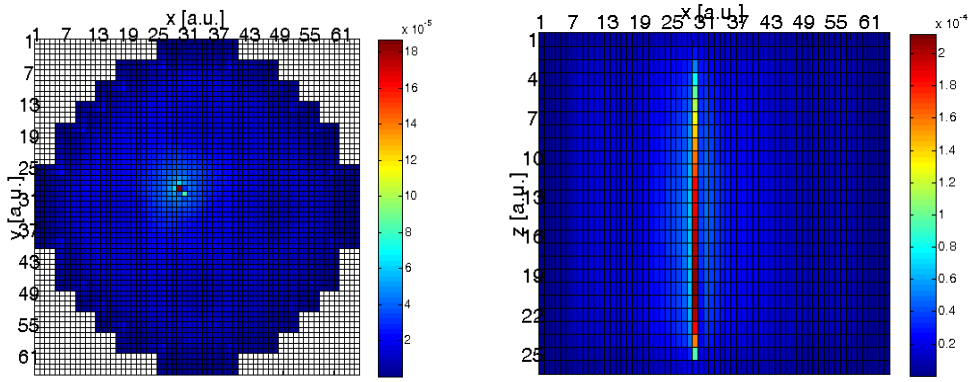

Fig. 48 Radial and axial amplitude distributions of thermal noise (coarse mesh, at the middle of vibrating fuel assembly.

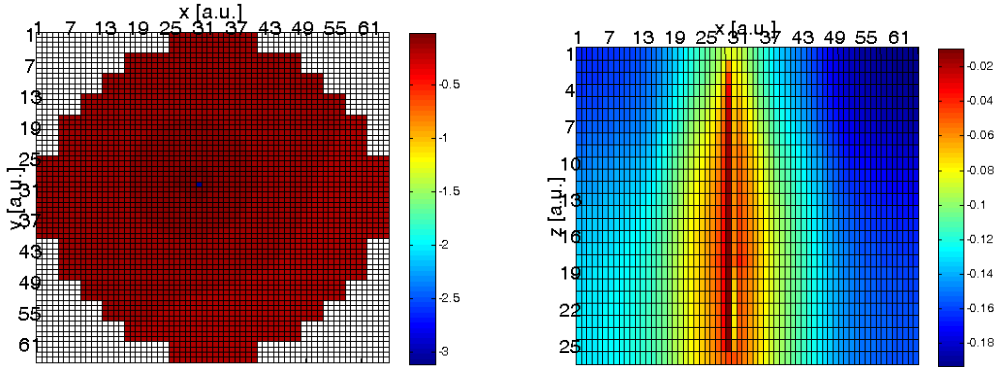

Fig. 49 Radial and axial phase distributions of thermal noise (coarse mesh, at the middle of vibrating fuel assembly.

Further, in *Fig. 42-Fig. 49* the radial and axial distributions of the amplitude and the phase of the two-group noise induced by vibrating fuel assembly for both fine and coarse mesh subsystems are presented, respectively.

6.8. Conclusions

In the present section some preliminary results for the neutron noise induced by 3dimentinal fuel assembly vibrations simulated via modified coupled fine-coarse mesh CORE SIM core simulator were presented and discussed. In general, these results resolve the expected behaviour of the neutron flux in the case of fuel assembly vibrations. This was the first attempt to simulate the neutron noise due to 3-dimensinal fuel assembly vibrations (i.e. its fundamental mode). In order to model the fully realistic displacement of the vibrating fuel assembly, the current model should be modified in such a way that it is able to resolve the node size of a sub millimetre range at the fine mesh level. This latter would require much heavier computer simulations (in terms of time and memory). Therefore, before performing any qualitative analysis of the simulated results, further investigation is necessary to clarify the way to improve the obtained results (by for example implementing other and faster numerical methods) and is planned to be performed in the future.

7. PROPOSAL FOR 2016-2017

1. Further development and improvement of the coupled coarse-fine mesh CORE SIM-based model presented in the current Stage and used for simulating the noise induced by three dimensional fuel assembly vibrations. The main goal is to obtain the realistic displacement (in the sub millimetre range) of the fuel assembly during vibrations at the fine mesh scale. This can be achieved by using more advanced and faster numerical techniques for solving governing CORE SIM equations. The results will have some significance for reactor diagnostics and surveillance of the noise induced by fuel assembly vibrations.
2. Further investigation of the point-kinetic component of the noise induced by fuel assembly vibrations. In order to obtain more realistic simulation results, the model used in the present Stage will be extended (to the three dimensional model which allows to use eight ex-core detectors) and complimented with the modelling of the noise induced by core barrel vibrations. The further validation of the point-kinetic component from ex-core detector signals against the exact reactivity component will be performed.
3. Analysis of new ex-core measurements, taken in R-4 after power increase. The aim is to further investigate the effect of the power uprate by 18.6 %, which was achieved in R-4 in 2015. A comparison with the results from last year could give the first step in a starting trend analysis.
4. Further development and test of the mode separation model as applied to 3-D "wobbling" type or "tilting" vibrations. The basic theory was developed and tested on measurements in the present Stage, but further tests are necessary to assess its applicability, as well as to follow up the "wobbling" type vibrations. Such components can be identified if both the upper and lower ex-core detectors are utilised simultaneously and the symmetry relationships are taken into account to enhance such components, similarly to how the beam and shell mode components can be enhanced by suitable combinations of the signals of only the lower or the upper detectors. Extending the formerly purely 2D model to 3-D can benefit even the diagnostics of the beam mode vibrations, if e.g. the reactivity component is estimated from the sum of 8 detectors instead of 4. It is suggested that some measurements are evaluated retrospectively, since measurement data are available. One suitable case would be the measurements in R2. This is because the characteristic of the beam mode vibrations of R2 differ from those of R3 and R4. It would be interesting to compare R2 with R3 and R4 even what regards the tilting mode vibrations.
5. A basic study in neutron noise was outlined in Section 5 of this present report, showing how the modulation of a moderating or scattering medium, without the presence of fissile material, will induce non-trivial (correlated) fluctuations both in pulse count and current mode of the detectors. It is suggested that an experimental verification of the theoretical predictions be made during the next Stage. As mentioned also in Section 5, in addition to its own research value, this study could also give some indirect support to our efforts in the determination of the void fraction from neutron noise measurements.

The idea is that neutrons emitted independent from each other from a source with simple Poisson statistics (Am-Be or Pu-Be source), slowing down and diffusing in a non-multiplying medium, which are hence originally uncorrelated, become correlated if the medium in which the slowing down and diffusion takes place is fluctuating (e.g of a result of a perturbation, such is the presence of two-phase flow). The experiment requires a neutron source in a water tank, and two neutron detectors. Bubbles introduced in the water between the source and the detectors would act as a suitable perturbation. Such an experiment can be performed both in Chalmers and at our collaboration partners, the EPFL Lausanne.

6. A pilot study of the possibility of using fission chambers for zero power noise experiments. In zero power noise experiments, the subcritical reactivity is determined from the statistics of the individual counts: either from the time correlations between two consecutive counts (Ross-alpha method) or from the relative variance of the number of detection as a function of the measurement time (variance to mean or Feynman-alpha method). Application of these methods meets difficulties at higher neutron fluxes (high count rates), due to dead-time problems. This could be circumvented by the use of fission chambers; however, at high count rates these operate in the so-called Campbell mode. In this mode the individual counts are not distinguishable, since the pulses induced by the counts strongly overlap. So far, from the higher moments of the detector current, only the mean count rate could be determined, but not the correlations or variance of the pulse count. However, recently we managed to generalise the theory of fission chamber currents to make it possible to extract both the time correlations and the variance of the counts from the detector current. In order to be able to apply the method in practice, further theoretical studies and numerical simulations are needed, which is suggested to be performed in the next stage. Possibly some experimental study, or verification of the method, can also be included in the next Stage, either in Ringhals, or at some of our collaborating partners (such as the Technical University of Budapest, or CEA).

8. ACKNOWLEDGEMENT

This one-year contract was performed by funding from Ringhals Vattenfall AB, contract No. 630217-031. Contact person from Ringhals was Adj. Prof. Henrik Nylén.

REFERENCES

[1] J. A. Thie, “Core motion monitoring”, *Nuclear Technology* **45**, pp 5-45 (1979).

[2] I. Pázsit, J Karlsson, N. Garis, “Some developments in core-barrel vibration diagnostics”, *Annals of Nuclear Energy* **25**, pp 1079-1093 (1998).

[3] V. Dykin, C. Montalvo, H. Nylén, I. Pázsit, Ringhals Diagnostics and Monitoring, Final Research Report 2012-2014, CTH-NT-304/RR-19 (2014).

[4] R. B. Pérez, R. T. Wood, "A stochastic method for nuclear power plant diagnosis" (1988).

[5] I. Pázsit, H. Nylén, C. Montalvo-Martin, "Refined method for surveillance and diagnostics of the core barrel vibrations of the Ringhals PWRs" (2014).

[6] I. Pázsit, C. Montalvo Martin, H. Nylén, T. Andersson, A. Hernández-Solis and C. Bernitt Carterno, "Developments in core-barrel motion monitoring and applications to the Ringhals PWRs,"*To appear in Nuclear Science Engineering* (2015).

[7] C. W. Mayo, "Detailed neutron noise analysis of pressurized water reactor internal vibrations", *Atomkernenergie* **29**, pp 9-13 (1977).

[8] G. Kosály, "Noise investigations in boiling-water and pressurized-water reactors", *Progress in Nuclear Energy* **5**, pp 145-199 (1980).

[9] I. Pázsit, C. Demazière, C. Sunde, P. Bernitt, A. Hernández-Solís, Final Report on the Research Project Ringhals Diagnostics and Monitoring Stage 12 (2008).

[10] B. Severinsson (July 2013), "Brusmätningar för analys av härdhöljesvibrationer på Ringhals 3. Utförda mellan 2013-02-26 och 2013-07-05". Ringhals internal report, UH-rapport 2245846 / 2.0.

[11] B. Severinsson (Sept. 2013), "Brusmätning för analys av Härdhöljesvibrationer på utförda under 2013". Ringhals internal report, UH-rapport 2233461 / 2.0.

[12] M. Nilsson (October 2010), "Brusmätning för att söka lågfrekventa störningar i R3, 100826. Ringhals internal report, UH-rapport 2099930 / 2.0.

[13] C. Sunde, C. Demazière and I. Pázsit (2007), Final Report on the Research Project Ringhals Diagnostics and Monitoring, Stage 11. CTH-NT-206/RR13, Chalmers University of Technology, Sweden.

[14] I. Pázsit, C. Demazière, C. Sunde, P. Bernitt and A. Hernández-Solís (2008), Final Report on the Research Project Ringhals Diagnostics and Monitoring, Stage 12. CTH-NT-220/RR-14, August 2008, Chalmers University of Technology, Sweden.

[15] I. Pázsit, C. Montalvo Martín, V. Dykin and T. Tambouratzis (2010), Final Report on the Research Project Ringhals Diagnostics and Monitoring, Stage 13. CTH-NT-230/RR-15, March 2010.

[16] I. Pázsit, C. Montalvo Martín, V. Dykin and H. Nylén (2011), Final Report on the Research Project Ringhals Diagnostics and Monitoring, Stage 14. CTH-NT-253/RR-15, December 2011.

[17] V. Dykin, C. Montalvo Martín, H. Nylén and I. Pázsit (2012), Ringhals Diagnostics and Monitoring Annual Research Report 2012, CTH-NT-269/RR-17, December 2012.

[18] V. Dykin, C. Montalvo Martín, H. Nylén and I. Pázsit (2013), Ringhals Diagnostics and Monitoring, Annual Research Report 2013, CTH-NT-286/RR-18.

[19] V. Dykin, C. Montalvo Martín, H. Nylén and I. Pázsit (2014), Ringhals Diagnostics and Monitoring, Final Research Report 2014, CTH-NT-304/RR-19.

[20] I. Pázsit. H. N. Tran, V. Dykin and A. Jonsson (2013) Research and Development Program in Reactor Diagnostics and Monitoring with Neutron Noise Methods, Stage 18. SSM Internal Report No. 2013:04 ISSN: 2000-0456. Available at www.stralsakerhetsmyndigheten.se.

[21] N. H. Tran, I. Pázsit and H. Nylén (2015), "Investigation of the ex-core noise induced by fuel assembly vibrations in Ringhals-3 PWR", *Annals of Nuclear Energy* **80**, pp 434 - 446 (2015).

[22] C. Demaziére (2011) CORE SIM: A multi-purpose neutronic tool for research and education, Ann. nucl. Energy 38, 2698-2718

[23] I. Pázsit, C. Demazière (2011), Noise Techniques in Nuclear Systems, Chapter in Handbook of Nuclear Engineering, Vol. 3, Reactors of Generation II, Springer, New York, USA.

[24] T. Yamamoto, Personal communication. Kyoto University Research Reactor Institute, 2014.

[25] I. Pázsit and L. Pál, Neutron Fluctuations - A Treatise on the Physics of Branching Processes. Elsevier Ltd, Oxford, New York, Tokyo (2008).

[26] L. Pál and I. Pázsit, Neutron fluctuations in a multiplying medium randomly varying in time. *Physica Scripta* **74**, 62-70 (2006)

[27] L. Pál and I. Pázsit, Theory of neutron noise in a temporally fluctuating multiplying medium. *Nucl. Sci. Engng* **155**, 425 - 440 (2007)

[28] G. Perret, G. Girardin, P. Frajtag, and M. Hursin, "Decay constant and delayed neutron fraction measurements in CROCUS," TM-41-14-02-Rev1, 2014.

[29] F. J. Sweeney, J. March-Leuba and C. M. Smith (1985), "Excitation Sources for Fuel Assembly Vibrations in a PWR", *Trans. Am. Nuc. Soc.* Vol. **49**, pp 334-335.

CHALMERS UNIVERSITY OF TECHNOLOGY
SE 412 96 Gothenburg, Sweden
Phone: + 46 - (0)31 772 10 00
Web: www.chalmers.se